NASA-CR-202158

FINAL
IN-34-CR
OCIT

A Final Report
Grant No. NAG5-2924
June 1, 1995 - August 31, 1996

TORSIONAL BUCKLING TESTS OF A SIMULATED SOLAR ARRAY

Submitted to:

National Aeronautics and Space Administration
Goddard Space Flight Center
Greenbelt, MD 20771

Attention:

Mr. John Decker, Code 722.1
Mechanical Systems Division

Submitted by:

E. A. Thornton
Professor

SEAS Report No. UVA/528525/MANE97/101
August 1996

DEPARTMENT OF MECHANICAL, AEROSPACE
AND NUCLEAR ENGINEERING

SCHOOL OF
ENGINEERING
& APPLIED SCIENCE

University of Virginia
Thornton Hall
Charlottesville, VA 22903

Abstract

Spacecraft solar arrays are typically large structures supported by long, thin deployable booms. As such, they may be particularly susceptible to abnormal structural behavior induced by mechanical and thermal loading. One example is the Hubble Space Telescope solar arrays which consist of two split tubes fit one inside the other called BiSTEMs. The original solar arrays on the Hubble Space Telescope were found to be severely twisted following deployment and later telemetry data showed the arrays were vibrating during daylight to night and night to daylight transition. The solar array twist however can force the BiSTEM booms to change in cross-section and cause the solar arrays to react unpredictably to future loading. The solar arrays were redesigned to correct for the vibration, however, upon redeployment they again twisted.

To assess the influence of boom cross-sectional configuration, experiments were conducted on two types of booms, 1)booms with closed cross-sections, and 2) booms with open cross-sections. Both models were subjected to compressive loading and imposed tip deflections. An existing analytical model by Chung and Thornton was used to define the individual load ranges for each model solar array configuration. The load range for the model solar array using closed cross-section booms was 0-120 Newtons and 0-160 Newtons for the model solar array using open cross-section booms. The results indicate the model solar array with closed cross-section booms buckled only in flexure. However, the results of the experiment with open cross-section booms indicate the model solar array buckled only in torsion and with imposed tip deflections the cross section can degrade by rotation of the inner relative to the outer STEM. For the Hubble Space Telescope solar arrays the results of these experiments indicate the twisting resulted from the initial mechanical loading of the open cross-section booms.

Table Of Contents

List of Figures

List of Tables

Nomenclature

Arabic	Description
A	Boom Cross-Sectional Area
a	Length Between Strain Gage 1 and Lower End of Test Article
b	One Half Length of Spreader Bar
b'	One Half Width of the Solar Blanket
b_w	BiSTEM Strip Width
d	Boom Diameter
E	Modulus of Elasticity
EA	Axial Stiffness
EΓ	Warping Stiffness
EI	Bending Stiffness
F	Boom Tensile Load
F_h	Horizontal Load
F_x	Solar Blanket Membrane Force per Unit Length
GJ	Boom Torsional Rigidity
I	Moment of Inertia
I_E	Sum of the Area Moments of Inertia
L	Length of Boom
M	Moment
P	Compressive Load on a single Boom
P_{cr}	Critical Buckling Load
R_m	Mean Radius
r_i	Inside Radius
r_o	Outside Radius
s_1	Laser Displacement Sensor 1
s_2	Laser Displacement Sensor 2
t	Strip Thickness
w'	Lower Spreader Bar Displacement

Nomenclature

w1	Boom 1 Tip Displacement
w2	Boom 2 Tip Displacement

Greek symbol	Description
α	Overlap Angle, see Figure 2.6
β	Boom Torsional Buckling Eigenvalue
ε_{a1}	Axial Strain Boom 1
ε_{a2}	Axial Strain Boom 2
ε_b	Bending Strain
Φ	BiSTEM Angle of Twist, see Figure 4.12
λ	Boom Flexural Buckling Eigenvalue
θ	Swept Angle, see Figure 2.7
σ	Stress

Chapter 1

Introduction

From the beginning of the space program to the present, spacecraft have needed to communicate with their controllers here on earth. These communication systems use solar arrays supported by deployable appendages to generate needed electricity.

1.1 Deployable Appendages

Deployable appendages are structural members that are long, slender beam-like booms. The uses for these booms are numerous. Some examples of past applications are low gain antenna, supports for payloads, and larger systems such as solar arrays. For some solar arrays the booms are comprised of two concentric tubes. Each of the tubes is split thus possessing an incomplete circular cross-section. While these booms are stowed each STEM (storable tubular extendible member) is flattened and rolled up onto drums, each resembling a carpenter's tape. Then during deployment the stored elastic energy forces the tubes into their original shape. Booms with this configuration were used for the solar arrays of the Hubble Space Telescope.

1.2 Hubble Space Telescope

The Hubble Space Telescope (Figure 1.1) is an unmanned orbiting telescope that is providing scientists an unprecedented means for exploration of deep space.

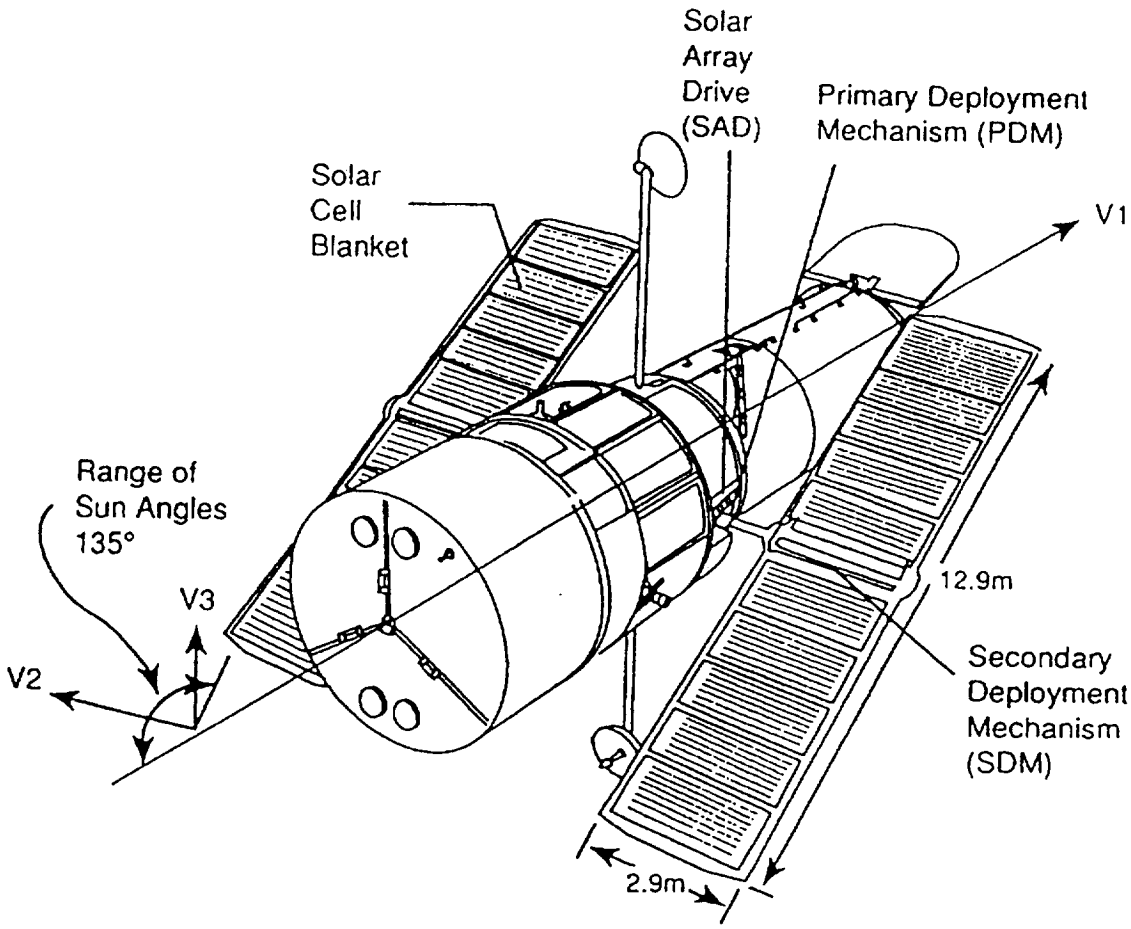

Figure 1.1: Hubble Space Telescope

The telescope's 2.4 meter primary mirror makes it possible for astronomers to document the visible realm of the universe with ten times the resolution and fifty times the sensitivity than that of any other telescope yet built, [1]. The Space Telescope is much more than an optical device, it is in fact, an orbiting space observatory. Aboard the Space Telescope are six major instruments designed to analyze the in-coming light. These instruments are two cameras to photograph the objects of the cosmos, a photometer to measure the magnitude of the entering light, two spectrographs to spread the gathered light into its component colors and several guidance sensors to position and locate objects in space. The various instruments and sensors acquire electrical power from two sets of solar arrays both measuring 12.9 meters in length and 2.9 meters in width [2]. The Space Telescope was launched into orbit aboard the Space Shuttle Discovery on April 24, 1990. The successful deployment from the Shuttle was achieved one day later at an altitude of 615 kilometers.

1.3 Pointing Disturbances

Shortly after the deployment, a significant, potentially long term complication was observed from telemetry data. The telescope pointing control system was experiencing large disturbances, mostly during the transition from daylight to eclipse and eclipse to daylight. The data [3] showed that disturbances occurred at a frequency near 0.1 Hz. Further investigation revealed the dominant frequency about the V1 and V2 axes (see Figure 1.1 for axes orientation) was 0.1 Hz and 0.6 Hz about the V3 axis, also with a prominent 0.1 Hz frequency component. Evidence [4]

suggesting the pointing disturbances were caused by the solar arrays were that the fundamental bending modes of the arrays were predicted to be near 0.1 Hz, and the slight differences in stiffness of the booms could explain the beating phenomena between the vibration histories. Moreover, the flexible arrays were the most likely sources of disturbances due to large thermal gradients that would occur at transitions from daylight to eclipse and eclipse to daylight..

1.4 Vibrations

Once the Space Telescope was seen to be experiencing these significant complications an attempt to understand and predict what was happening to the Space Telescope was undertaken by NASA, its contractors and academia. The dynamic response of the solar arrays were predicted analytically by Thornton and Kim [5] using two methods, uncoupled and coupled thermal-structural analysis. The uncoupled model is consistent with classic heat transfer which assumes rigid bodies for the purposes of writing the energy conservation equation. In terms of the Space Telescope solar arrays, that means the temperature gradients are calculated assuming the motion of the solar array does not affect the incident, absorbed heat fluxes. The published results predict a thermally induced vibration for the first bending mode to occur at 0.097 Hz. The second model coupled the effect of the boom's deformation with the absorbed heat flux. Again, in terms of the Space Telescope, this means the solar array booms' motion are affected by the incident, absorbed heat fluxes. This model established a stability criterion predicting conditions for which thermal flutter of the solar array's may occur and its accompanying dynamic response. The results

predict a maximum temperature gradient of 20 K across the boom depth which develops in about 120 s and causes the booms to experience a tip deflection of about 0.38 m.

Both uncoupled and coupled models provide key parameters describing the behavior of the solar arrays. The parameters for understanding the static and dynamic response of the arrays are the thermal and surface properties of the boom material, as well as the boom stiffness and thermal expansion coefficient. Another parameter important for the boom design is the boom initial compressive force which lowers the solar array's natural frequencies. Finally, these models showed the ratio of the thermal and structural response times, the solar inclination angle and the system damping are important parameters in determining the possibility of thermal flutter.

These predictions were very similar to those made by NASA. According to a paper presented at the 61st Shock and Vibration Symposium [6], NASA and their contractors concluded by the results of analytical models that the temperature gradient caused the solar array deformations and vibrations. With this information NASA, ESA and its contractors were able to redesign and produce a next generation of solar arrays in time for the Space Telescopes first servicing mission.

1.5 First Servicing Mission: Condition of Original Solar Arrays

In December 1993 the Space Shuttle Endeavour successfully captured and attached the Space Telescope to the cargo bay for its first servicing mission. What was suggested previously only through telemetry data, was now clearly evident to the astronauts. The Solar Arrays (Figure 1.2) were badly disfigured and were damaged.

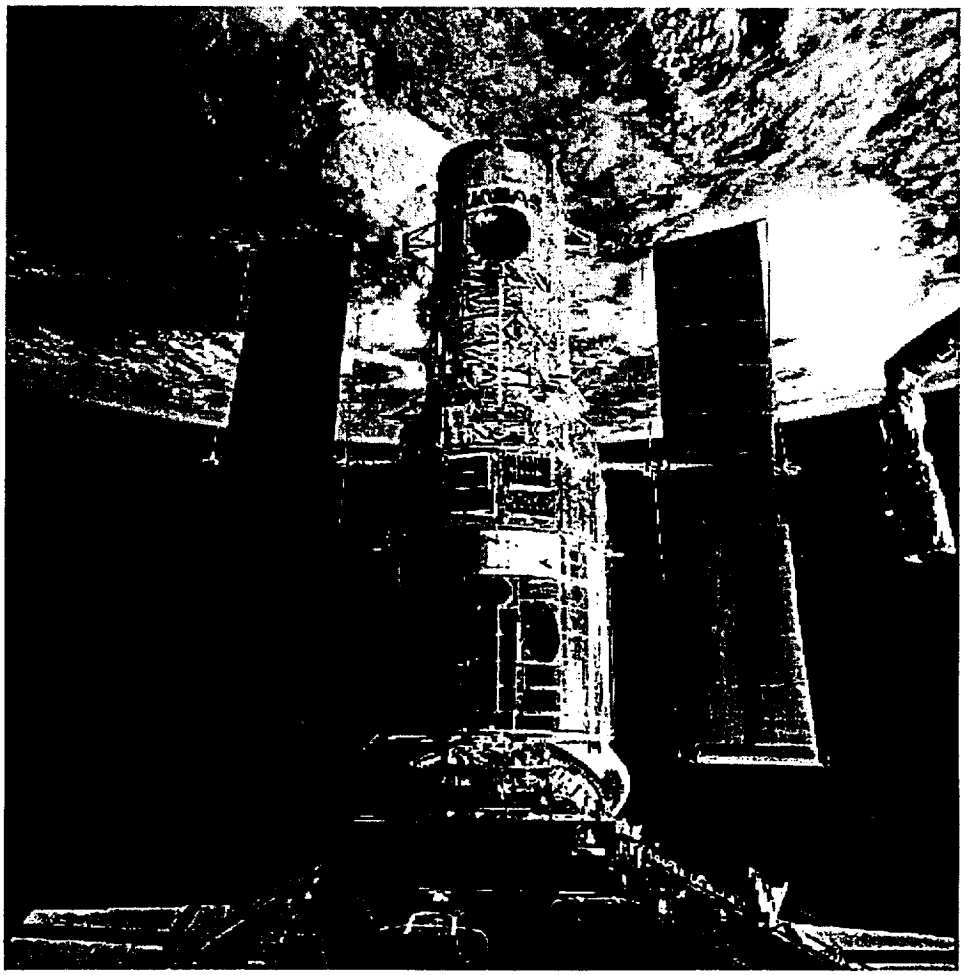

Figure 1.2: Original Solar Arrays

The scheduled list of repairs included a retraction of the arrays by the Secondary Deployment Mechanism (Figure 1.1), disconnection of the existing arrays, connection of redesigned arrays and finally, redeployment. Although both wings were damaged, the wing with the least amount of damage was successfully retracted, disconnected from the Space Telescope and stowed to bring back to earth. The astronauts noted the other wing was twisted severely and at least one boom did not appear to be parallel with the solar blanket. Closer inspection of the wing revealed the solar array indeed did have a torsional deflection and one BiSTEM buckled (Figure 1.3) leaving the outer STEM opened enough to allow the inner STEM to locally separate from the outer STEM. The crew unsuccessfully tried to retract the damaged wing. Finally, it was decided that astronaut Kathryn Thornton would unbolt the array and jettison it overboard. After these dramatic events, redesigned solar arrays were successfully mounted and deployed.

1.6 First Servicing Mission: Deployment of Redesigned Solar Arrays

Once the original solar arrays had been detached and replaced with the redesigned arrays, the deployment was achieved while the Space Telescope was still mounted to the Space Shuttle in the cargo bay. One at a time, each wing was deployed completely. Once the Secondary Deployment Mechanism started to push the BiSTEM outward bringing with them the solar array blanket and thermal shields, the process went as expected. Until the array reached near the end of its deployment no appreciable vibrations nor deflections were observed by the astronauts. But with most of the deployment achieved successfully, the arrays began to torsionally deform

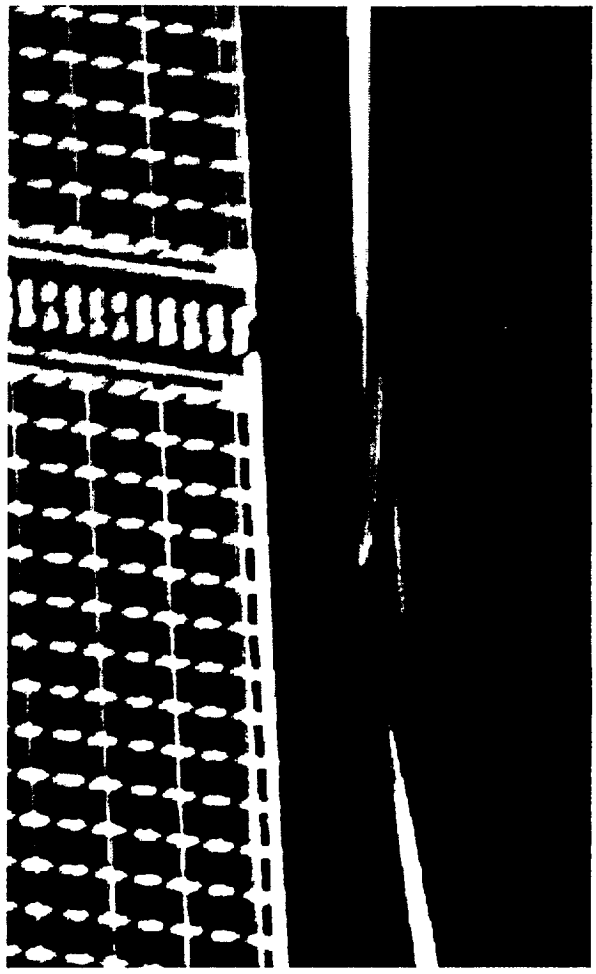

Figure 1.3: BiSTEM Failure

(Figure 1.4). This action continued until the array deployment reached its mechanical stops completing the deployment. Video tapes show that the sudden cessation of the arrays deployment coincided with the onset of a torsional vibration of the arrays as well as the thermal shielding stretching and contracting along their respective BiSTEMs. Within a short time of its start, the solar arrays torsional vibration and the oscillation of the thermal shields covering the BiSTEMs damped out. The resulting steady state configuration of the solar array was a permanent torsional deflection. The Space Telescope remained captured and fixed to the Shuttle through several daylight to night and night to day transitions. During this time, no appreciable vibrations were observed. NASA at that time decided the arrays had assumed a stable condition and later deployed the Space Telescope into orbit about the earth.

1.7 Buckling

When the Space Telescope was deployed with the redesigned solar arrays, the steady state torsional deformation appeared very similar to the torsional deformation of the original solar arrays upon their deployment. While this deformation did not appear to endanger the mission of the Space Telescope it was apparent that further study was necessary to correct this unwanted configuration.

Initial analysis centered around flexural buckling. This analysis, [5], assumed a symmetrical solar array and flexural deformations. The boom Euler buckling force P was computed to be 48.30 Newtons. When deployed, a typical boom force was 14.80 Newtons, hence flexural buckling was not a problem. In

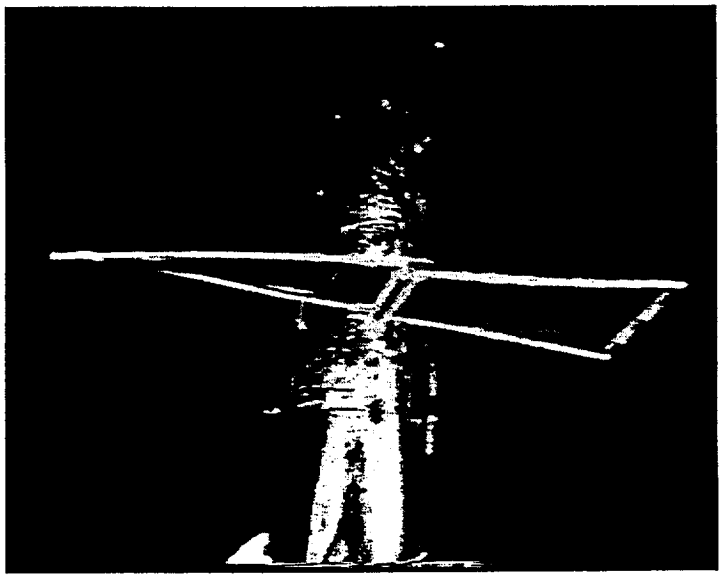

Figure 1.4: Deployed Redesigned Solar Arrays

another paper, Chung and Thornton [7] identified the deformation as a torsional buckling and presented an analytical model to predict the conditions this may occur.

For the model that was presented (Figure 1.5), several basic assumptions were made: 1) torsion implied symmetric twisting about the x axis, 2) the solar blanket was taken to be an inextensible membrane whose thermal expansions and contractions are neglected, 3) the solar blanket was subjected to uniform tension in the x direction and the membrane tensile force was assumed constant, 4) the right and left BiSTEM booms were assumed to be identical cantilevered beams, each subjected to a constant axial compressive force, 5) boom y deflection was neglected for torsional deformations, 6) the thermal effects were neglected and finally, 7) the spreader bar was assumed rigid. With these assumptions Chung and Thornton developed an analytical model for torsional buckling. The analysis led to the transcendental equation 1.1 whose roots are the critical buckling values for the boom forces P.

$$-\frac{\beta BC}{bD}+\frac{CF_x b'^3}{3bL}+bP\lambda=0 \qquad 1.1$$

Figure 1.5 illustrates that L is the boom length, b is one half the length of the spreader bar and b' is one half the width of the solar blanket. In equation 1.1, F_x is the solar blanket tension, and P is the axial compressive force. The coefficient B in equation 1.1 is defined by

$$B=GJ-\frac{PI_E}{A} \qquad 1.2$$

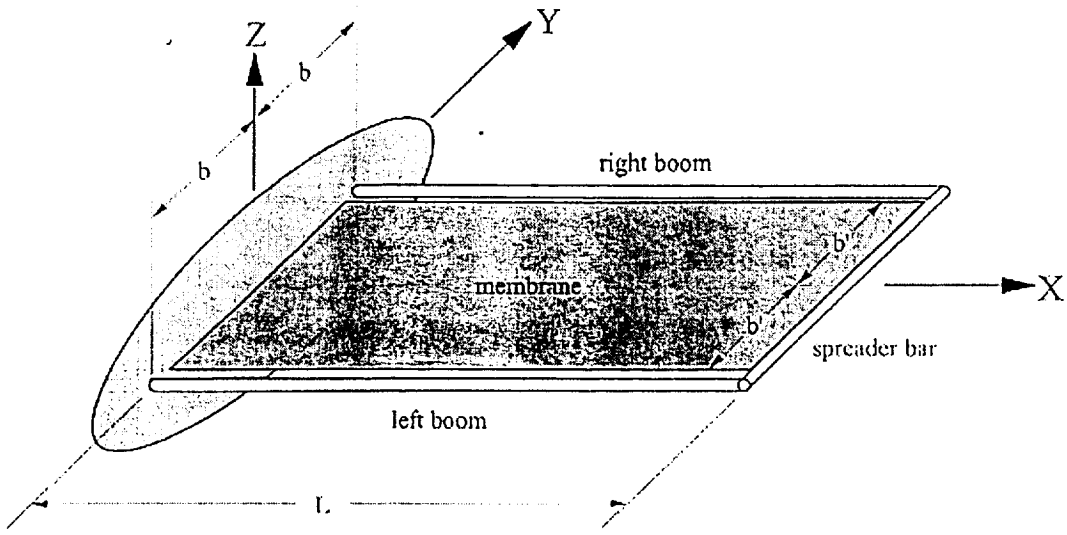

Figure 1.5: Analytical Model of Solar Array

where GJ is the booms torsional rigidity, I_E is the sum of the area moments of inertia and A is the boom cross-sectional area. The coefficient C in equation 1.1 is defined by

$$C = \tan\lambda L - \lambda L \qquad 1.3$$

where λ^2=P/EI and EI is the boom bending stiffness. In equation 1.1, β is

$$\beta^2 = \frac{GJ}{E\Gamma} - \frac{PI_E}{EA\Gamma} \qquad 1.4$$

where $E\Gamma$ is the warping stiffness. Finally the coefficient D, is defined as

$$D = \sinh\beta L - \frac{(1-\cosh\beta L)^2}{\sinh\beta L} - \beta L \qquad 1.5$$

When the properties of the solar array are used in these equations, the predicted torsional buckling load is 14.97 Newtons compared with the 14.80 Newton load imposed on each of the original solar array booms. This comparison provided the catalyst for an experimental study investigating torsional buckling.

1.8 Objective

The basic objective of this thesis is to develop a detailed understanding of the mechanics behind the torsional buckling problem. The means to achieve this objective is an experimental study to demonstrate the phenomena and generate information suitable for comparison to analytical and computational investigations.

1.9 Scope

Chapter 2 begins with a physical description of the Hubble Space Telescope's solar arrays and how they are deployed. Next, a description of the solar array booms is presented along with a history of their behavior. Finally, a description of the solar

array modification is presented. Chapter 3 begins with a description of the test apparatus for a solar array load simulation. Then a preliminary experiment with a model solar array using 1.27 cm diameter closed cross-section aluminum tubes is described. Continuing, a discussion of the model solar array and data acquisition system that was used is presented. This discussion is followed by an outline of test procedures, a summary of test results and a discussion of the results. Chapter 3 ends with the presentation of possible sources of experimental error, a summary of the experiment and finally, a comparison of predicted versus experimental results.

Chapter 4 begins with the presentation of the modifications made to the test rig for an experiment with 2.18 cm diameter BiSTEMs like those used on the Hubble Space Telescope. Continuing, a description of the model solar array and the data acquisition system is presented. Next test procedures and results will be discussed and summarized. Finally, sources of experimental error and a comparison of predicted versus experimental results is presented. Chapter 5 will give a summary of the experiments and the conclusions that can be made as a result. Chapter 5 ends with recommendations for future work as a result of this study.

Chapter 2

Hubble Space Telescope Solar Arrays

The Hubble Space Telescope has two sets of solar arrays, or wings, each set attached 180^0 apart about the circumference of the telescope mounted on the forward shell and light shield. From these solar arrays the power necessary to run the onboard electronics is generated. Without the solar array system functioning properly the mission of the Space Telescope could be compromised severely .

2.1 Solar Array Description

The solar arrays are 12.9 meters in length and 2.9 meters in width. These arrays (Figure 2.1) are made up of two solar cell blankets per wing. The blankets are made from a glass fiber-reinforced Kapton ® and are covered with 47,960 solar cells [8]. Initially, the array performance is rated at 4.52 kW at 34 V and at 70^0 C, then 3.70 kW after five years of service. The blankets are attached at one end to a spreader bar and the other to a stowage drum (Figure 2.2). For storage the blankets are rolled up on the stowage drum which rotates on a central spar. The drum and spar, called the Secondary Deployment Mechanism provide structural support for the deployed solar arrays and the deployment mechanism. The upper and lower blankets and an embossed cushion remain tightly rolled onto the Stowage Drum until they are to be unfurled.

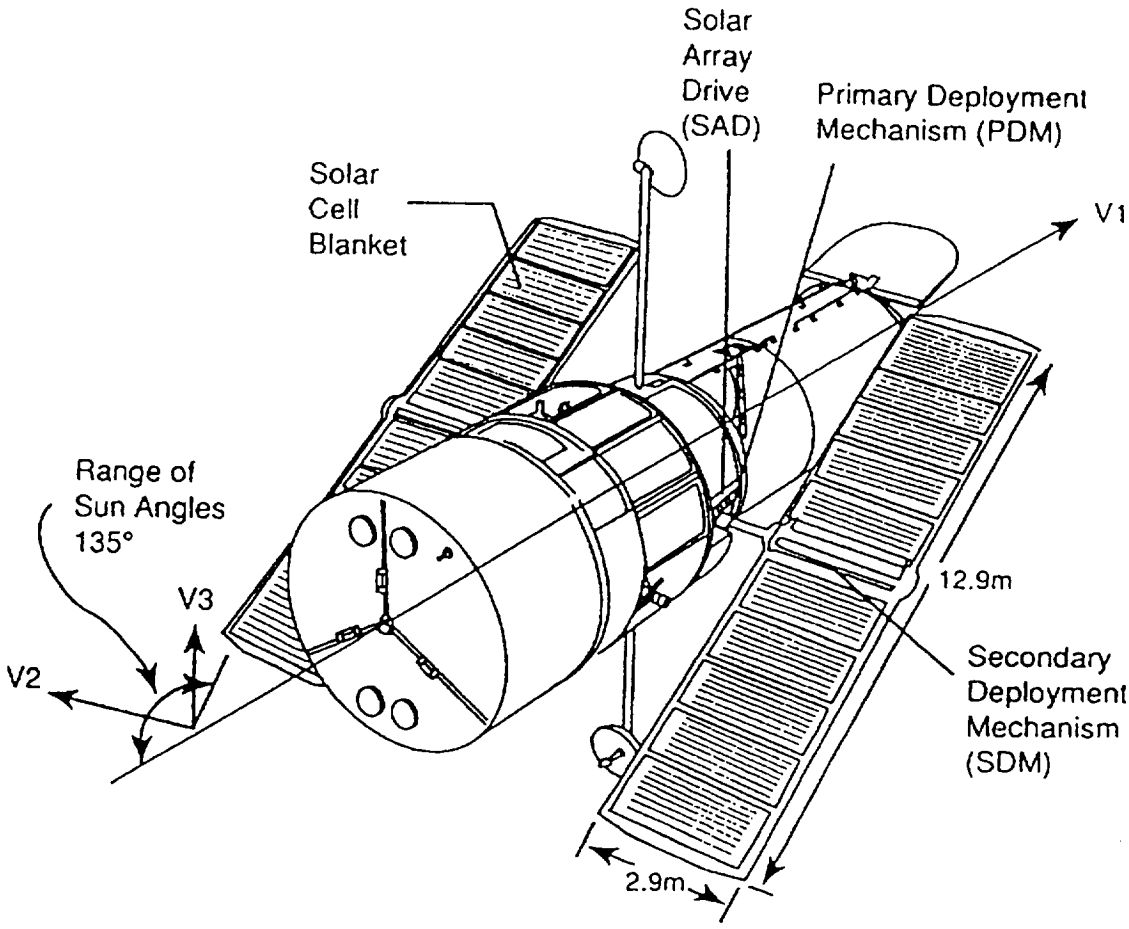

Figure 2.1: Hubble Space Telescope

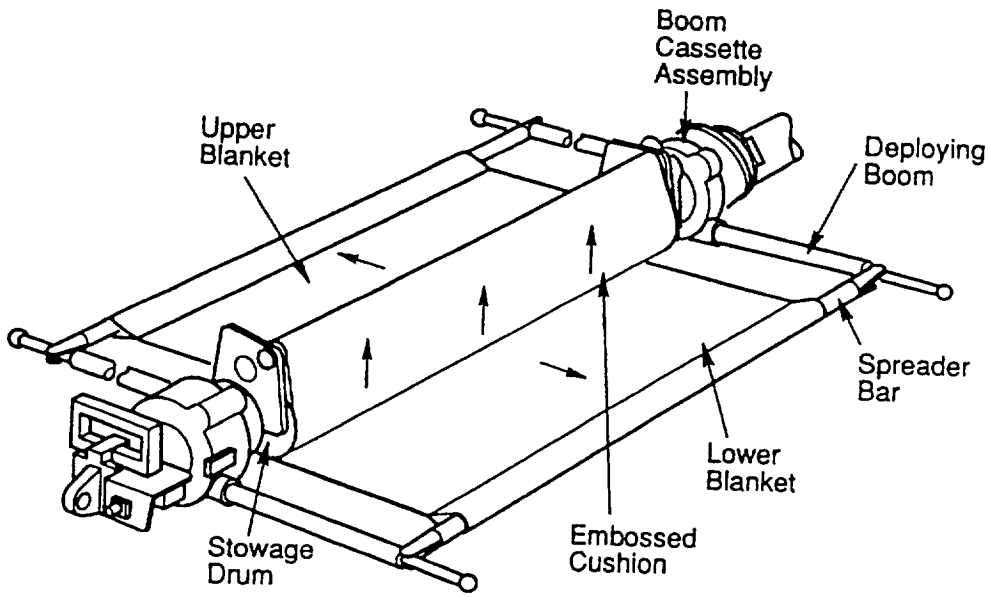

Figure 2.2: Original Solar Array

Once the solar arrays are to be deployed, latches holding the rolled up array assembly to the hull of the telescope are released. The Primary Deployment Mechanism rotates the still rolled up arrays 90^0, thus positioning them on a radius outward from the center of the telescope. Once in this position, the Secondary Deployment Mechanism pushes out the BiSTEMs, connected by the spreader bar and unfurls the solar cell blankets. The blankets being deployed from the stowage drum create an offset from the spreader bar end to the stowage drum (Figure 2.2). When viewed from the side along the axis of the stowage drum, a right triangle is formed with the BiSTEMs being one side, the radius of the stowage drum, 3.56 cm, being another side and finally the solar blanket being the third side, the hypotenuse of the triangle (Figure 2.3).

2.2 BiSTEMs

The primary structural members of the solar arrays are the BiSTEMs. A BiSTEM is constructed of two STEMs, configured during deployment (Figure 2.4) such that one fits inside the other and the gap of the inner STEM is 180^0 rotated from the gap of the outer. This deployed BiSTEM cross section configuration, however, is only fixed at both ends. This means, that between the ends only friction between the contacting surfaces of the inner and outer STEMs prevents them from deforming into a different geometry. When the BiSTEM is stowed (Figure 2.5) each STEM is separated from the other, flattened and rolled up onto a drum. Then during deployment, the drums rotate, similar to that of meshed gears, causing the STEMs to fit one into the other. The energy within the strips induced during their flattening is

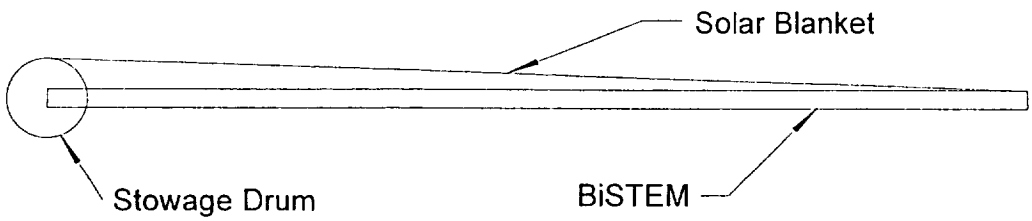

Figure 2.3: Solar Blanket Offset

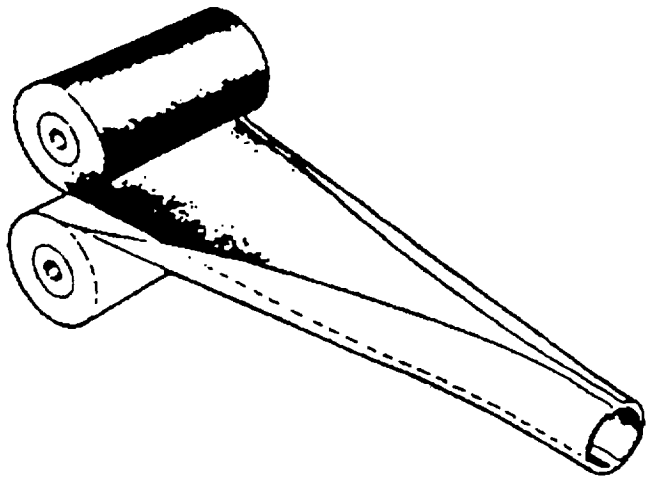

Figure 2.4: BiSTEM

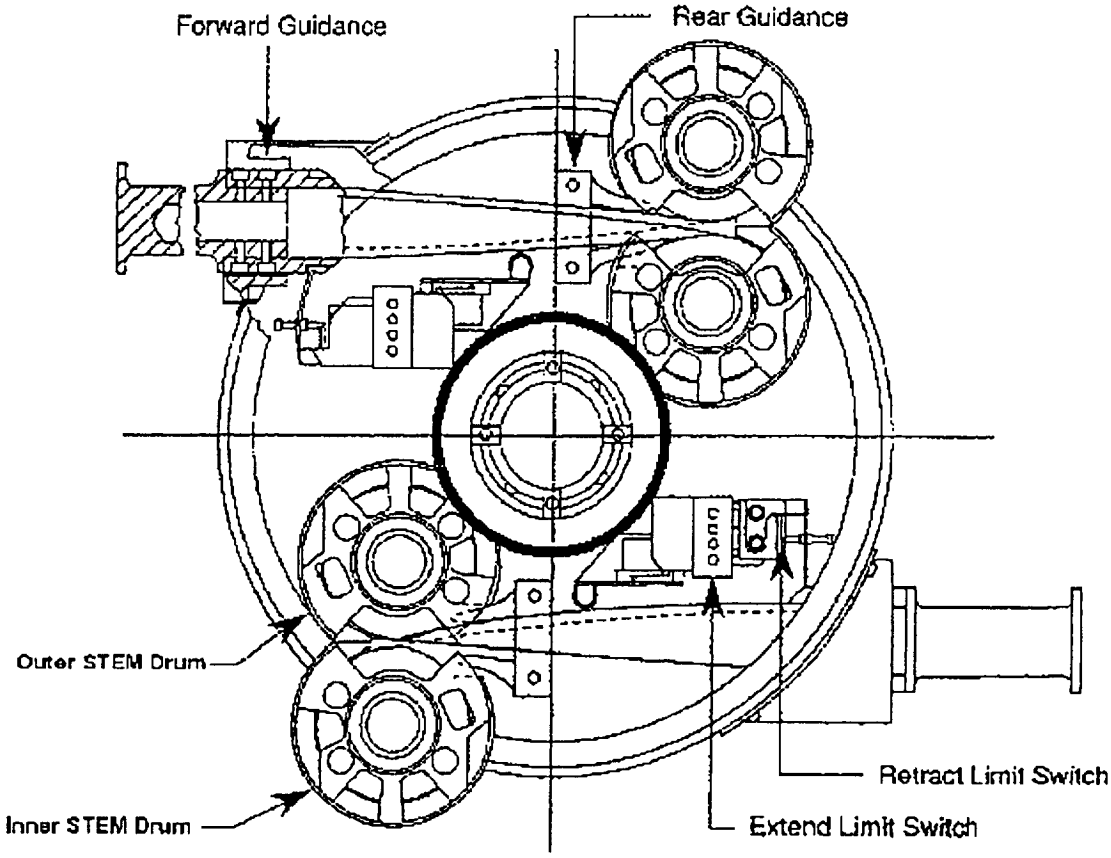

Figure 2.5: Boom Actuator Mechanism

then naturally released allowing the STEMs to assume their nearly circular cross section. The two open cross section tubes forming a BiSTEM act in bending, as if it were a single slender beam. However, in torsion, the BiSTEM reacts as two open cross section tubes, and therefore a BiSTEM has a very low torsional stiffness. From the geometry of the BiSTEM (Figure 2.6) the moments of inertia are [9]:

$$I_{11} = \frac{d^3 t}{8}[\pi + 2(\pi - \sin\alpha\cos\alpha)] \qquad 2.1$$

$$I_{22} = \frac{d^3 t}{8}[\pi + 2(\pi + \sin\alpha\cos\alpha)] \qquad 2.2$$

and from Figure 2.7 the torsional constant is,

$$J = \frac{t^3 R_m \theta}{3} \qquad 2.3$$

where, R_m, in equation 2.3 is the average of the outside radius of the STEM and the inside radius of the STEM, and t is the tube wall thickness. The properties of the Hubble Space Telescope BiSTEMs described in this section are presented in Table 2.1 [9].

Table 2.1: BiSTEM Properties

d	Tube Diameter (cm)	2.18
t	Strip Thickness (cm)	0.013
b_w	Strip Width (cm)	6.35
α	Overlap Angle (rad.)	1.34
A	Cross Section Area (cm^2)	0.16
I_{11}	Moment of Inertia (cm^4)	0.089
I_{22}	Moment of Inertia (cm^4)	0.104
z_{11}	Section Moduli (cm^3)	0.081
z_{22}	Section Moduli (cm^3)	0.0058
EI_{min}	Minimum Bending Stiffness ($N\text{-}m^2$)	171.
EA	Axial Stiffness (N)	3.11E6
GJ	Torsional Rigidity ($N\text{-}m^2$)	0.0065
$E\Gamma$	Warping Stiffness ($N\text{-}m^4$)	0.50

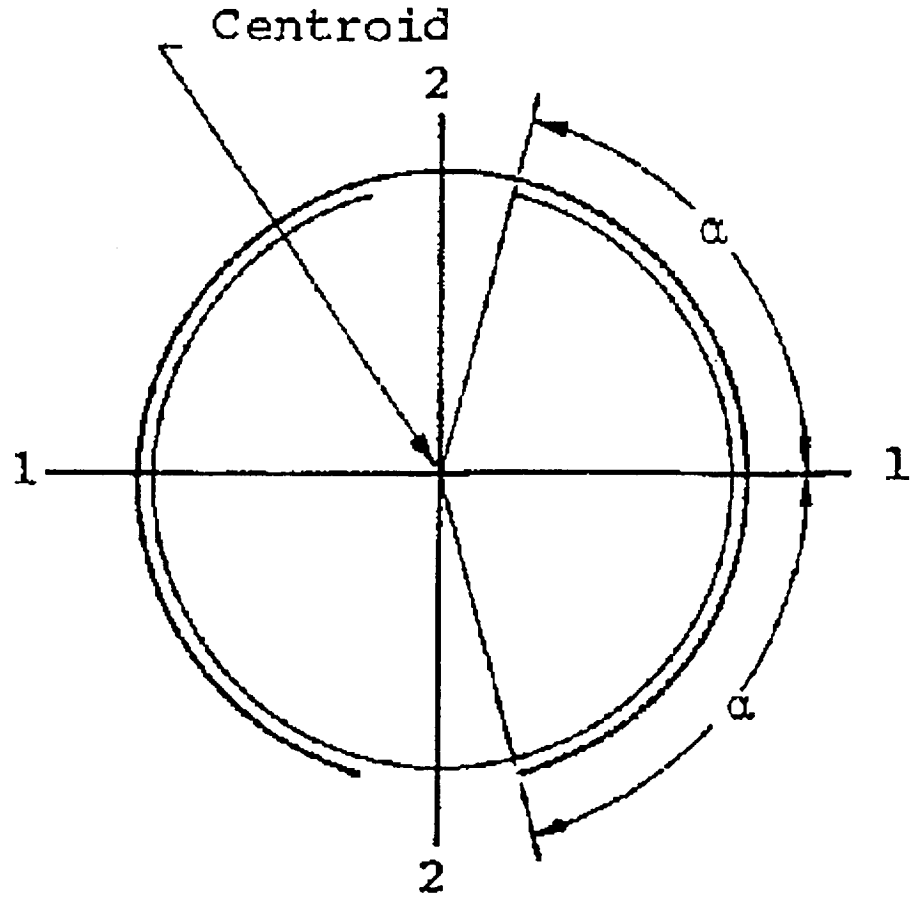

Figure 2.6: BiSTEM Cross Section

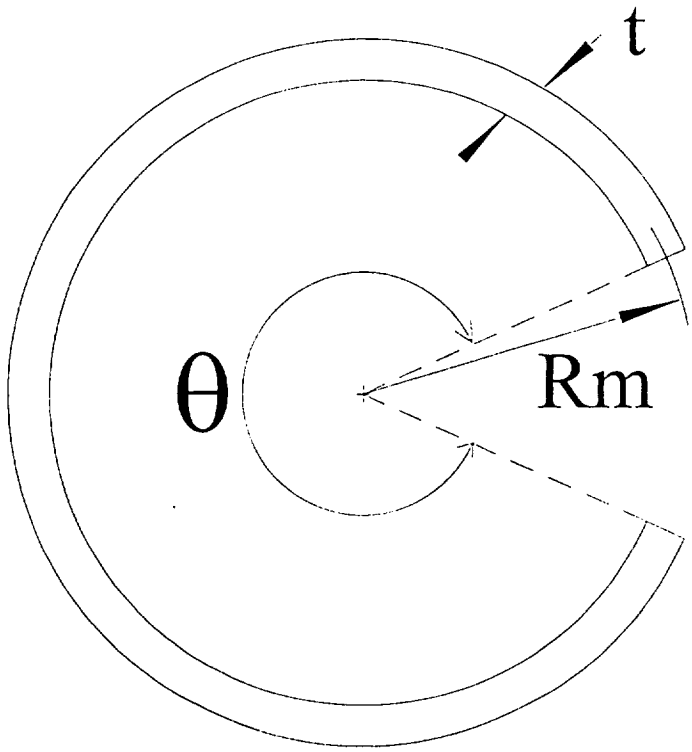

Figure 2.7: Open Cross Section Tube

2.3 Solar Array Modifications

After the Space Telescope was deployed in April of 1990 and the thermally induced vibrations were experienced, the European Space Agency was charged to redesign the solar arrays needed to reduce the BiSTEM bending due to thermal gradients and mitigate any possible damaging vibrations. The BiSTEMs (Figure 2.8) received a cylindrical shaped thermal shielding bellows system covering their entire length. According to ESA tests the thermal gradient across the BiSTEM was reduced by 21 ^{0}C with the addition of the thermal shielding, [3]. To reduce further the chance of a thermally induced vibration, several other systems were modified. The boom actuator mechanism received a brake to prevent the drum from rotating once the solar arrays had been deployed. To compensate for thermal expansion and contraction of the solar blanket a system of springs was attached between the spreader bar and the solar blanket. The spring system, allowing expansion and contraction of the solar blanket ensured a constant tension. To compensate for variations in deployment rate between BiSTEMs attached to the same solar blanket a Teflon ® coated aluminum bellows end condition was attached between the end of the BiSTEM and the spreader bar. Once deployed, the thermally shielded BiSTEMs and blanket tensioning mechanism reduced the temperature gradient from 24 ^{0}C to 3 ^{0}C , and eliminated the thermally induced vibrations, [3].

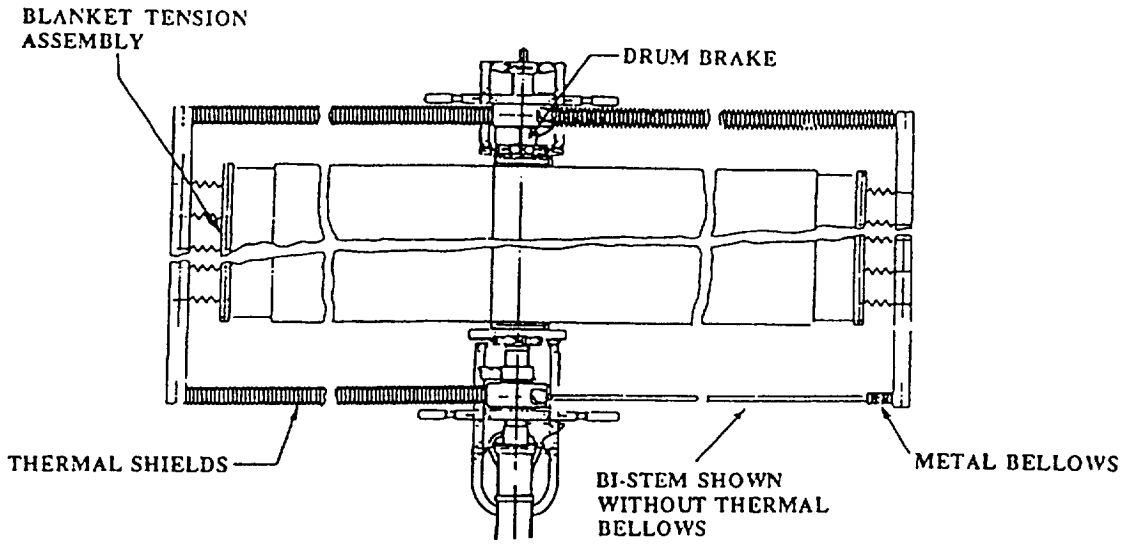

Figure 2.8: Redesigned Solar Array

Chapter 3

Model Solar Array with Closed Cross Section Booms

Because of their unique construction the BiSTEMs used on the Hubble Space Telescope may or may not respond in accordance with predictions of classical beam theory. To serve as a base-line reference this model uses closed cross-section 1.27 cm outside diameter aluminum booms which should correspond closely to classical beam behavior. With the closed-cross section booms, an adequate comparison with predictions for buckling loads based on beam theory should be possible. This chapter presents the experimental program and a summary of the results.

3.1 Objectives

The laboratory experiments presented here were designed to investigate the physical phenomenon of solar array buckling with booms made from closed-cross section tubes. The objective of the experimental study is to characterize: (1) quasi-static behavior of the model solar array in terms of tip deflection as a function of compressive load, and (2) bending strain distribution in the model solar array booms as a function of load.

3.2 Test Fixture

A test fixture was designed and constructed for studying buckling associated with a simulated solar array in the laboratory. The fixture consists of a 2.90m x 1.22m x 1.22m rectangular aluminum frame containing supports for attaching model

solar arrays and a stepper motor/slide mounted on the top (Figure 3.1). Integral to the overall test fixture is a load cell and a plumb bob. The model solar array, consisting of two 1.27 cm aluminum booms, is positioned in the center of the frame along the 1.22 meter depth and each boom is positioned 30.48 cm left and right of the center along the 1.22 meter width. The support conditions for the booms were designed to represent the conditions present in the Hubble Space Telescope solar arrays. The booms are held at their top ends by set screws to an insert/base plate which is bolted to the top plate (Figure 3.2). The top plate is a 1.27 cm thick by 1.22m x 1.22m aluminum plate bolted to the top of the test frame. The lower end of the booms are connected to a bellows end condition which are themselves connected to the lower spreader bar (Figure 3.3). The bellows (Cajon flexible vacuum tubing model number 321-8-x-1) are constructed of two 1.27 cm outside diameter tubes connected by a 2.54 cm long section of corrugated stainless steel tube with an outside diameter of 1.91 cm. The lower spreader bar joins the two booms via their individual bellows end conditions. These end conditions allows the lower spreader bar to translate along the x, y, and z axes while constraining the boom to twist with the lower spreader bar (Figure 3.3). The bellows permits a rotation in the y-z plane, and represents a hinge with zero bending moment. The lower spreader bar is a solid 2.39 cm diameter, 55.88 cm long aluminum rod with 5.08 cm long threaded rods extending outward along the length. A canvas membrane is connected between the upper and lower spreader bars. The upper spreader bar is also a solid 2.39 cm diameter, 55.88 cm long aluminum rod (Figure 3.4). The upper spreader bar has a 11.43 cm long threaded rod screwed into it

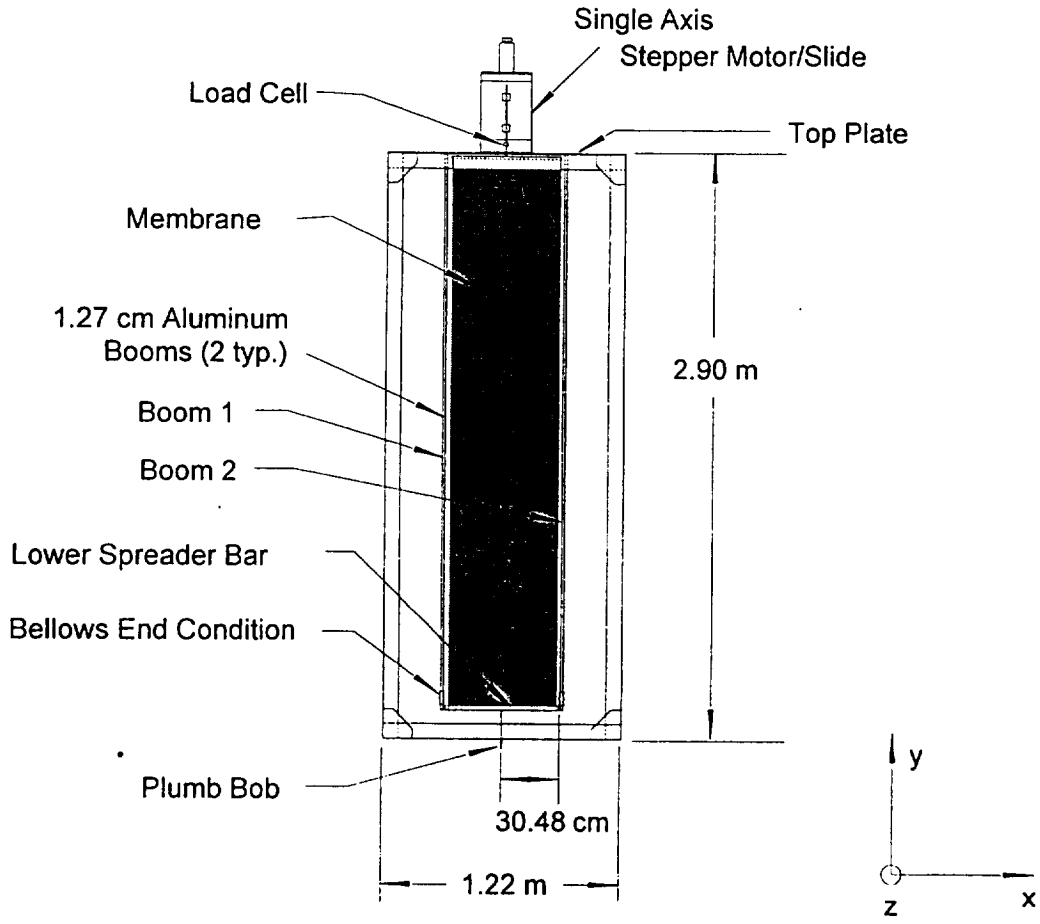

Figure 3.1: Test Fixture and Model Solar Array

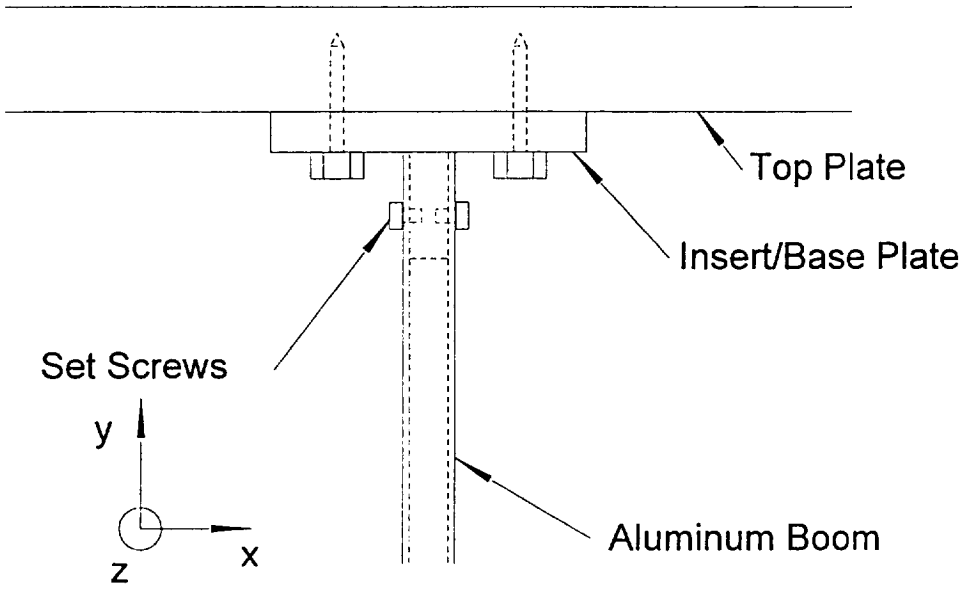

Figure 3.2: Fixed End

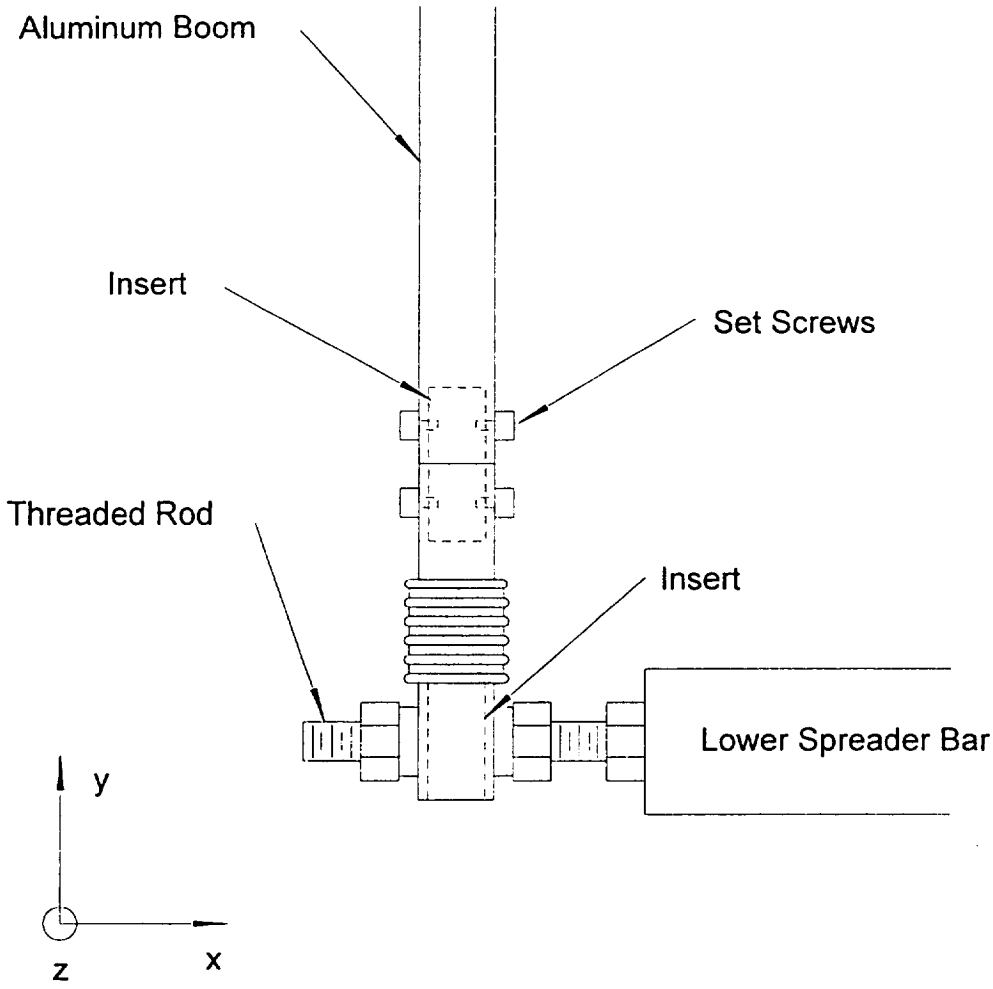

Figure 3.3: Lower End Condition

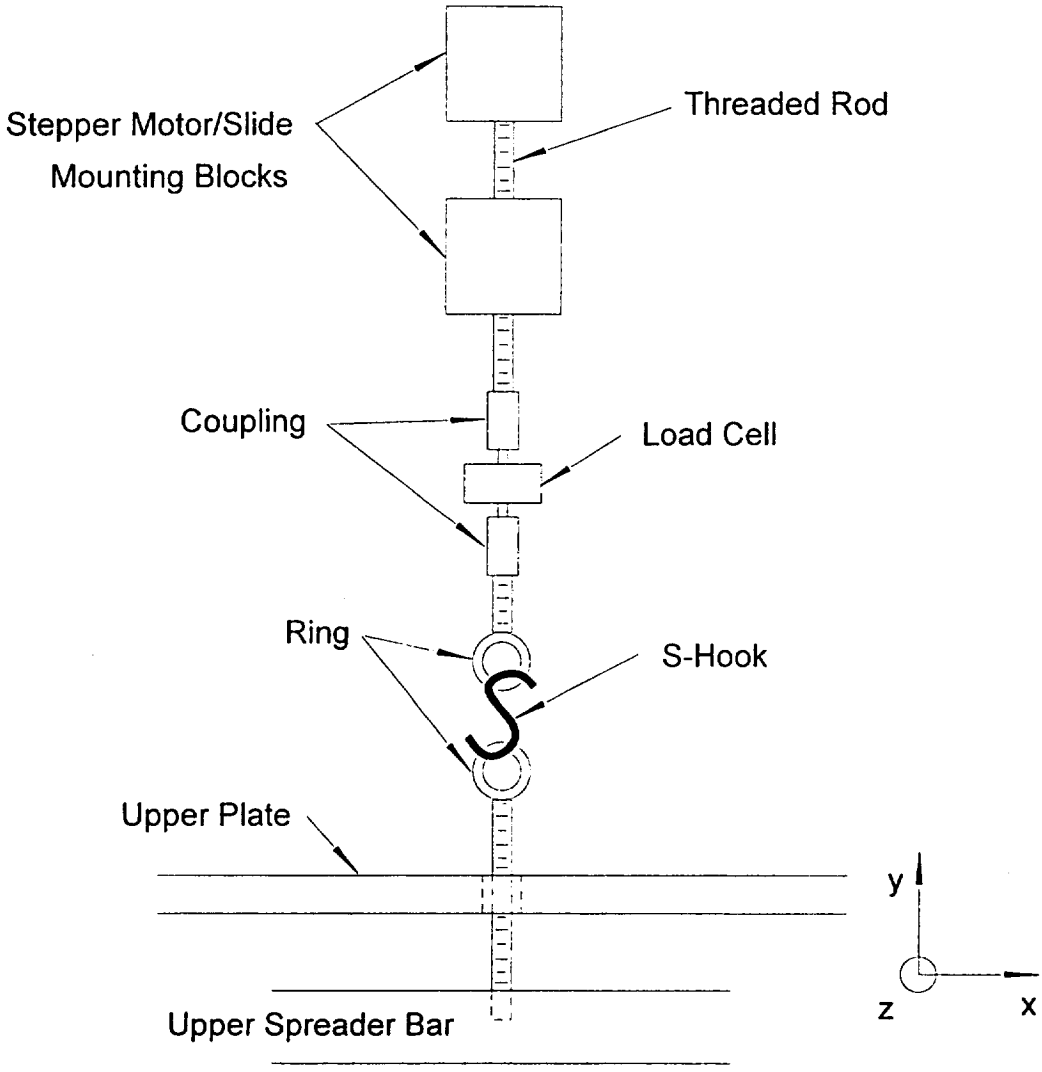

Figure 3.4: Upper Spreader Bar/Stepper Motor/Slide Mount

perpendicularly and centered along its length. The rod and upper spreader bar thus form a tee configuration. Attached to the top of this threaded rod is a ring by which an S - hook couples to another ring connected to the lower mount of an A.L. Design 0 - 444.8 Newton load cell model no. ALD-MINI-UTC-M. This S - hook coupling releases any spurious side loading to the load cell. The upper mount of the load cell is then coupled to a threaded rod which is threaded into the stepper motor/slide mounting blocks which are bolted to the single axis stepper motor/slide. The stepper motor drives a worm gear that controls the linear motion of the 30.48 cm square slide. The slides full range of motion is 15.24 cm along the y axis. Remotely controlled, the stepper motor causes the slide to lift the upper spreader bar thus imparting a tensile load in the membrane and creating a compressive load in the 1.27 cm aluminum booms.

Finally, a plumb bob is attached to the center of the lower spreader bar which points to a linear scale positioned horizontally along the depth and centered along the width of the test frame (Figure 3.5). Once the model solar array is loaded and deflects, the plumb bob indicates the motion of the spreader bar and the booms along the z axis.

3.3 Loading

The compressive load source utilized in this study was generated by the stepper motor/slide (Techno ISEL Inc. Model No. HL31SBM602050005 200mm) coupled to a 2.44 m x 55.88 cm canvas membrane which was attached to the lower spreader bar (Figure 3.6). The stepper motor/slide is operated at 120 volts and is

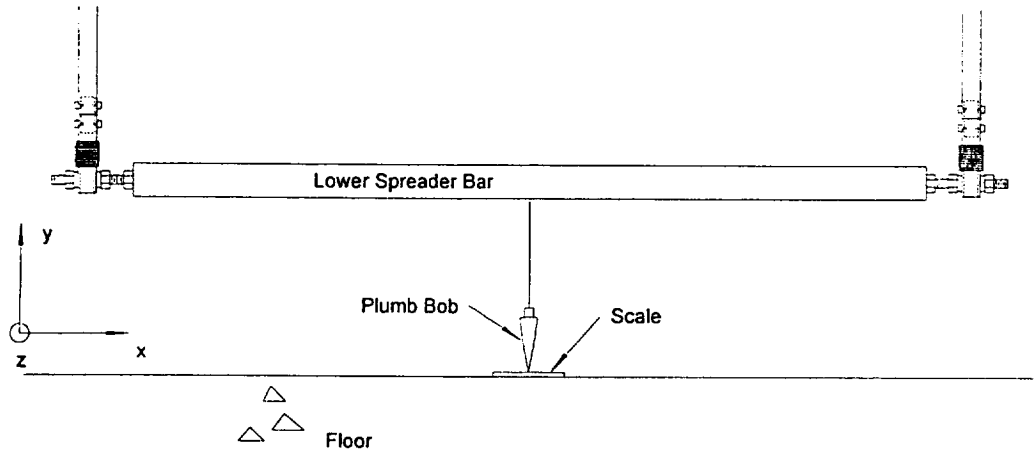

Figure 3.5: Lower Spreader Bar

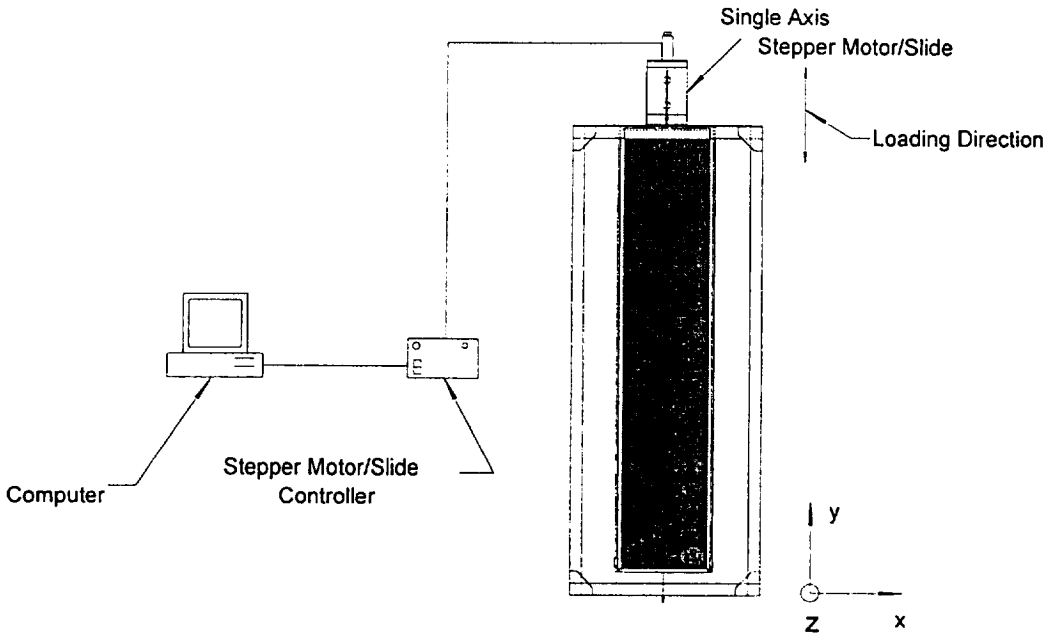

Figure 3.6: Loading

controlled by a MAC 001 controller (Techno ISEL Inc. Model No. H26T55). Programming the motion of the stepper motor/slide via the MAC 001 controller is performed using a Micron P75 computer with MAC 001 resident software. Loading is directed along the y axis of the solar array. An initial 5.08 cm stand-off between the upper spreader bar and the top plate is necessary at the beginning of a test to load the canvas membrane adequately in tension and thus impart a compressive load to the booms. The 5.08 cm stand-off is reduced during loading as the upper spreader bar is lifted along the y axis by the stepper motor/slide.

3.4 Booms

The model solar array buckling test was performed using thin-walled, closed-section 6061 T6 aluminum booms. The booms are 2.63 meters in length, L, with a 1.27 cm outside diameter and have a wall thickness of 0.089 cm. Booms 1 and 2 each have a Poisson's full bridge located 25.55 cm up from the lower spreader bar along the y axis. The full bridge consists of four Micro Measurements Inc. type CEA-13-125UT-350 gauges. Two gauges rotated 90 degrees one from the other are attached to one backing. Therefore, there are two backings for each full bridge. The two backings are bonded at 180 degree increments around the circumference of the boom. This configuration makes up one full bridge. The full bridges report the axial strain imparted to their respective boom, Figure 3.7.

Boom 1 was also instrumented with a pattern of eight channels of half bridges. Each half bridge consists of two gages. This decision to instrument only one beam fully was based on preliminary tests that showed the axial strain gages on either boom

reporting the same strain values for a given load, and the booms to be bending symmetrically. Figure 3.7 shows boom 1 identifying strain gage locations relative to the top fixed end condition. Boom 1 bending strains are monitored using Micro Measurements Inc. type WK-06-125AD-350 strain gauges. The two strain gages that form a half bridge were bonded at 180 degree increments around the circumference of the boom. Each wired half bridge makes up one channel. Signals from the strain gauges on the booms are fed to a data acquisition system.

3.5 Data Acquisition

The strain gauge data was collected using the Micro Measurements System 4000 data acquisition system. The load signal was measured using a Fluke 8026B multimeter. The Micro Measurements System 4000 system allows for data to be acquired, displayed and recorded during test runs. Due to the quasi-static nature of the experiment, incrementally loading the model solar array and waiting for a steady state configuration, the load data could be input into a spread sheet which would later be meshed with the strain data. Data files of strain information were then post-processed, joining them with the spread sheet containing the load information. A schematic of the data acquisition system utilized in the experiments is presented in Figure 3.8.

3.6 Test Procedures

Four tests were conducted using the model solar array and are outlined in Table 3.1.

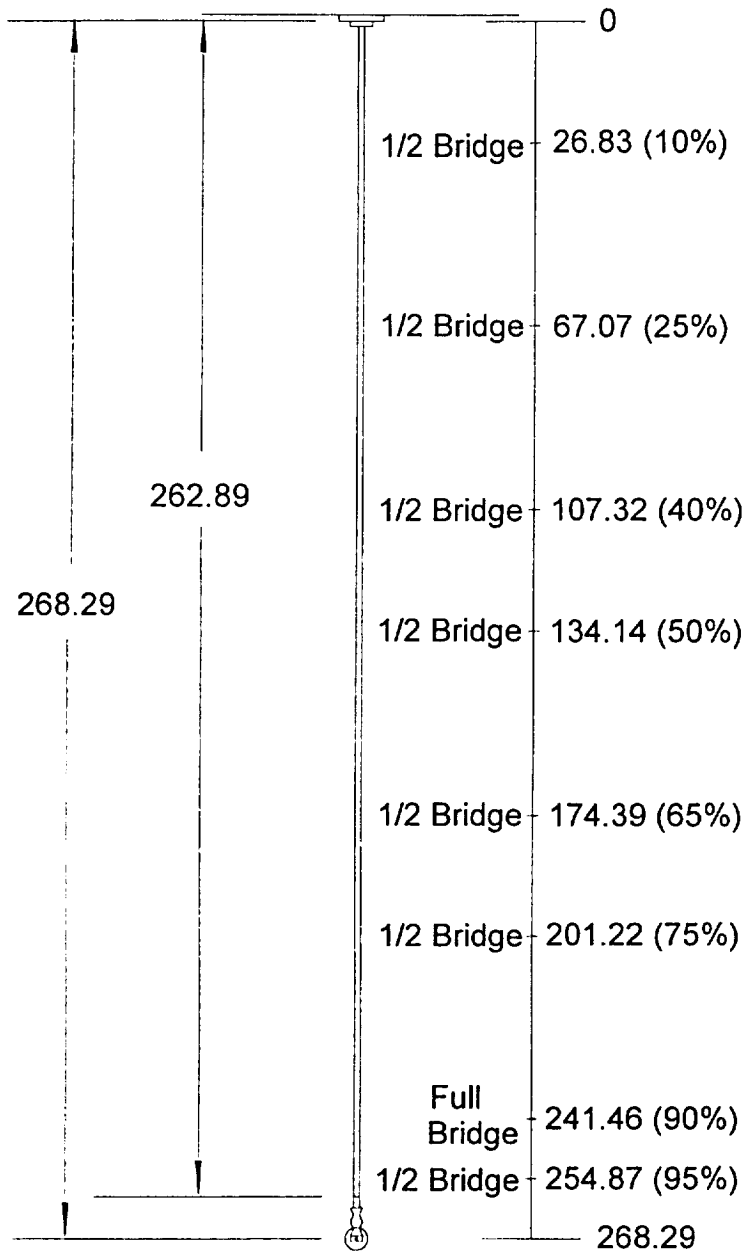

Figure 3.7: Boom 1 Strain Gauge Locations

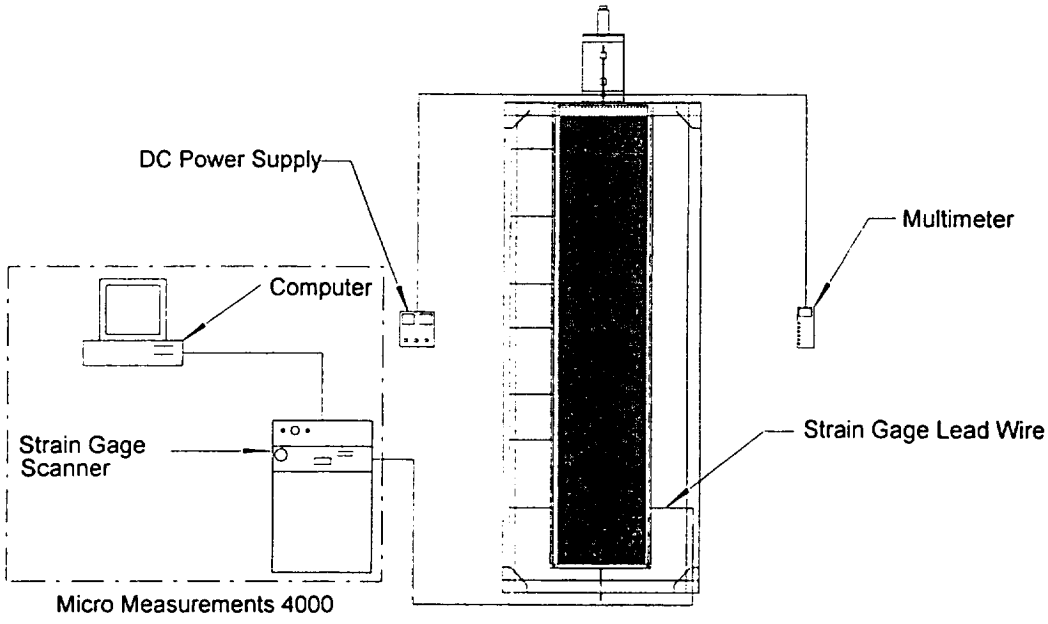

Figure 3.8: Data Acquisition

Table 3.1: Tests Conducted with Closed Cross-Section Booms

Test	Purpose
1	Determine axial strain as a function of applied vertical load.
2	Determine the bending strain distribution along boom 1 as a function of an applied horizontal load.
3	Characterize the buckling behavior of the model solar array with applied compressive load.
4	Determine fundamental bending vibration frequency as a function of boom compressive load.

3.6.1 Test Procedures: Tests 1 and 2

Test 1 determines the axial strain as a function of an applied vertical load, F. The vertical load, F, is the force in each boom caused by the weights shown in Figure 3.9. This test used the test apparatus described earlier in section 3.2 modified to support vertical weights. A 0.152 cm diameter steel rod was inserted through each boom at a distance 7.62 cm above the lower spreader bar. String was tied to either end of the 0.152 cm steel rods to form a loop which would support weights attached via S-hooks.

Using the test apparatus shown in Figure 3.9 with a no load condition, and a slack membrane, the strain gages were zeroed and calibrated with the Micro Measurement System 4000 resident software. An equal amount of weight was attached to both booms via the S-hooks and the axial strain values were recorded with the System 4000. More weight was added, evenly distributed between the booms and again the strain values were recorded. The process of adding equal amounts of weight to each boom and recording the strain data continued over the test regime, thus the force, F, applied to each boom varied from 0-124.5 Newtons.

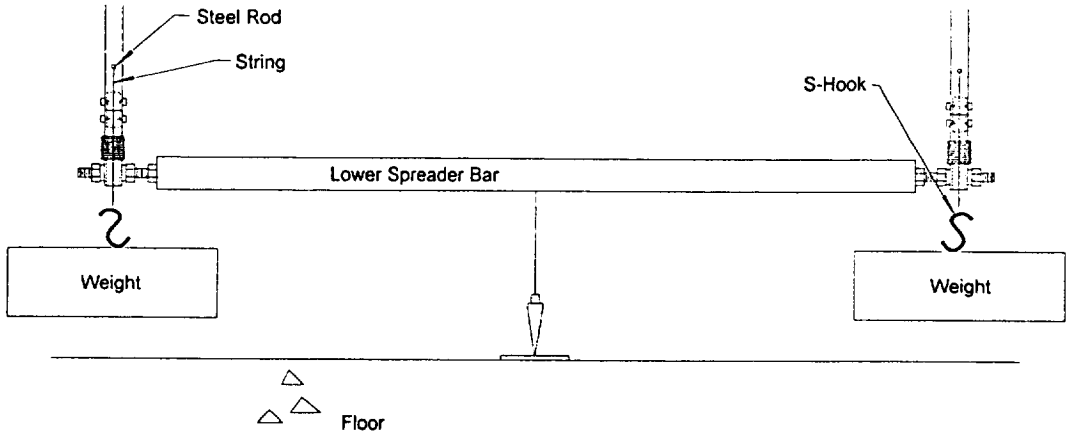

Figure 3.9: Test 1 vertical loading

Test 2 determined the bending strain distribution along the booms length as a function of an applied horizontal load. The test apparatus outlined in section 3.2 was again used with a single weight to apply a horizontal force, (figure 3.10). For this case, string was tied to both ends of the lower spreader bar to form a large loop. Approximately 0.91 m in front of the lower spreader bar was a pulley fixed in position by a portable vise. An S-hook, connected to the loop at the lower spreader bar, was attached to a string that went through the pulley and extended vertically towards the floor. The weight was attached to this end of the string via a second S-hook.

Using the test apparatus shown in Figure 3.10 and a no load condition, the strain gages were zeroed and calibrated with the Micro Measurements System 4000 resident software. The weight was attached to the S-hook hanging from the pulley and the strain data was recorded with the System 4000. The process of adding weight and recording strain data continued over the test regime, 0-9.68 Newtons.

3.6.2 Test Procedures: Tests 3 and 4

Tests 3 and 4 characterized the buckling behavior of the model solar array. Using the test apparatus shown in Figure 3.1 and a no load condition, the strain gages were zeroed and calibrated with the System 4000 resident software. The upper spreader bar was lifted using the stepper motor/slide. This action put the membrane in tension and imparted a compressive load to both booms. The bending and axial strain were then recorded using the System 4000, and the load cell value was noted in

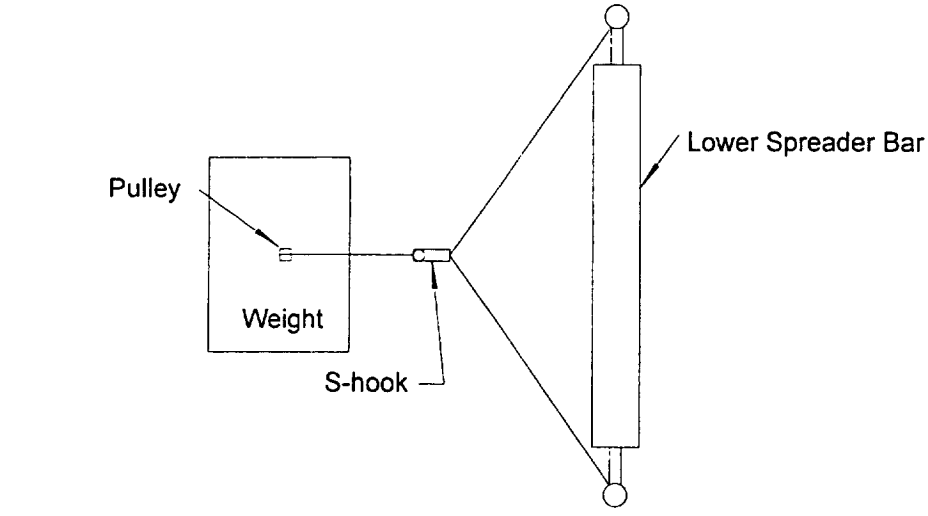

Top View

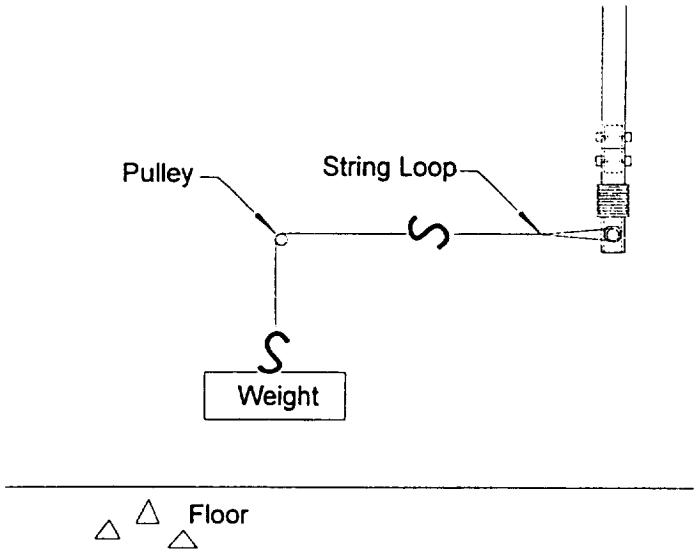

Side View

Figure 3.10: Test 2 horizontal loading

a log book. The load was then increased using the stepper motor/slide and the strain data and load cell value was recorded. This process of loading the model solar array and recording strain and load data continued over the test regime, 0-124.5 Newtons.

Test 4 also used the test apparatus shown in Figure 3.1 with the addition of a laser displacement sensor which monitored the movement along the z axis of the lower spreader bar, Figure 3.11. The laser displacement sensor output signal was read by a DAS-8 analog to digital card within the Micron P75 computer which was then displayed by Labtech Notebook. Test 4 started with the membrane in tension which imparted a compressive load to the booms. The booms were then deflected initially in bending by moving the lower spreader bar along the z axis. The lower spreader bar was then released and its vibratory motion was recorded by the laser displacement sensor. This motion was similar to that of a playground swing with both booms moving together in flexure. Once an adequate motion sample had been recorded the lower spreader bar was stopped. The boom's compressive load was increased by increasing the tensile load in the membrane. The lower spreader bar was again displaced along the z axis, released and again the motion was recorded by the laser displacement sensor. The process of increasing the load, moving the spreader bar, releasing it and recording its motion continued over the test regime, 0-124.5 Newtons.

3.7 Data Reduction

Tests 1-3 were each conducted three times. The repetition was done to insure the data was repeatable. Tables 3.2-3.4 are presented as sample data that is representative of the data taken for those tests. By inspection of each data set in each

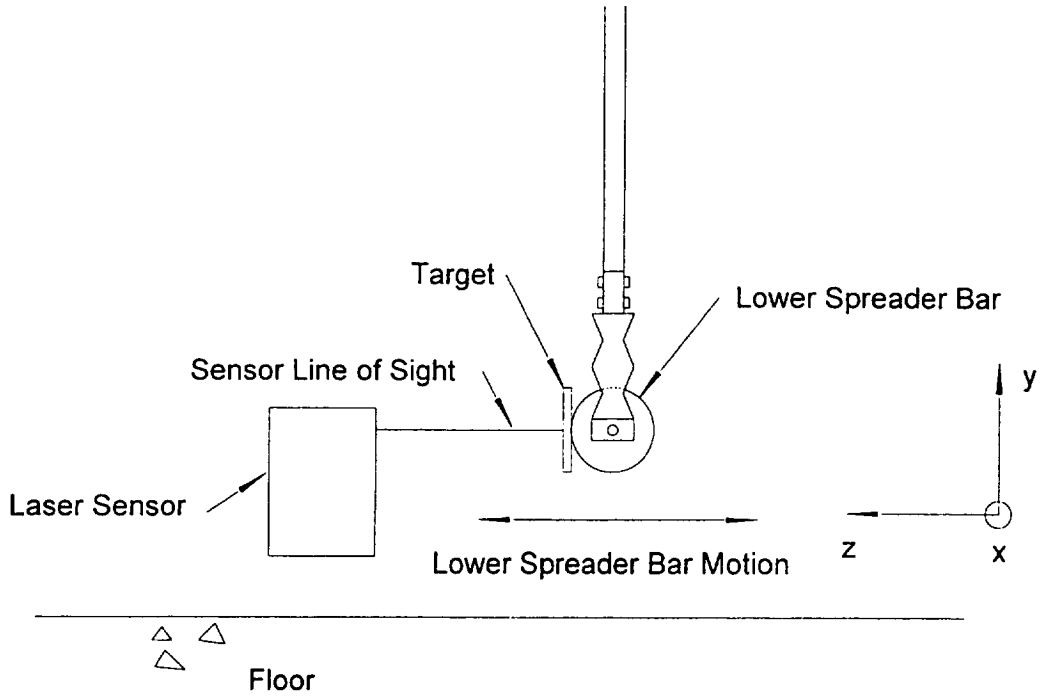

Figure 3.11: Test 4 bending vibrations

of tests 1-3 it was concluded that the data is repeatable. Test 4 frequency data, presented in Table 3.5, is the average period of three displacement cycles of the lower spreader bar. This method of reduction was used because the frequency value of the individual periods were within 1% of each other. Therefore, the data for Test 4 was repeatable.

Table 3.2 summarizes axial strain, ε_a , versus vertical load F for Test 1. The vertical load data is the amount of weight suspended from each boom. The two columns of axial strain data reported as, ε_{a1}, and ,ε_{a2}, represent the axial strain in each boom. The axial strain values are an average of the gages mounted 180 degrees around the circumference of the boom.

Table 3.3 summarizes bending strain, ε_b, versus horizontal load , F_h for Test 2. The horizontal load data is the total weight suspended from the S-hooks acting on both booms. The bending strain data is the average of the absolute values of strain from each half bridge.

Table 3.4 summarizes the bending strain distribution, ε_b, versus compressive load, P for Test 3. The compressive load data is the total force exerted on the model solar array reported by the load cell. The portion of the reported load that is caused by the upper, and lower spreader bars, membrane, booms and retaining hardware such as screws are subtracted thus leaving the total amount of load acting on both booms, Figure 3.12. The bending strain data is the average of the absolute values of strain from each half bridge. Table 3.5 summarizes the fundamental bending frequency variation with the applied load. The frequency data was calculated using the average

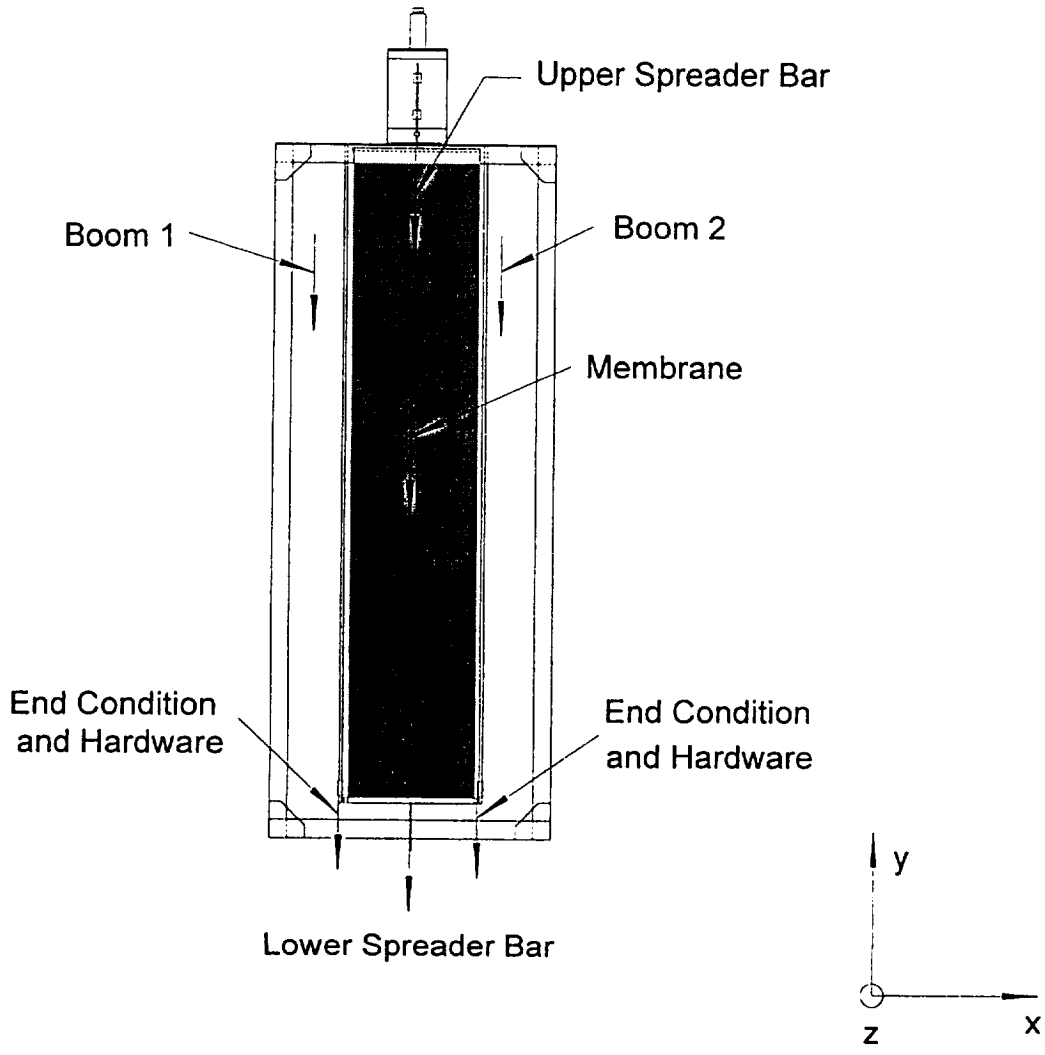

Figure 3.12: Weights acting on load cell

period of three displacement cycles of the lower spreader bar. The compressive load data for test 4 was processed using the same methodology as test 3.

Table 3.2: Test 1, Axial Strain vs. Vertical Load

Load (N) *	ε_{a1} (με)	ε_{a2} (με)
0	0	0
17.79	3	3
44.48	6	6
62.27	8	9
80.06	11	10
97.86	13	13
124.54	16	17

* Load in each boom

Table 3.3: Test 2, Bending Strain vs. Horizontal Load

Horizontal Load (N) *	4.98	5.96	6.94	7.92	9.68
Gauge Location (cm)	ε_b (με)	ε_b (με)	ε_b (με)	ε_b (με)	ε_b (με)
26.82	584	618	708	828	927
67.31	465	491	562	656	734
107.65	369	390	445	519	580
134.47	314	332	379	441	492
174.78	214	226	258	300	334
201.78	152	160	182	212	236
255.42	31	32	37	42	47

* Total load applied to two booms

Table 3.4: Test 3, Bending Strain Distribution

Compressive Load (N) *	109.29	111.42	113.56	115.69	117.83
Gauge Location (cm)	ε_b (με)	ε_b (με)	ε_b (με)	ε_b (με)	ε_b (με)
26.82	52	50	54	71	69
67.31	234	275	345	488	614
107.65	363	431	547	782	1008
134.47	406	482	616	886	1157
174.78	360	431	553	800	1054
201.78	282	338	436	633	839
255.42	51	63	84	119	163

* Total load applied to two booms

Table 3.5: Test 4, Frequency Distribution

Load (N) *	Frequency (hz)
8.94	0.52
19.6	0.52
34.6	0.50
53.8	0.46
62.3	0.44
75.1	0.40
92.2	0.35
109.	0.29
117.	0.29
124.	0.41
128.	0.58
130.	0.67

*Total load applied to two booms

3.8.1 Discussion of Results, Tests 1 and 2

Tests 1 and 2 results are presented in Figures 3.13 and 3.14 respectively each showing a least squares linear curve fit for the data. Figure 3.13 represents the relationship between the axial strain and the weight hung from the ends of the booms. The scatter reported in the axial strain, ε_a, is attributed to the inability of the strain gauges to resolve the very small signals. The relationship described by this graph is linear, that is if we increase the weight hung from the booms the axial strain will also increase by a constant factor. This relationship provides one positive check in determining the validity of the test apparatus.

Figure 3.14 represents the relationship between the horizontal load and the bending strain at gauge location 1 near the fixed end, (Figure 3.7). The relationship described by this graph is also linear. Increasing the horizontal load at the free end forces the tips of the booms to bend away from their static position in the direction of

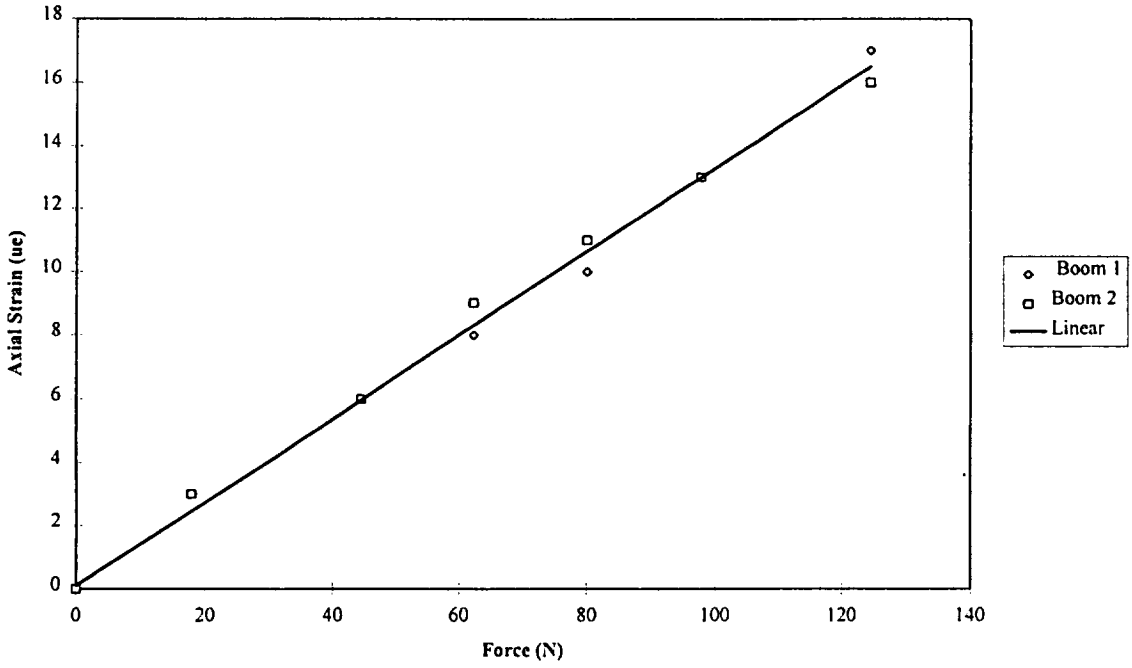

Figure 3.13: Test 1 vertical load-axial strain

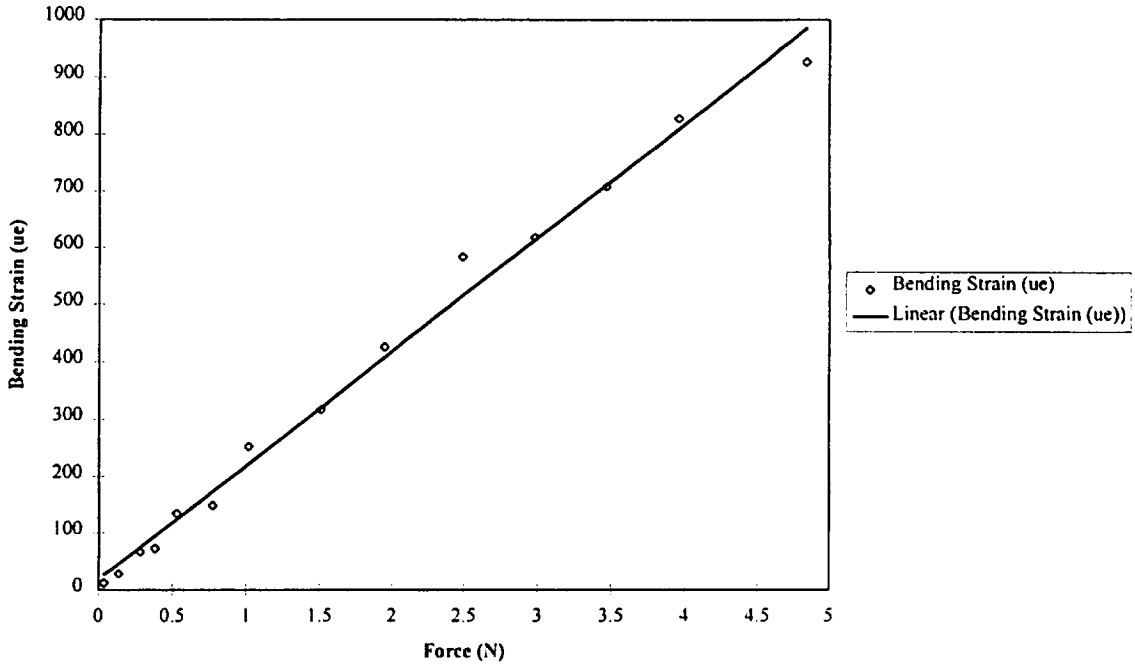

Figure 3.14: Test 2 bending strain at gage location 1

the applied horizontal load. This increased bending provides increased bending strain, again this relationship provides further assurance the test apparatus is functioning properly. Here it is worthy to note that the bending strains are much larger than the axial strain previously shown.

3.8.2 Discussion of Results, Tests 3 and 4

The results for test 3 are presented in figures 3.15 and 3.16. Figure 3.15 represents the relationship between the bending strain distribution at the strain gage channels for boom 1 for increasing loads applied by the membrane. Also shown in Figure 3.15 are polynomial curve fitting lines for each set of data corresponding to a load. The polynomial equations are second order. The relationship shows three significant details. First, near either end of the booms the values for the bending strain are at their minimums and approach zero. Second, the maximum value for the bending strain occurs near the center of the booms' length. Finally, with increasing compressive load imparted to the booms the overall bending strains increase.

Figure 3.16 shows the relationship between the maximum bending strain values at the center of the boom length from each curve of Figure 3.15 and the corresponding compressive load on boom 1. There are two significant results from this graph. The first is the boom force approaches an asymptote near 115-120 Newtons. Second, with increasing load, the bending strain increases nonlinearly as the force approaches the horizontal asymptote.

The results for test 4 are presented in Figure 3.17. Figure 3.17 represents data showing the relationship between the bending frequency and the total applied

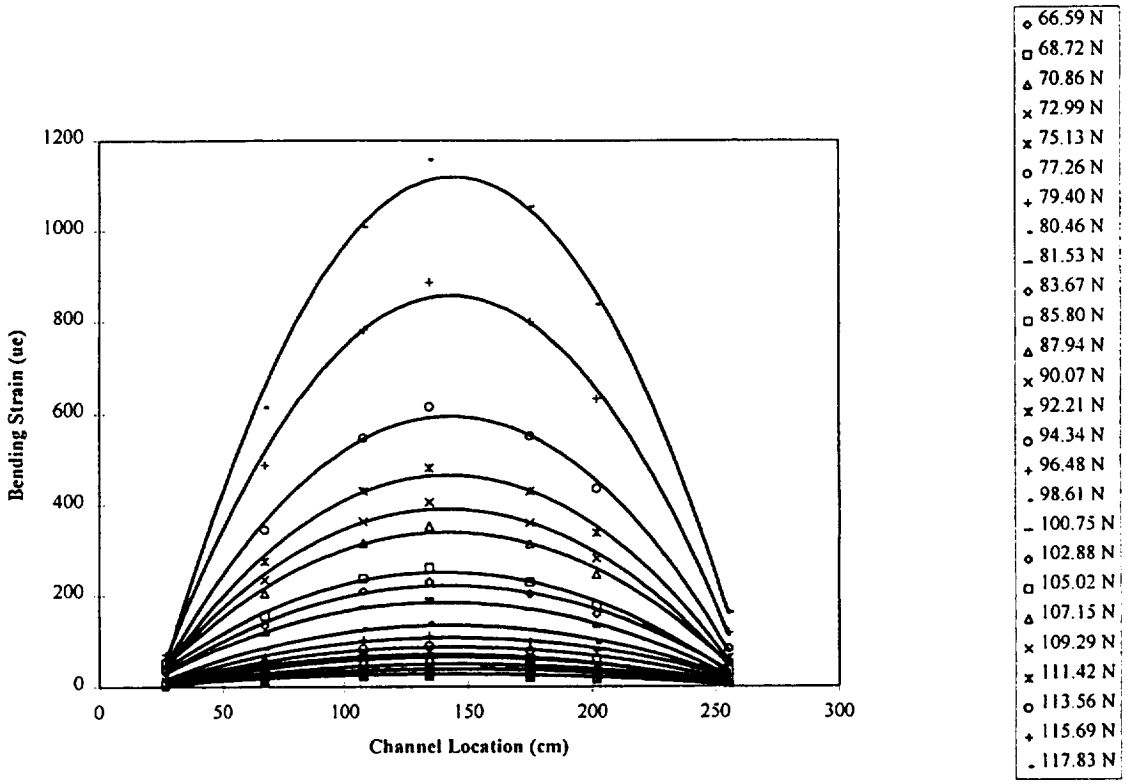

Figure 3.15: Test 3 bending strain profiles

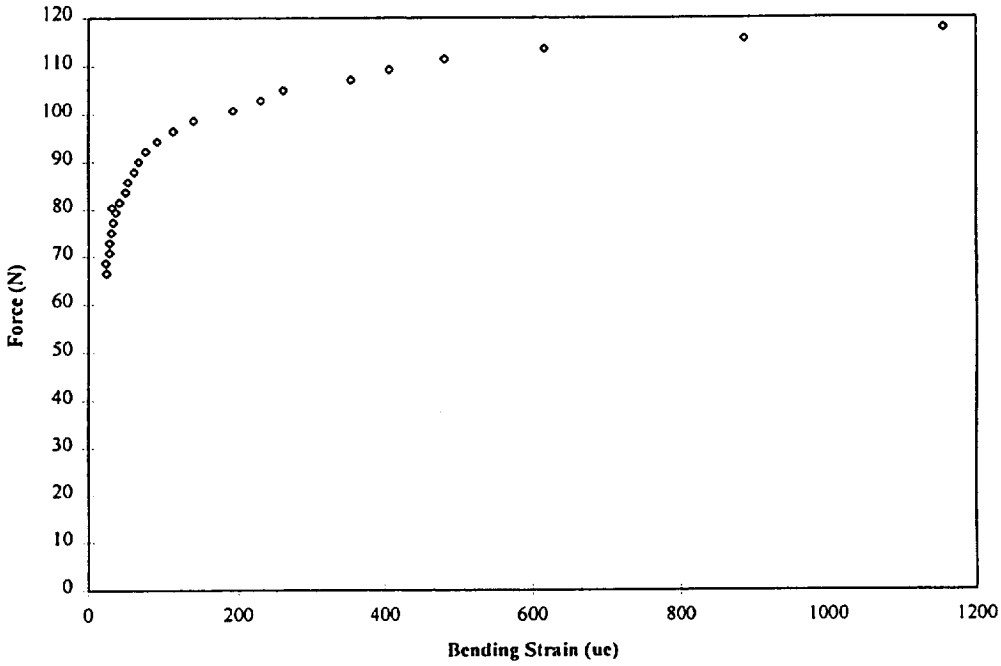

Figure 3.16: Test 3 maximum bending strain

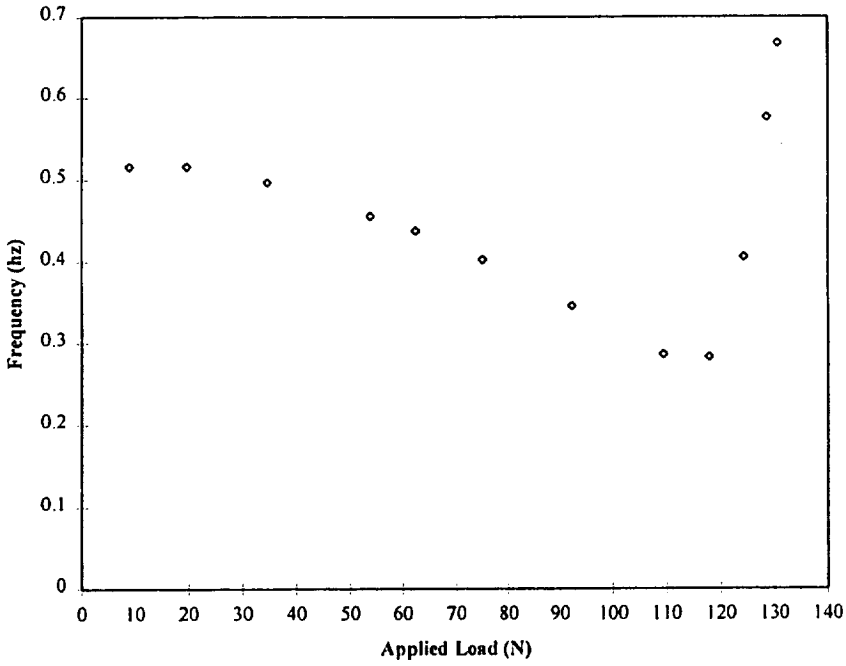

Figure 3.17: Test 4 bending vibration frequency versus applied load

compressive load applied to both booms. This graph shows two significant details. First, as the compressive load is increased, the bending vibration frequency decreases. Second, there is a distinct minimum in the curve at an applied force of about 115 Newtons. According to classical beam theory, the vibration frequency approaches zero as the load approaches the buckling load. This result did not occur in the experiment because nonlinear effects began to dominate, instead the frequency approached a minimum value. At the minimum frequency, the applied force of 115 N is the estimated buckling force. After this minimum with an increase in compressive load the frequency value increases.

3.9 Experimental Error

The sources of error for this experiment consist of those associated with the strain gauges, load cell, laser sensor and the data acquisition system. The strain gauges used to detect bending strain were the Micro Measurements WK-06-125AD-350 with a gage factor error of 2.02 +/- 1.0% (24^0 C) which correlates to a strain error of 600 με +/- 6 με. The strain gauges used to detect axial strain were the Micro Measurements CEA-13-125UT-350 with a gauge factor error of 2.16 +/- 1.0% (24^0 C) which correlates to a strain error of 10 με +/- 0.1 με. The data acquisition system was equipped with a 4270A Micro Measurements strain gauge scanner. Shunt calibration was performed using an installed calibrated resistor. The Micro Measurement software was configured to calibrate and zero channels. The resolution of the 4270A scanner was 1με with a drift of +/- 3με after operating at 23.89 ^{0} C, [10]. The load cell used to detect the tensile load imparted to the membrane was an A.L. Design

ALD-MINI-UTC-M-100 with an error of 20 mV +/- 0.04 mV F.S. The load cell signal was read by a Fluke 8026B Digital Multimeter with an error of +/- 200 mV +/- 0.1% of reading + 1 digit. Therefor a reading of 4 mV has an error of +/- 1.004 mV. The laser sensor used to detect the linear displacement of the lower spreader bar was a Keyence LB-11/LB-70. The signal from the displacement sensor was sent through a Keithley Metrabyte DAS-8 analog to digital card then displayed by Labtech Notebook via a Micron P75 computer. The error associated with the displacement sensor is 1.6% of full scale, and the error of the DAS-8 card is +/- 0.01% (of reading) plus +/- 1 bit. The error for the buckling load was calculated using the root mean square method. The error associated with the flexural buckling is +/- 0.46 Newtons.

3.10 Comparison of Experiment and Analysis

The results from tests 1 - 4 are compared with fundamental mechanics of material analyses.

3.10.1 Tests 1 and 2

The axial strain, ε_a, versus vertical load, F, results, Figure 3.13 produced a linear relationship where the slope of the fitted straight line is $\varepsilon_a/F = 0.13\ \mu\varepsilon/N$.

From strength of materials,

$$\sigma = \frac{F}{A} \qquad 3.1$$

where, σ, in equation 3.1 is the stress in the boom and, A, is the cross sectional area of the boom. From Hooke's law,

$$\varepsilon_a = \frac{\sigma}{E} \qquad 3.2$$

where, E, in equation 3.2 is the modulus of elasticity for the boom material.

Combining equations 3.1 and 3.2 gives,

$$\frac{\varepsilon_a}{F} = \frac{1}{EA} \qquad 3.3$$

Using data supplied by Reynolds Metals, Table 3.6, the boom manufacturer, Tull Metals, the supplier, and fundamental strength of materials analyses [11] the relationship of axial strain versus vertical load is predicted to be $\varepsilon_a/F = 0.115\ \mu\varepsilon/N$.

Table 3.6: Boom Properties

a	241.46 cm
L	262.89 cm
I	0.0578 cm^4
r_o	0.64 cm
r_i	0.55 cm
E	69E9 Pa

The absolute percent difference between experimental and predicted values is 13%. The relatively high percent difference between experimental and predicted is due to the very small strain values encountered in the experiment.

The bending strain versus horizontal load, Figure 3.14, also produced a linear relationship where the slope of the fitted straight line is $\varepsilon_b/F_h = 199.57\ \mu\varepsilon/N$.

From mechanics of materials,

$$M = \frac{F_h}{2} a \qquad 3.4$$

Figure 3.18 illustrates that, M, is the applied moment to each boom from the horizontal load, $F_h/2$, acting over a length of, a. Figure 3.18 also illustrates that, r_o, is the boom outside radius. The stress in the boom, σ , is,

$$\sigma = \frac{Mr_o}{I} \qquad 3.5$$

where, I, in equation 3.5 is the moment of inertia. From Hooke's law,

$$\varepsilon_b = \frac{\sigma}{E} \qquad 3.6$$

where, E, in equation 3.6 is the modulus of elasticity. Combining equations 3.5 and 3.6 gives,

$$\frac{\varepsilon_b}{F_h} = \frac{ar_o}{2EI} \qquad 3.7$$

where,

$$I = \frac{\pi}{4}(r_0^4 - r_i^4) \qquad 3.8$$

and, r_i, is the boom's inside radius. Using data shown in, Table 3.6, the relationships of bending strain versus horizontal load is predicted to be ε_b/F_h = 192.74 $\mu\varepsilon$/N. The difference for this relationship between experimental and predicted values is 3%. The results of tests 1 and 2 when compared to the predicted results gives the experimentalist confidence the test procedures and the test configuration can be used to produce accurate results.

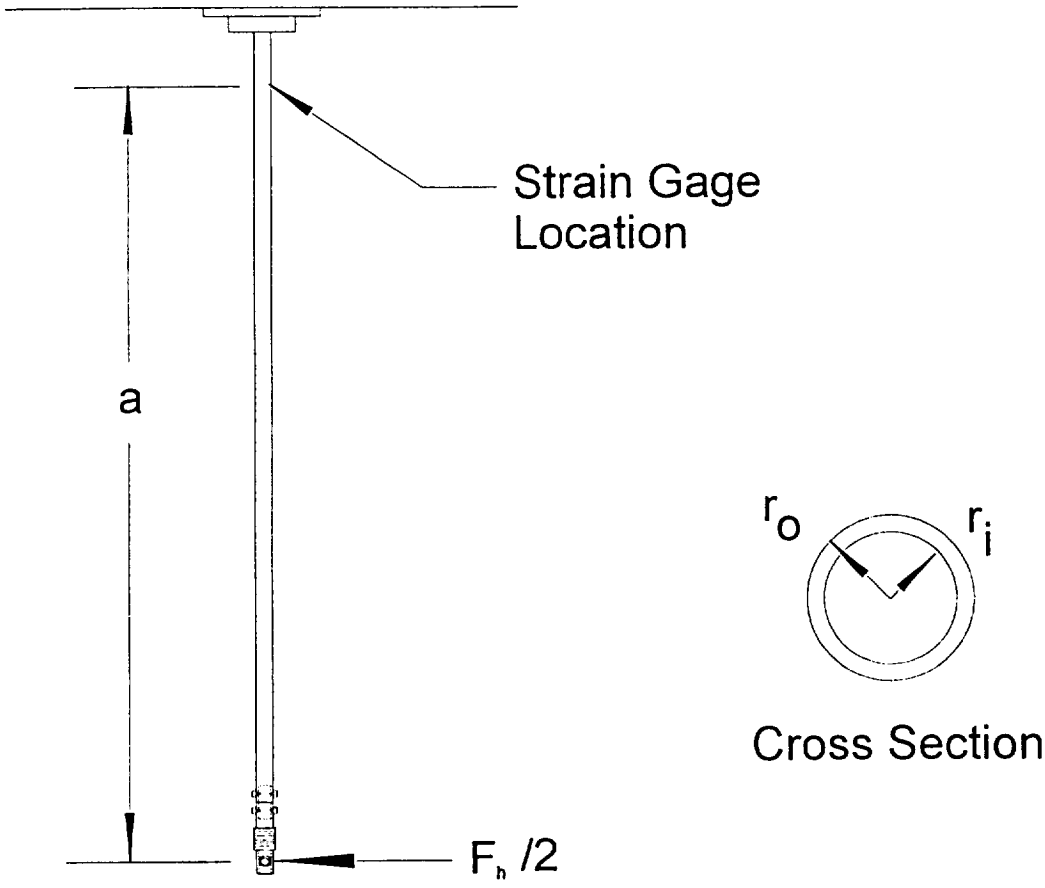

Figure 3.18: Gauge Location

3.10.2 Tests 3 and 4

The trend of Figure 3.16 illustrates with increasing load, the bending strain increases nonlinearly as the force approaches a horizontal asymptote. The asymptote in this case is the critical buckling load. The experimental results show the critical buckling load to be approximately 117 Newtons.

The experimental model can be compared to results using *Euler's formula,*

$$P_{cr} = \frac{\pi^2 EI}{L^2} \qquad 3.9$$

because the line of action of the compressive force, P, passes through the fixed end supports of the booms as in the case of a simply supported beam [5]. In equation 3.9, L is the length of the boom, and, I, (equation 3.8), is the moment of inertia. Using, equation 3.9, and data from Table 3.6, the critical buckling load, P_{cr}, for the booms is estimated to be 114 Newtons. Comparing the absolute difference between the experimental and predicted values is 3%.

The bending vibration and buckling load curve compares the bending vibration frequencies versus the applied compressive load, Figure 3.17. The trend of the graph reaches its minimum value for frequency near 120 Newtons. Using the load value corresponding to the minimum frequency and comparing that value, 120 Newtons, to the predicted critical buckling load, 114. Newtons there is a 5 % difference. The torsional buckling of the model solar array with 1.27 cm closed cross-section booms is 400 Newtons.

3.11 Closing Comments

From this series of tests using closed cross-section booms several conclusions can be made. First, buckling for the model solar array with the closed cross-section booms occurs in flexure. Second, torsional buckling could not be induced over the load range of 0-124.5 Newtons. Thus, the closed cross-section booms provide large enough torsional stiffness so that for the solar array the torsional buckling load is greater than the flexural buckling load. Finally, the results of the tests gave the experimentalist the confidence that the test apparatus and procedures implemented would produce accurate results for investigating the buckling behavior of the solar array with BiSTEM booms.

Chapter 4

Model Solar Array with BiSTEM Booms

A model solar array was constructed using 2.18 cm outside diameter BiSTEM booms. These BiSTEMs are duplicates of those on the Hubble Space Telescope except the model solar array BiSTEMs are shorter in length. With the BiSTEM booms, a comparison with predictions for buckling loads based on classical beam behavior will be made. This chapter presents the experimental program and a summary of the results.

4.1 Objectives

The laboratory experiments presented here were designed to investigate the physical phenomenon of solar array buckling with booms made from BiSTEMs. The objective of the experimental study is to characterize: (1) quasi-static behavior of the model solar array in terms of tip deflection as a function of load, (2) quasi-static behavior of the model solar array in terms of lower spreader bar angle of twist as a function of load, (3) localized buckling of the BiSTEMs as a function of horizontal deflection when loaded near the critical buckling load, and (4) individual BiSTEM twist as a function of horizontal deflection when loaded near the critical buckling load.

4.2 Test Fixture

A test fixture was designed and constructed for studying buckling associated with a simulated solar array in the laboratory. The same fixture was used for this set

of experiments as described in Section 3.2. Integral to the over all test fixture is a load cell and two laser displacement sensors (Figure 4.1). The model solar array, consisting of two 2.18 cm outside diameter stainless steel BiSTEMs, is positioned in the test fixture 57.4 cm along the 1.22 meter z axis and each BiSTEM is positioned 33.02 cm left and right of the center along the 1.22 meter x axis.

The support conditions were designed to represent the conditions present on the Hubble Space Telescope. The booms are held at their top ends by set screws to an insert/base plate bolted to the top plate (Figure 4.2). The fixed end conditions of the BiSTEMs are offset 3.6 cm along the z axis to simulate the solar array blanket/BiSTEM geometry that is on the Hubble Space Telescope. The top plate is a 1.27 cm thick by 1.22 m x 1.22 m aluminum plate bolted to the top of the test frame. The lower end of the booms are connected to bellows which are themselves connected to the lower spreader bar (Figure 4.3). The bellows (Cajon flexible vacuum tubing model number 321-24-x-1) are constructed of two 3.81 cm outside diameter tubes connected by a 2.54 cm long section of corrugated stainless steel tube with an outside diameter of 5.08 cm. The lower spreader bar joins the two booms via their individual bellows end conditions. These end conditions allow the lower spreader bar to translate along the x, y, and z axes while constraining the boom to twist with the lower spreader bar (Figure 4.3). The bellows permit a rotation in the y-z plane, and represents a hinge with zero bending moment.

The lower spreader bar is a solid 2.39 cm diameter, 55.88 cm long aluminum rod with 8.89 cm long threaded rods extending outward along the

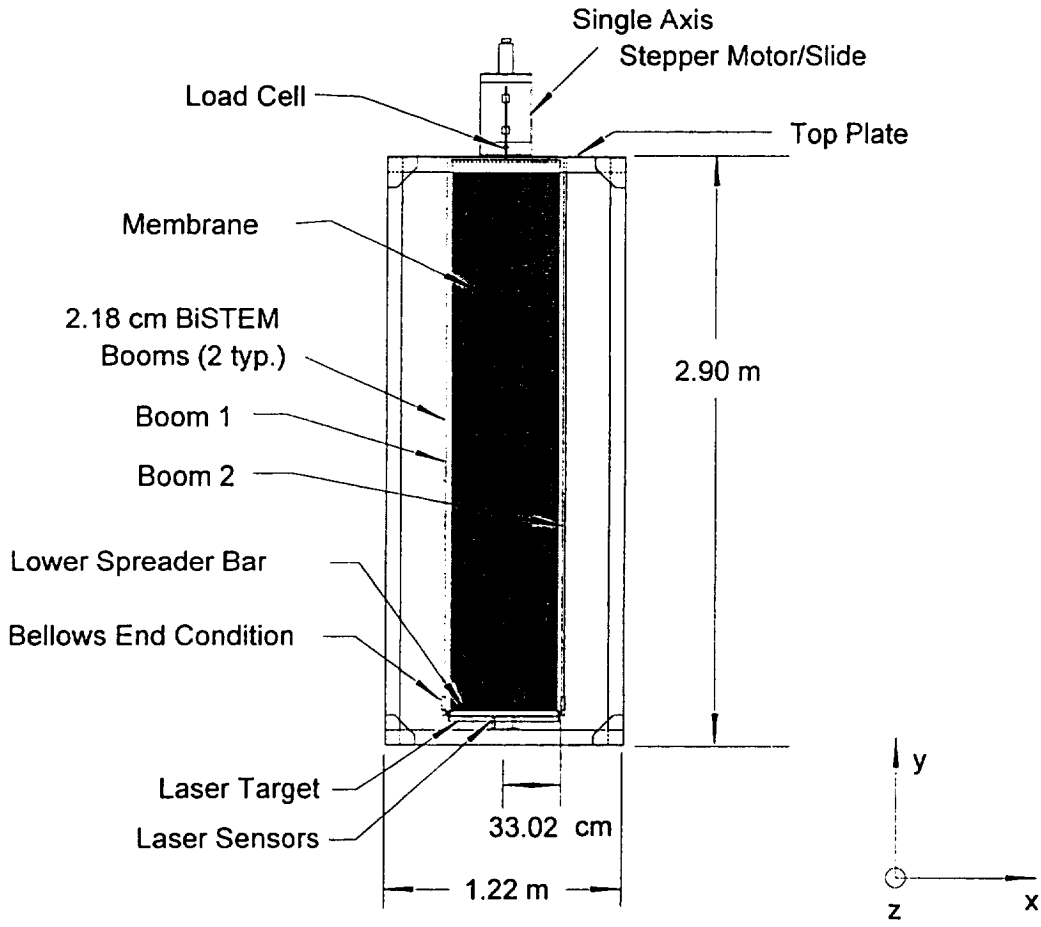

Figure 4.1: Test fixture and model solar array with BiSTEMs

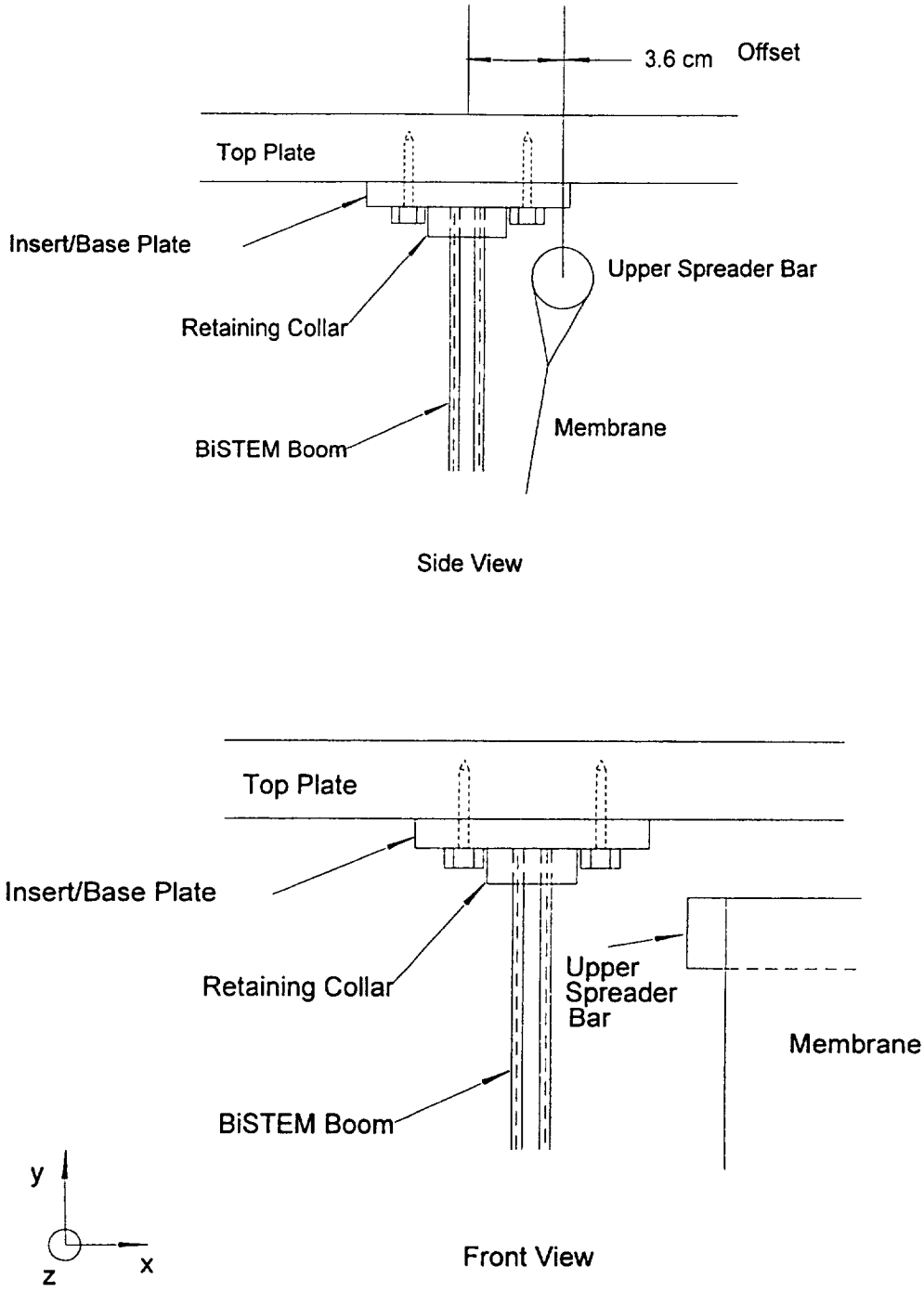

Figure 4.2: BiSTEM fixed end

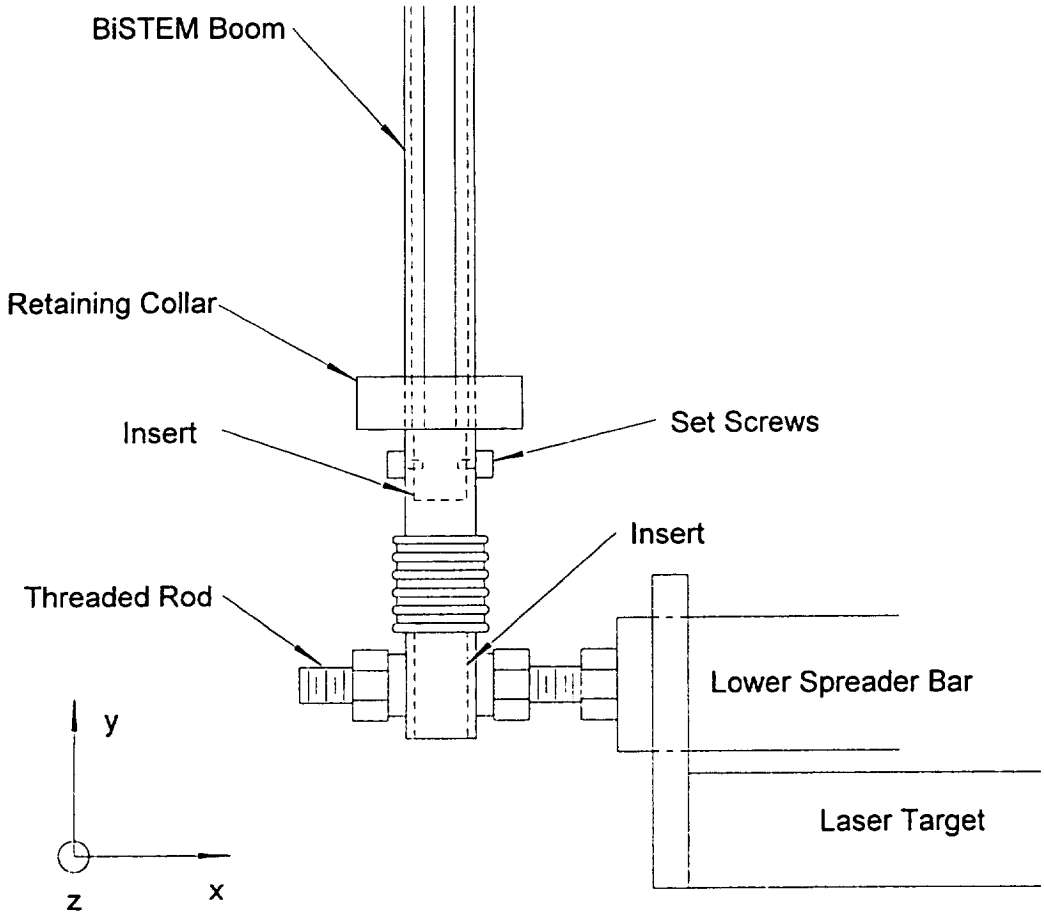

Figure 4.3: BiSTEM lower end condition

length. A canvas membrane is connected between the upper and lower spreader bars. The upper spreader bar is also a solid 2.39 cm diameter, 55.88 cm long aluminum rod (Figure 4.4). The upper spreader bar has a 11.43 cm long threaded rod screwed into it perpendicularly and centered along its length. The rod and upper spreader bar thus form a tee configuration. Attached to the top of this threaded rod is a ring by which an S - hook couples to another ring connected to the lower mount of an A.L. Design 0 - 444.8 Newton load cell model no. ALD-MINI-UTC-M. This S - hook coupling releases any spurious side loading to the load cell. The upper mount of the load cell is then coupled to a threaded rod which is threaded into the stepper motor/slide mounting blocks which are bolted to the single axis stepper motor/slide. The stepper motor drives a worm gear that controls the linear motion of the 30.48 cm square slide. The slides full range of motion is 15.24 cm along the y axis. Remotely controlled, the stepper motor causes the slide to lift the upper spreader bar thus imparting a tensile load in the membrane and creating compressive loads in the 2.18 cm BiSTEM booms.

Finally, two Keyence laser displacement sensors model no. LB-70/LB-11 are attached to the base of the test fixture and point at a target attached to the lower spreader bar (Figure 4.5). Once the model solar array is loaded and deflects, the laser sensors indicate the motion of the spreader bar along the z axis.

4.3 Loading

The compressive load source utilized in this study was generated by the stepper motor/slide (Techno ISEL Inc. Model No. HL31SBM602050005 200mm)

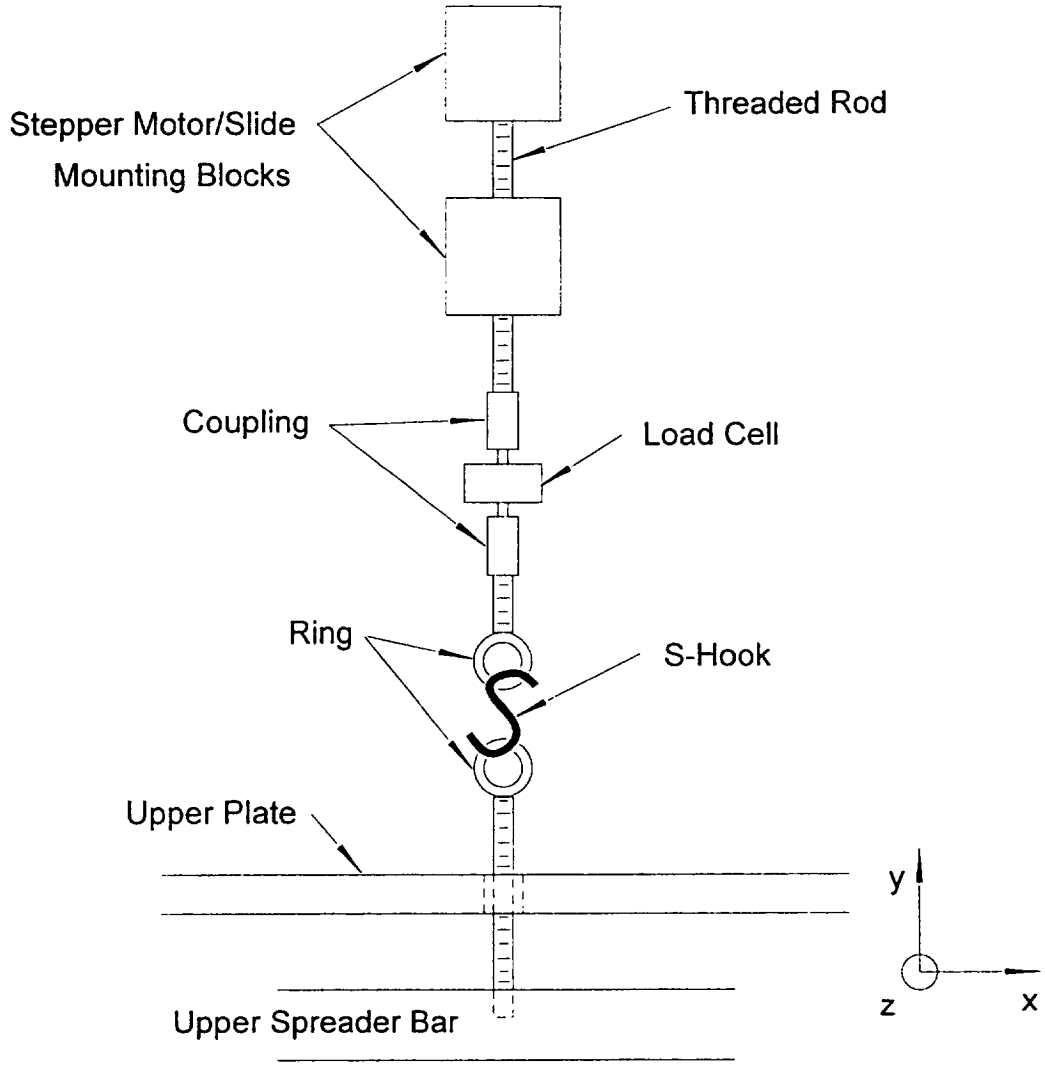

Figure 4.4: Upper spreader bar/stepper motor/slide mount

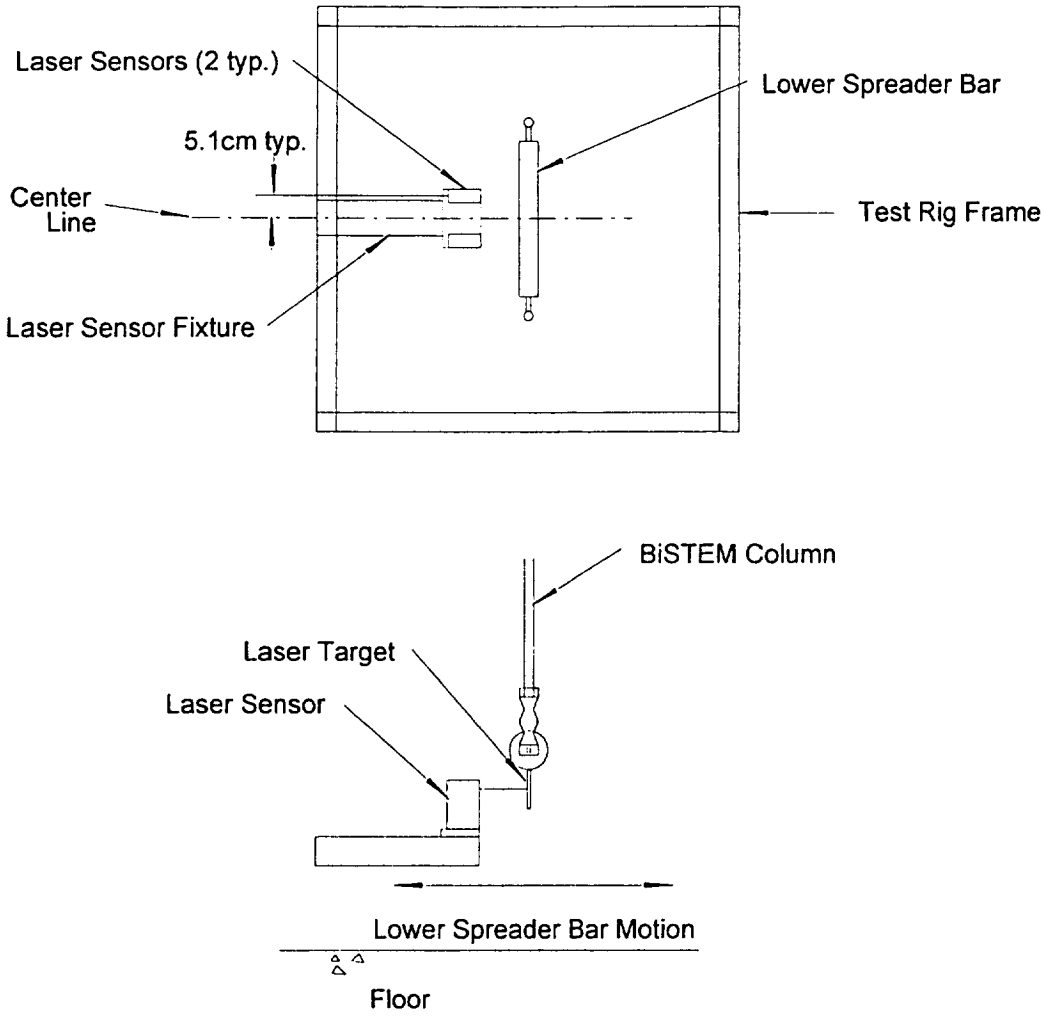

Figure 4.5: Lower spreader bar/laser displacement sensors

coupled to the 2.44 m x 55.88 cm canvas membrane which was attached to the lower spreader bar (Figure 4.6). The stepper motor/slide is operated at 120 volts and is controlled by a MAC 001 controller (Techno ISEL Inc. Model No. H26T55). Programming the motion of the stepper motor/slide via the MAC 001 controller is performed using a Micron P75 computer with MAC 001 resident software. Loading is directed along the y axis of the solar array. An initial 3.81 cm stand-off between the upper spreader bar and the top plate is necessary at the beginning of a test to load the canvas membrane adequately in tension and thus impart a compressive load to the booms. The 3.81 cm stand-off is reduced to 1.0 cm during loading as the upper spreader bar is lifted along the y axis by the stepper motor/slide.

4.4 Booms

The model solar array buckling test was performed using stainless steel BiSTEM booms. The booms are 2.66 meters in length, L, with a 2.18 cm outside diameter and each STEM of the BiSTEM has a wall thickness of 0.01 cm. Booms 1 and 2 each have tufts of tape centered in the outer STEM's seam, attached to the inner STEM (Figure 4.7). The tufts of tape are spaced approximately 30 cm apart along the length of each boom. This pattern of tape tufts evenly spaced along the length of each boom allows for visible inspection of whether the inner and outer STEMs twist during loading, and if so, twist independent of each other or if the STEMs twist in unison.

4.5 Data Acquisition

The displacement data was collected using two Keyence laser displacement sensors model no. LB-70/LB-11. The load data was collected by an A.L. Design

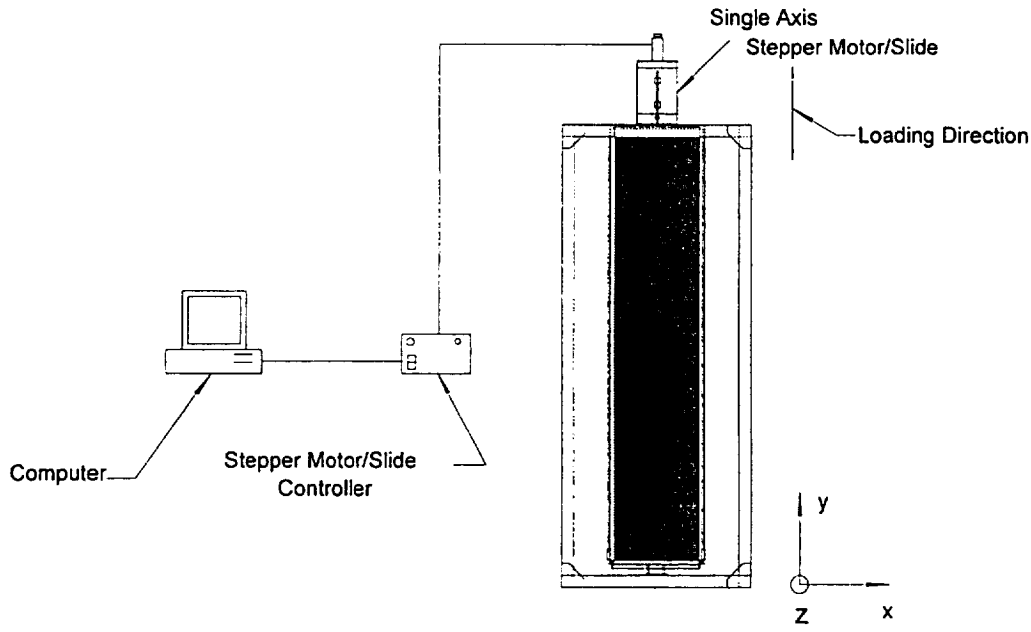

Figure 4.6: Loading model solar array with BiSTEMs

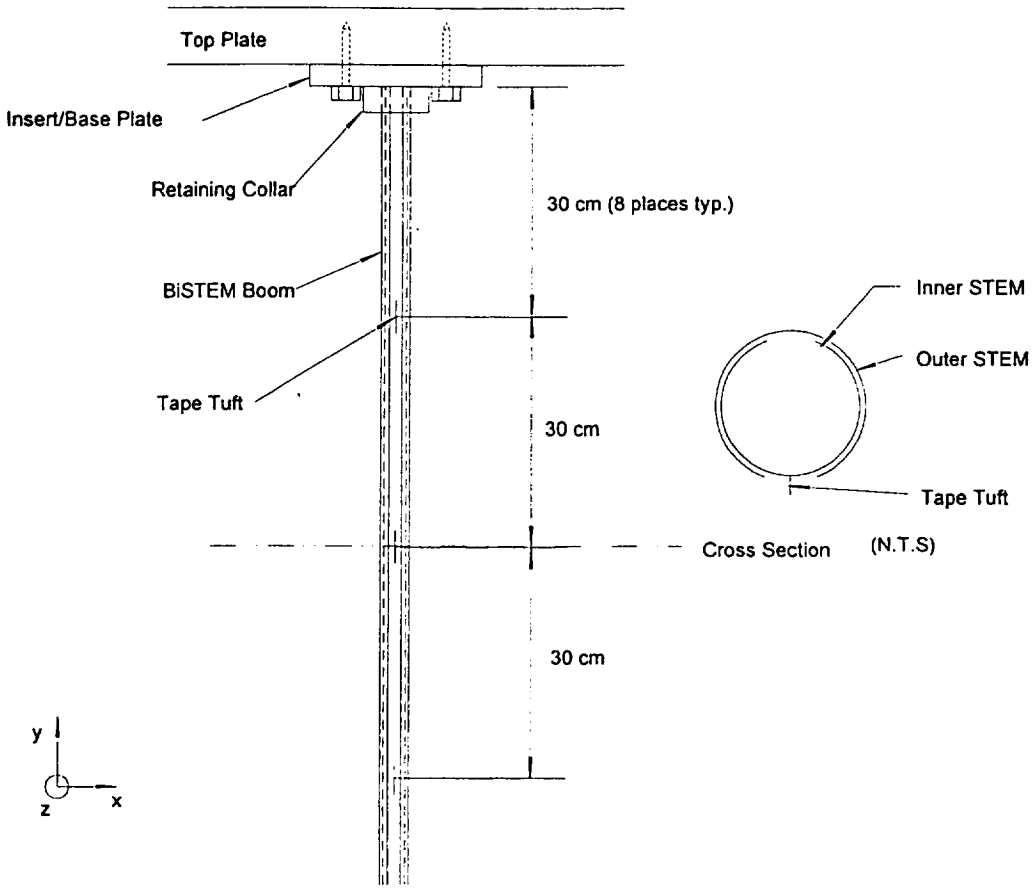

Figure 4.7: BiSTEM boom

0 - 444.8 Newton load cell model no. ALD-MINI-UTC-M. The signals from both the load cell and displacement sensor were sampled by a Keithly Metrabyte EXP-GP 16 multiplexing board. A Keithly Metrabyte DAS-8 analog to digital card received the data signal from the EXP-GP 16 converted the signal from an analog to a digital signal to be displayed by a Micron P75 computer using Labtech Notebook software. This PC based data acquisition system allows the information to be collected, displayed, and stored dynamically while a test is in progress. A schematic of the data acquisition system utilized in the experiments is presented in Figure 4.8.

4.6 Test Procedures

Three tests were conducted using the model solar array and are outlined in Table 4.1.

Table 4.1: Tests Conducted

Test	Purpose
1	Characterize the buckling behavior of the model solar array with applied compressive load in configuration 1.
2	Characterize the buckling behavior of the model solar array with applied compressive load in configuration 2.
3	Describe the local buckling behavior of the BiSTEMs and whether they twist with both an applied compressive load near the critical buckling load and an imposed horizontal displacement.

4.6.1 Tests Procedures: Tests 1 and 2

Test 1 characterized the buckling behavior of the model solar array using the test apparatus shown in Figure 4.1 with the BiSTEMs oriented in configuration 1. Figure 4.9 illustrates configuration 1 with the BiSTEM seam turned away from the membrane. This configuration is opposite to that on the Hubble Space Telescope.

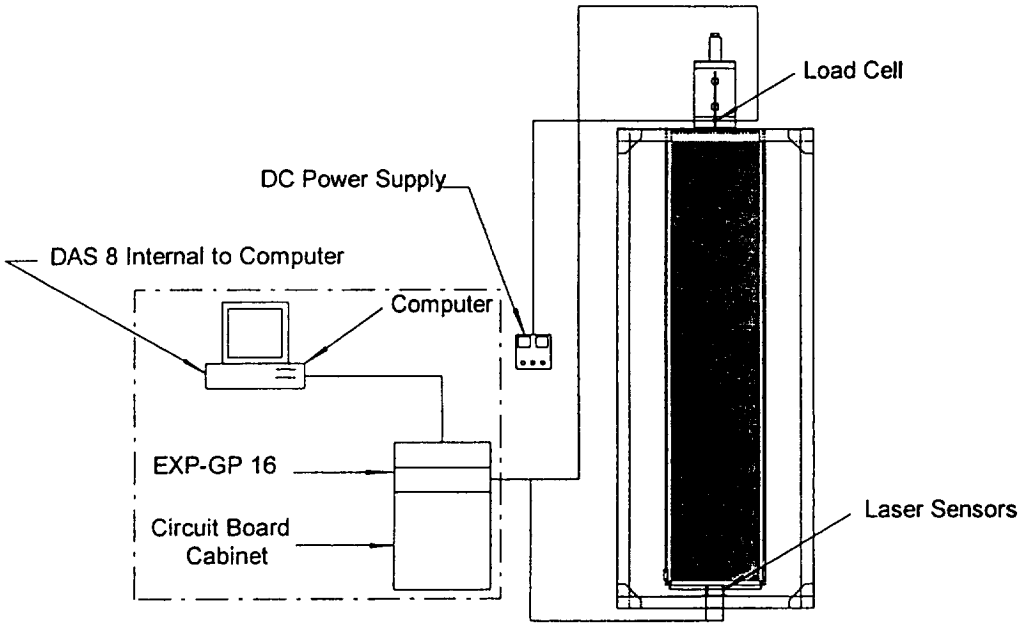

Figure 4.8: Data acquisition system

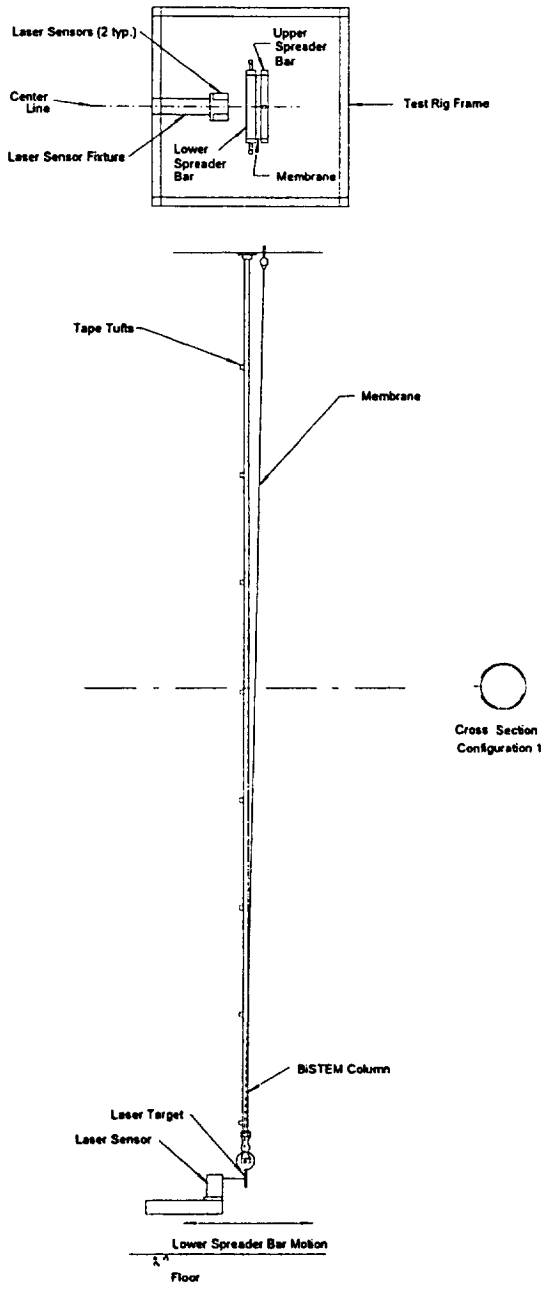

Figure 4.9: Test 1 Buckling behavior

Configuration 2 has the BiSTEM seam turned toward the membrane. The upper spreader bar was lifted using the stepper motor/slide. This action put the membrane in tension and imparted a compressive load to both booms. While the load was increased steadily through the test regime of 0 to 135 Newtons the laser displacement sensors and the load cell recorded the motion of the lower spreader bar and the compressive load respectively.

Test 2 also characterized the buckling behavior of the model solar array using the test apparatus shown in Figure 4.1. However test 2 was conducted in configuration 2 (Figure 4.10). This configuration is the same as that on the Hubble Space Telescope. The test procedure for test 2 was identical to that of test 1 with the load range 0 to 160 Newtons.

4.6.2 Test Procedures: Test 3

Test 3 describes the local buckling behavior of the BiSTEMs and whether they twist with both an applied compressive load, P near the critical buckling load and an imposed horizontal displacement. The compressive load, P, is the sum of the force in booms 1 and 2. The horizontal displacement, w', is the distance the center point of the lower spreader bar is moved along the z axis after the compressive load is applied (Figure 4.11). This test used the test apparatus described earlier in section 4.2 modified to use a single weight to apply a horizontal force displacing the lower spreader bar, w'. Although Figure 4.11 shows the horizontal displacement in one direction of the z axis horizontal displacement was imposed in the opposite direction as well. To achieve the displacement, string was tied to both ends of the lower

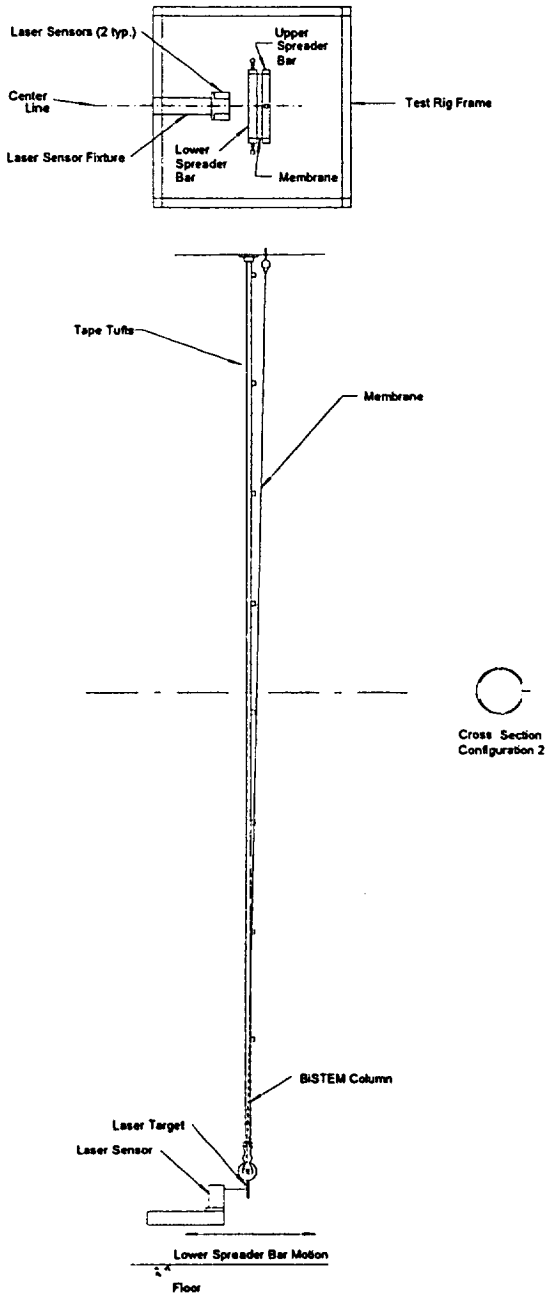

Figure 4.10: Test 2 Buckling behavior

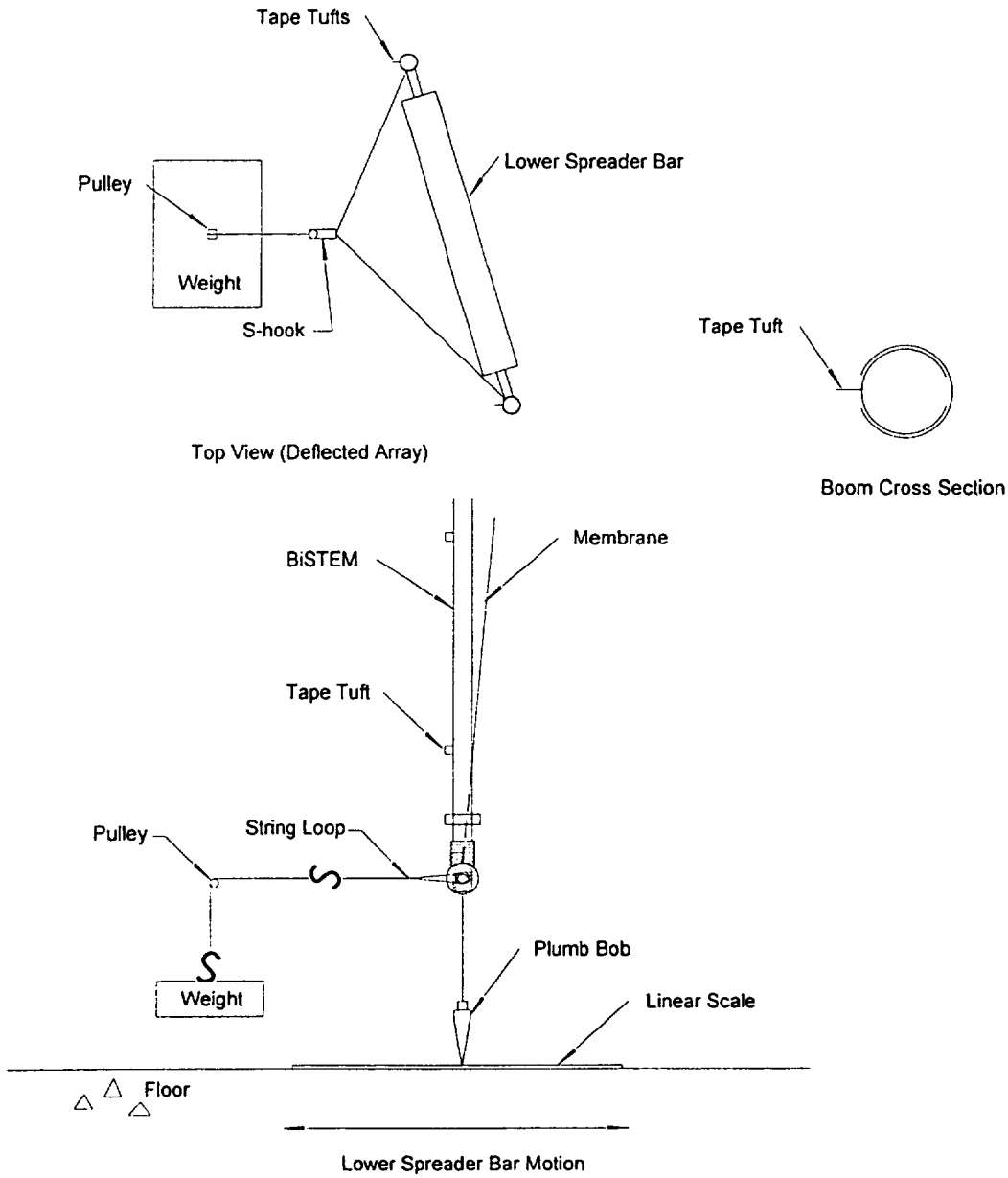

Figure 4.11: Test 3 Local buckling and twisting

spreader bar to form a large loop. Approximately 0.91 m in front of the lower spreader bar was a pulley fixed in position by a portable vise. An S-hook, connected to the loop at the lower spreader bar, was attached to a string that went through the pulley and extended vertically towards the floor. The weight was attached to this end of the string via a second S-hook.

Using the test apparatus shown in Figure 4.11 with an applied load near the critical buckling load, a weight was attached to the S-hook hanging from the pulley. The load cell data was recorded by the data acquisition system and the horizontal displacement was noted. The BiSTEMs were then inspected for twist and the pattern and magnitude of local buckling was noted. The process of increasing the horizontal displacement by increasing the weight hung by the S-hook and noting the BiSTEMs twist and local buckling continued by increasing the horizontal force from 0 - 6.9 Newtons. The identical procedure was followed to displace the lower spreader bar in the opposite direction along the z axis by attaching the loop, string and weight to the other side of the lower spreader bar.

4.7 Data Reduction

The angle of twist data is calculated from geometry shown in Figure 4.12 where s_1 and s_2 are measured in inches.

$$\Phi = \tan^{-1}\left(\frac{s_1 - s_2}{3}\right) \qquad 4.1$$

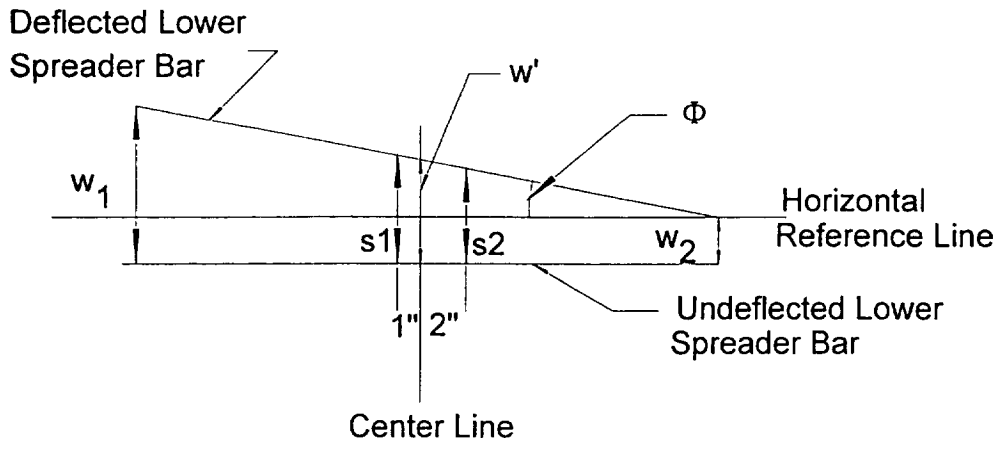

Figure 4.12 Spreader bar movement

The boom tip data is also calculated from geometry shown in Figure 4.12. The tip displacement data is the amount of movement that each boom tip moves along the z axis relative to their no load condition position.

$$w_1 = s_1 + 12(\tan\Phi) \qquad 4.2$$

$$w_2 = s_2 - 11(\tan\Phi) \qquad 4.3$$

The compressive load data is the total force exerted on the model solar array reported by the load cell. A portion of the reported load is caused by the weights of upper, and lower spreader bars, membrane, booms and retaining hardware as shown in Figure 4.13.

Figures 4.14, 4.15 and 4.16 illustrate the compressive load, P, versus boom tip displacements, w1 and w2, and, the angle of twist, Φ, and , the center displacement, w', respectively for test 1. The motion along the z axis of the center of the lower spreader bar, w', was calculated using the values from the laser displacement sensor 1, s1, and laser displacement sensor 2, s2, as shown in Figure 4.12.

$$w' = \frac{2}{3}(s_1 - s_2) \qquad 4.4$$

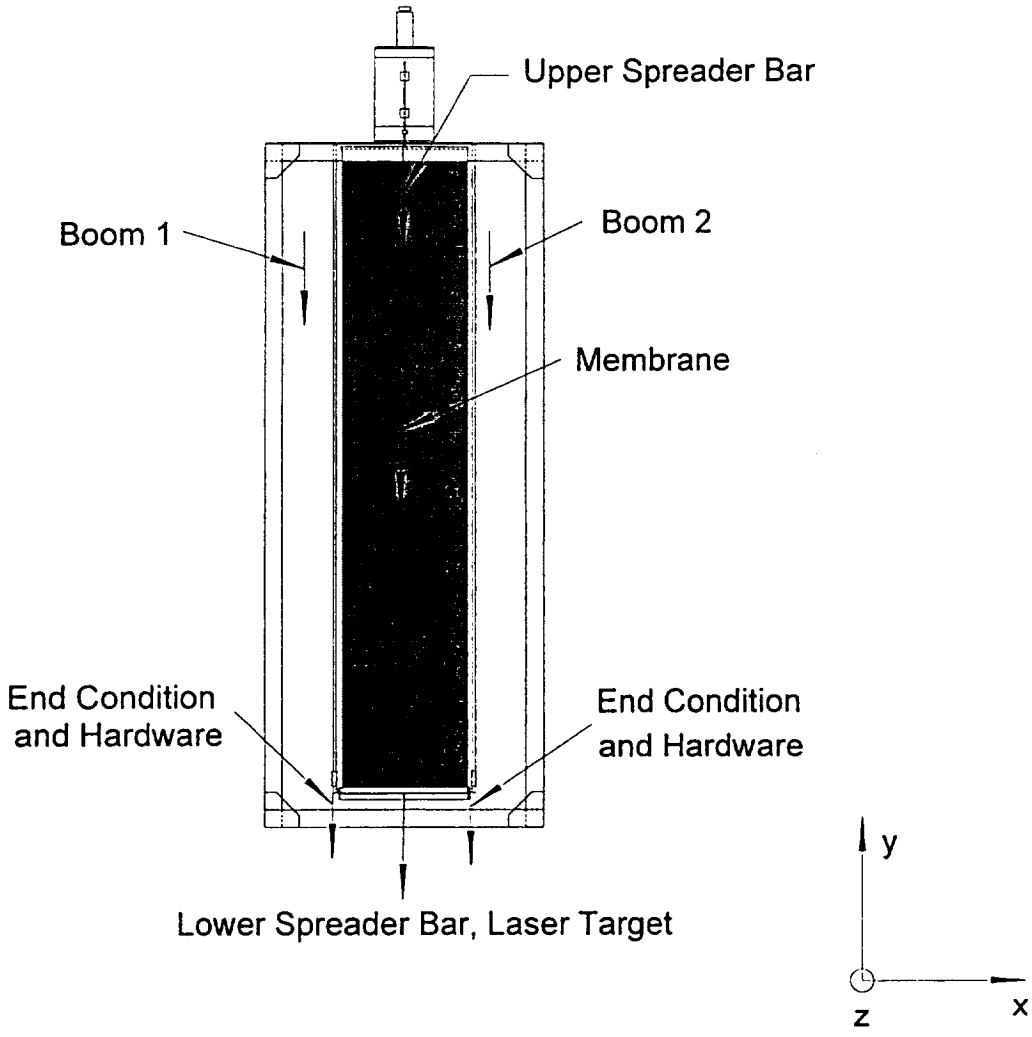

Figure 4.13: Model solar array weights acting on load cell

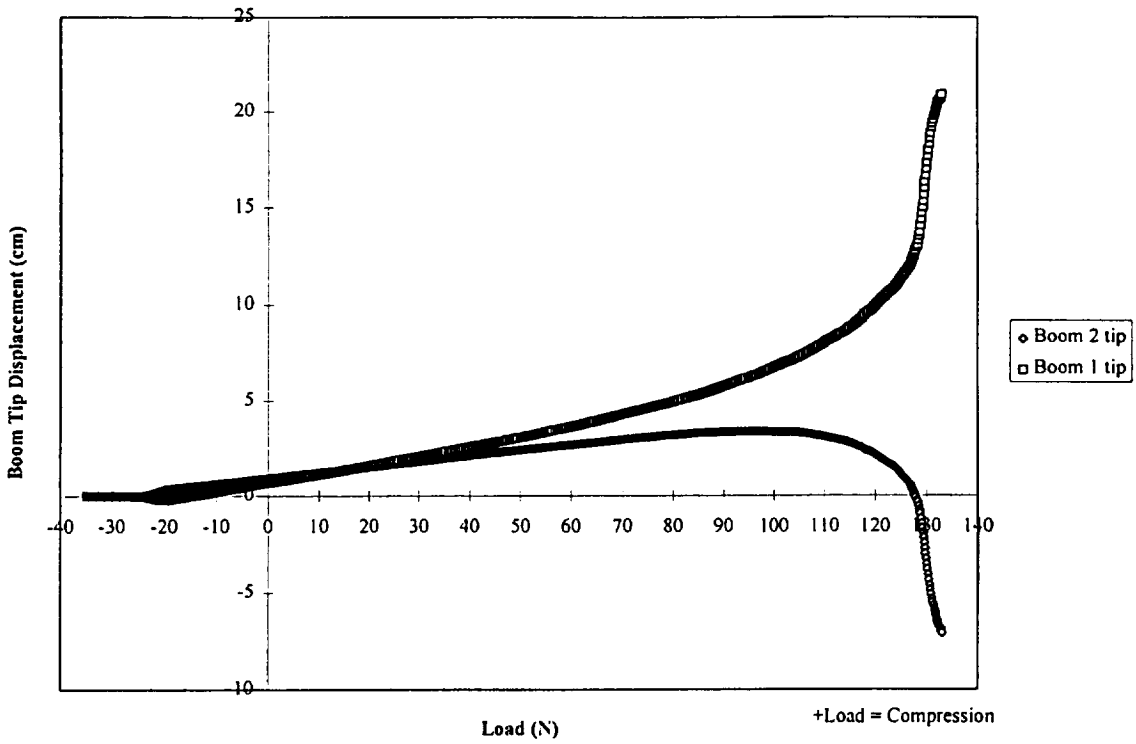

Figure 4.14: Test 1 Boom tip displacement

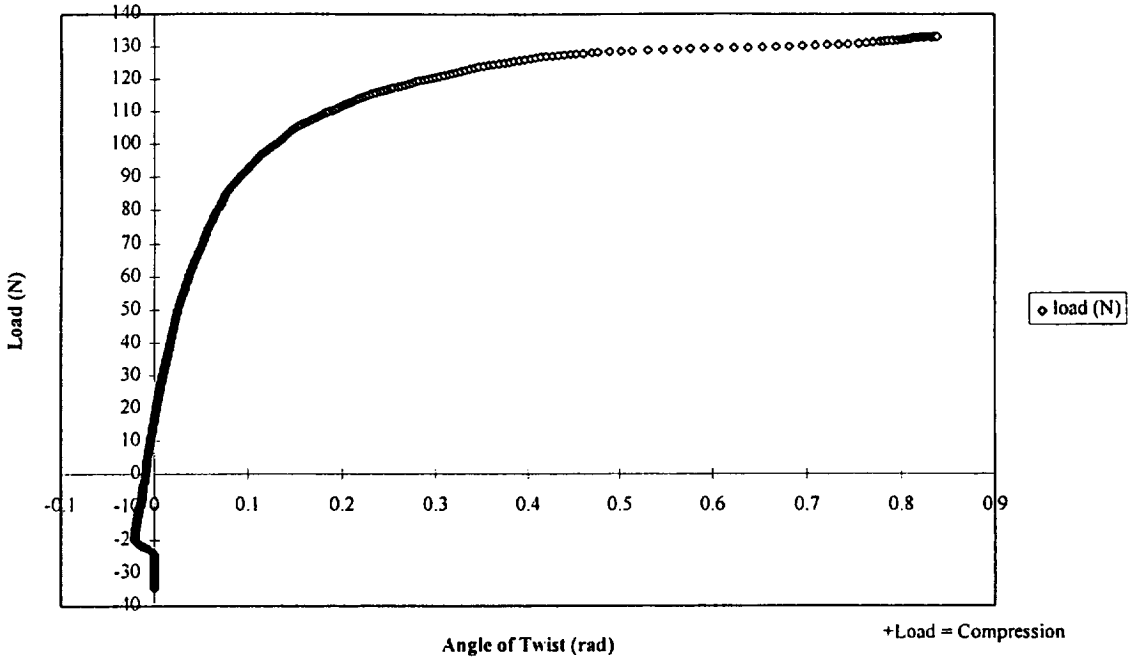

Figure 4.15: Test 1 Compressive load-angle of twist

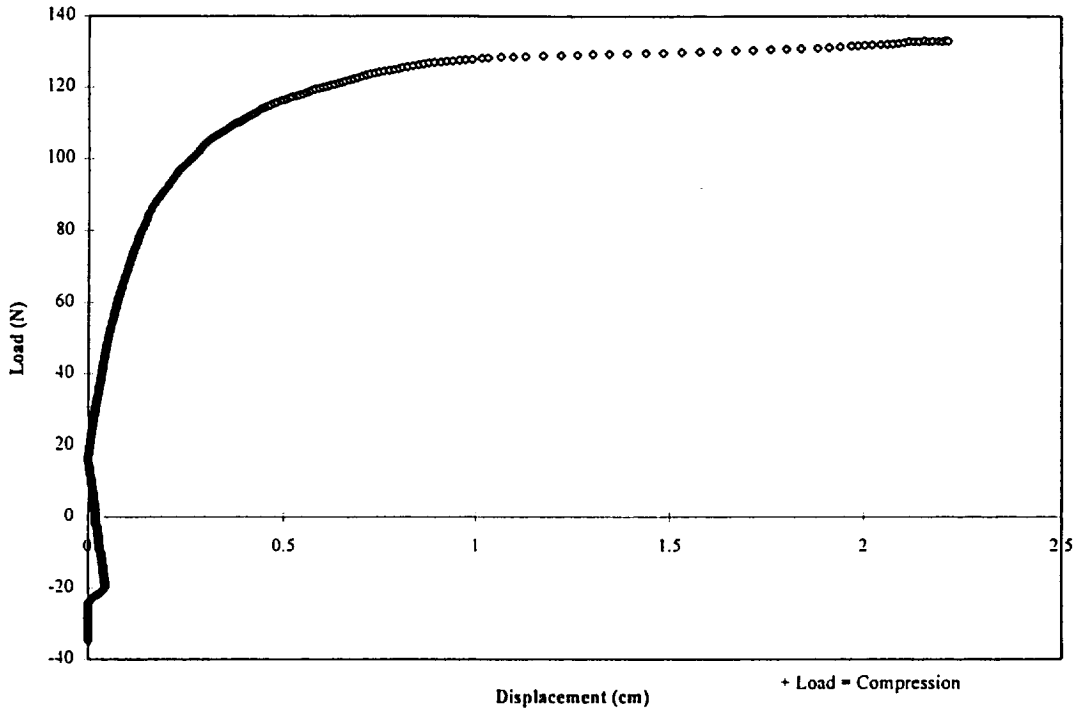

Figure 4.16: Test 1 Center displacement

Figures 4.17, 4.18 and 4.19 illustrate the compressive load, P, versus tip displacements, w1 and w2, and the angle of twist, Φ, and, the center displacement, w', respectively for Test 2. Test 2 data was processed identically to that of Test 1.

Table 4.2 summarizes the horizontal displacements, w', and loading, P, that the booms were subjected to for test 3. These displacements were in the direction shown in Figure 4.11.

Table 4.2: Test 3, Load and displacement for local buckling test

BiSTEM Load *(N)	-17.08	115.29	135.58	160.13
Horizontal Load *(N)	w' (cm)	w' (cm)	w' (cm)	w' (cm)
0	0	0	0	0
0.98	1.27	1.27	2.22	1.59
1.96	2.86	3.50	3.81	4.76
4.90	7.62	12.07	13.34	12.07
6.86	9.53	12.70	14.61	13.34

*Total load applied to two booms

Table 4.3 summarizes the horizontal displacements, w', and loading, P, that the booms were subjected to for test 3 displaced in the opposite direction shown in Figure 4.11. The BiSTEM load data is the total force exerted on the model solar array reported by the load cell. The horizontal displacement data is the amount of displacement along the z axis the lower spreader bar was moved once the compressive load was introduced.

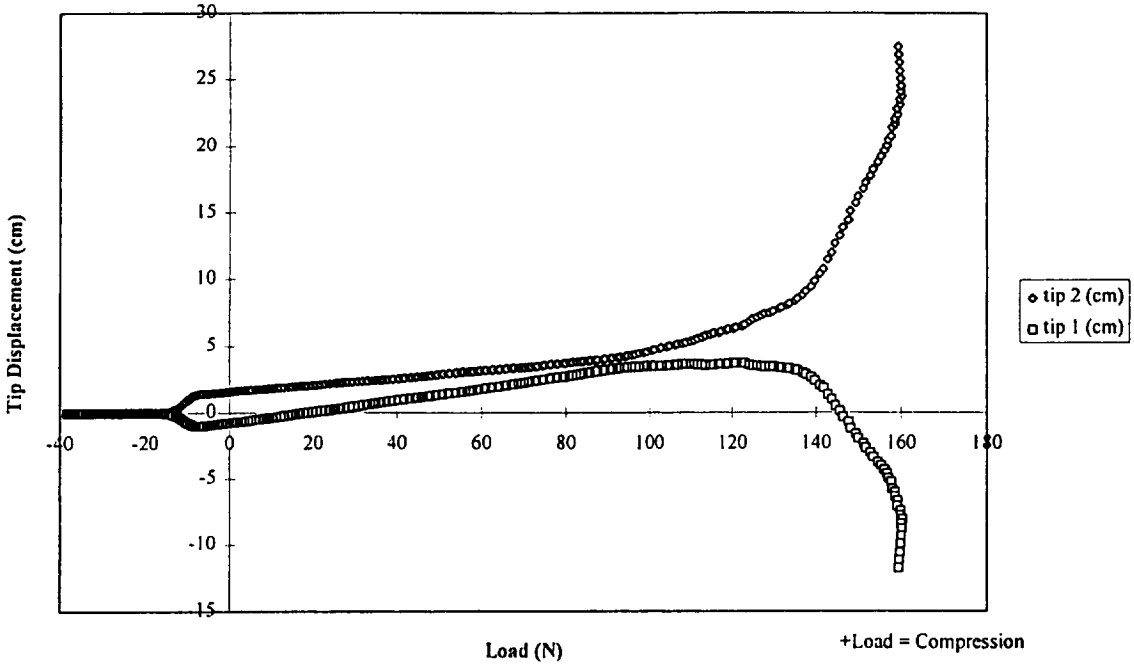

Figure 4.17: Test 2 Tip displacement

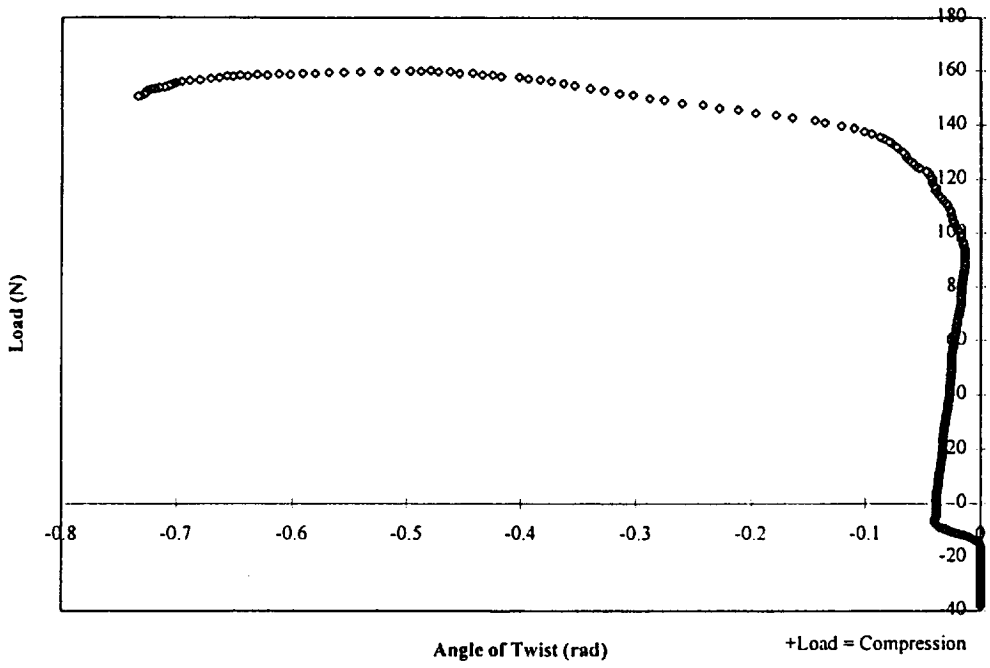

Figure 4.18: Test 2 Angle of twist

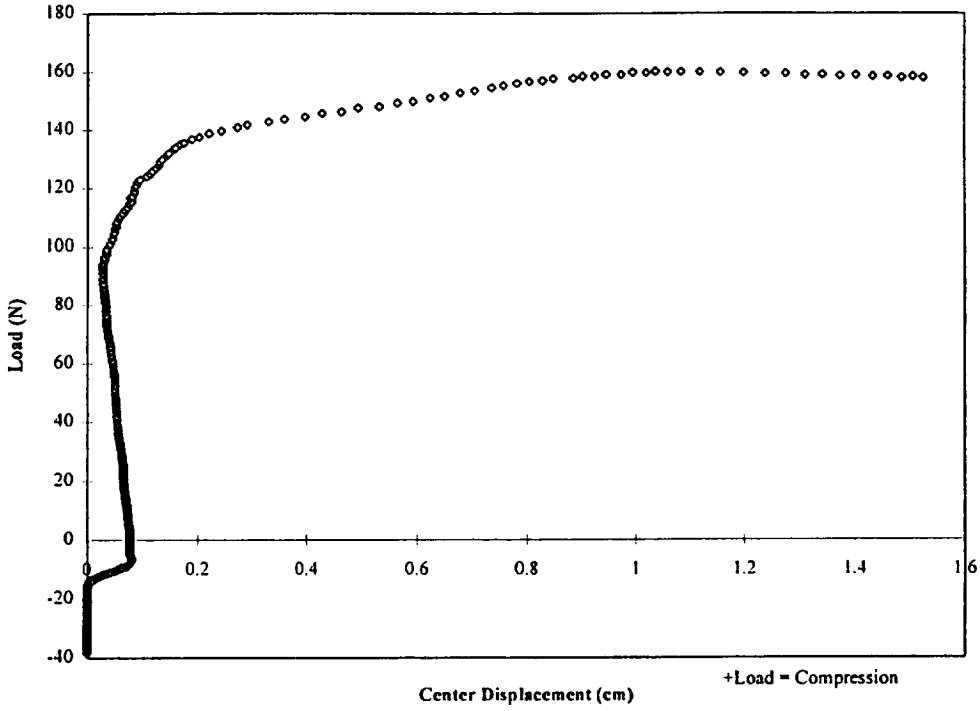

Figure 4.19: Test 2 Center displacement

Table 4.3: Test 3, Load and displacement for local buckling test

BiSTEM Load *(N)	-17.08	89.67	117.43	138.78
Horizontal Load *(N)	w' (cm)	w' (cm)	w' (cm)	w' (cm)
0	0	0	0	0
0.98	2.24	1.60	2.24	1.91
1.96	3.51	3.81	3.51	3.81
4.90	6.99	6.99	9.53	9.53
6.86	14.30	11.43	11.13	10.16

*Total load applied to two booms

Test 3 was conducted once. Repetition of this test was not possible due to the plastic deformations that occurred to the booms and the lack of replacement BiSTEMs. Tests 1 and 2 were each conducted three times. The repetition was done to insure the data was repeatable . Figures 4.14, 4.15, 4.16, 4.17, 4.18 and 4.19 are presented as sample data that is representative of the data taken for those tests. By inspection of each data set in each of tests 1 and 2 it was concluded that the data is repeatable.

4.8.1 Discussion of Results, Tests 1 and 2

The results of test 1 are presented in Figures 4.15 and 4.16. Figure 4.15 represents the relationship between the angle of twist of the lower spreader bar for increasing load applied by the membrane. Before the solar array was loaded, the BiSTEMs supported their own weight as well as that of the lower spreader bar and the membrane. This loading due to effects of gravity are illustrated in the tabularized and graphical results as the trends beginning as a negative value. The trend of the graph illustrates initially as the load was increased the spreader bar did not twist. As the load approached -20 Newtons the lower spreader bar slightly twisted counter-

clockwise then began twisting clock wise throughout the remainder of the test. There are two significant results from this graph. The first is the boom force approaches an asymptote near 135 Newtons. Second, with increasing load, the clock wise twist of the lower spreader bar increases nonlinearly as the force approaches the vertical asymptote.

Figure 4.16 represents the relationship between the displacement of the center point of the lower spreader bar along the z axis for increasing loads applied by the membrane. The results from this graph are similar to those illustrated by Figure 4.15.

The results of test 2 are presented in Figure 4.18, 4.19. Figure 4.18 represents the relationship between the angle of twist of the lower spreader bar for increasing load applied by the membrane. The trend of the graph illustrates initially as the load was increased the spreader bar did not twist. As the load approached -10 Newtons the lower spreader bar slightly twisted clockwise then began twisting counter-clockwise throughout the remainder of the test. There are three significant results from this graph. The first is the boom force approaches an asymptote near 160 Newtons. Second, with increasing load, the counterclockwise twist of the lower spreader bar increases nonlinearly as the force approaches the vertical asymptote. Third the model solar array twisted opposite to that of the model solar array in configuration 1.

Figure 4.19 represents the relationship between the displacement of the center point of the lower spreader bar along the z axis for increasing loads applied by the membrane. There are two significant results from this graph. The first is the boom force approaches an asymptote near 160 Newtons. Second, with increasing load, the

displacement of the central point of the lower spreader bar increases nonlinearly as the force approaches the vertical asymptote.

4.8.2 Discussion of Results, Test 3

Figure 4.20 illustrates the local buckling locations of booms 1 and 2 with the BiSTEMs in configuration 1. Due to the twisted configuration of the model solar array boom tip 1 deflected further than boom tip 2. The local buckling increases in magnitude and frequency with increasing compressive load to the model solar array and horizontal displacement. The local buckling pattern shown in Figure 4.21 illustrates the location of all the sites of local buckling that occurred. This pattern of local buckling developed similarly at each compressive load level. The first locations for local buckling occurred on boom 1 at 9.2 cm from the fixed end condition and on boom 2 at 35.9 cm, 64.8 cm, and 101.6 cm from the fixed end condition. With increasing compressive load the magnitude of the local buckling on boom 1 at the same location increased but there were no more locations. With increasing compressive load the magnitude of the local buckling on boom 2 increased and new locations of local buckling occurred at 6.4 cm, 20.3 cm, and 88.9 cm.

A small amount of boom twist was observed at the highest compressive load level, 160.13 Newtons in both booms. The twist in each boom did not exist at the fixed end condition, gradually began and increased toward the center of the booms length then decreased and finally ceased at the bellows end condition. At the highest compressive load level and largest horizontal displacement value each boom was disturbed by a "flick" with a finger at the center of the booms

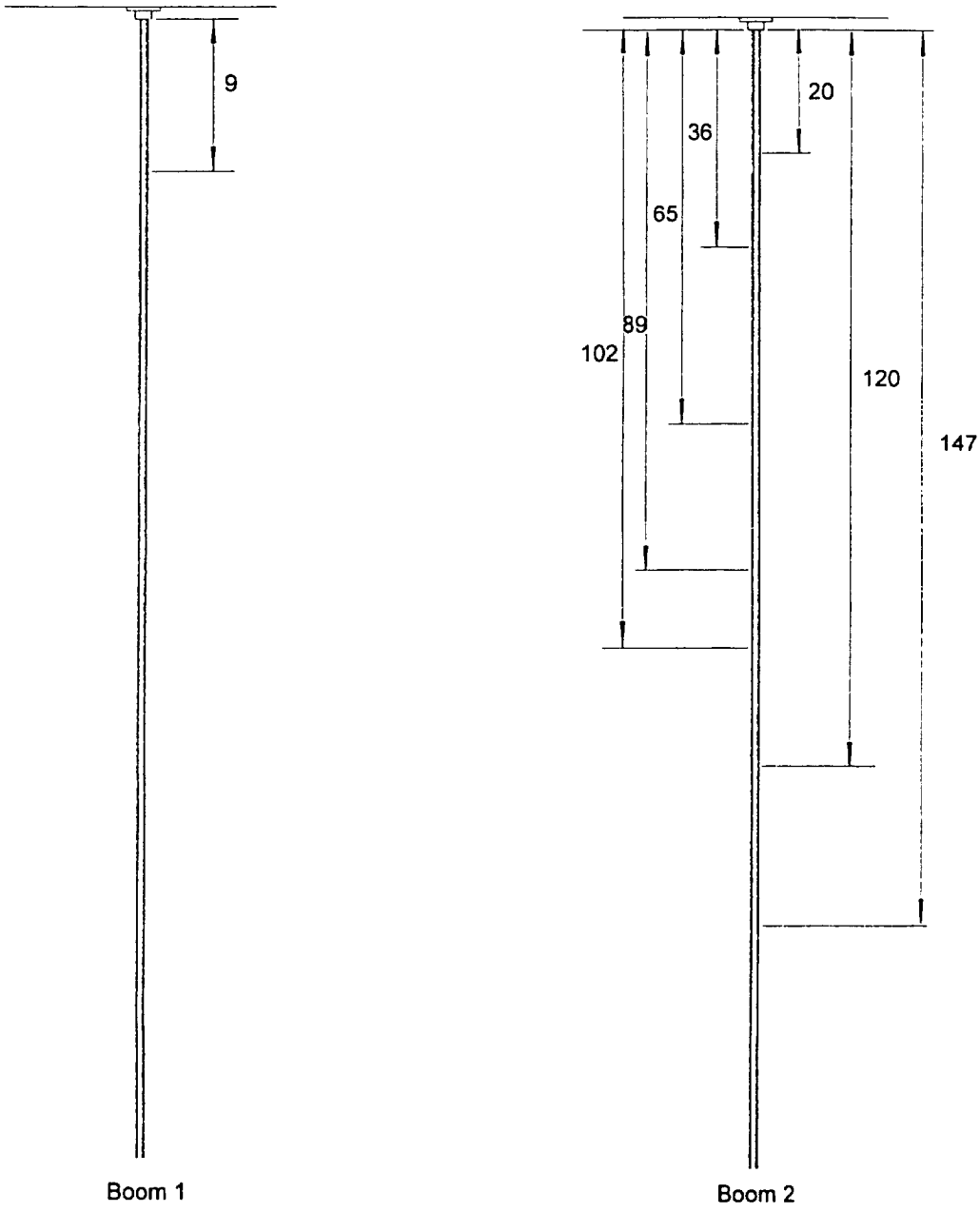

Figure 4.20: Local buckling locations

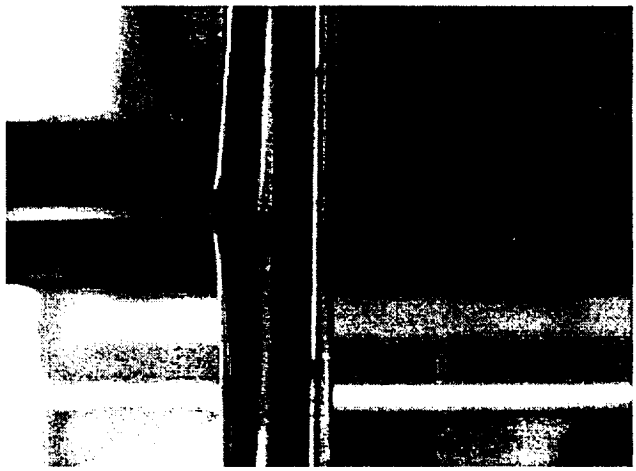

Figure 4.21: Local buckling of boom 2

length. There was no observable effect the disturbance had on boom 1. However, once disturbed, the inner and outer STEMs of boom 2 twisted relative to each other. This twisting of boom 2 inner and outer STEM had no observable effect on the rest of the model solar array. Once both the horizontal displacement and the compressive load were removed from the model solar array boom 2 inner and outer STEMs remained in their twisted configuration until another "flick" to the same location caused the inner and outer STEM to rotate back to their initial, unloaded position.

Comparing the data from Tables 4.2 and 4.3 the case of no imposed BiSTEM load reveals that the same amount of horizontal force displaces the lower spreader bar further when loading occurs in the opposite direction as that shown in Figure 4.11. This implies the bending stiffness is higher in one direction as opposed to the other.

4.9 Experimental Error

The sources of error for this experiment consists of those associated with the load cell, laser sensors and the data acquisition system. The load cell used to detect the tensile load imparted to the membrane was an A.L. Design ALD-MINI-UTC-M-10 with an error of 20 mV +/- 0.04 mV F.S. The laser sensors used to detect the linear displacement of the lower spreader bar was a Keyence LB-70/LB-11. The signals from the displacement sensors and load cell went through both Keithley Metrabyte EXP GP-16 multiplexer and DAS-8 analog to digital card. Labtech Notebook displayed the signals via a Micron P75 computer. The error associated with the laser sensors is 1.6% of full scale, the error of the DAS-8 card is +/- 0.01%

(of reading) plus +/- 1 bit and the EXP GP -16 has an error of +/- 0.015% (of reading) with a gain of 0.5. The error for the buckling load was calculated using the root mean square method. The error associated with the torsional buckling is +/- 0.6 Newtons.

4.10 Comparison of Experiment and Analysis

The results of tests 1 and 2 are compared with fundamental mechanics of material analysis. The trend of Figure 4.15, configuration 1, illustrates that with increasing load the angle of twist of the lower spreader bar increases nonlinearly as the force approaches a horizontal asymptote. The asymptote in this case is the critical torsional buckling load. The experimental results show the critical torsional buckling load to be approximately 135 +/- 0.6 Newtons. The trend of Figure 4.18, configuration 2, also illustrates that with increasing load the angle of twist of the lower spreader bar increases nonlinearly as the force approaches a horizontal asymptote. The asymptote in this case is the critical torsional buckling load. The experimental results show the critical torsional buckling load to be approximately 160 +/- 0.6 Newtons.

The experimental model can be compared to results using the transcendental equation 1.1 published in a paper by Chung and Thornton [7] and outlined in Chapter 1, Section 7. Using, equations 1.1 - 1.5, data supplied by Aero Astro, [9] Table 4.4, the BiSTEM manufacturer, and measurements from the model solar array, the critical torsional buckling load, P_{cr}, for the booms was calculated to be 151 Newtons.

Table 4.4: Model Solar Array Properties

Γ	2.586×10^{-12} m^6
ρ	7010.0 kg/m^3
A	1.613×10^{-5} m^2
b'	0.23 m
b	0.33 m
E	193.0×10^9 N/m^2
EI	171.1 N·m^2
G	7.5×10^{10} N/m^2
I_E	1.948×10^{-9} m^4
J	8.67×10^{-14} m^4
L	2.66 m

Comparing the absolute difference between the experimental configuration 1 and the predicted value is 10 %. Comparing the absolute difference between the experimental configuration 2 and the predicted value is 5 %. The flexural buckling load was calculated to be 477 Newtons.

4.11 Closing Comments

From this series of tests using BiSTEM booms several conclusions can be made. First, the buckling for the model solar array with BiSTEM booms occurs in torsion. Second, flexural buckling could not be introduced over the load range of 0 - 135 Newtons for configuration 1 and 0 - 160 Newtons for configuration 2. Third, the model solar array in configuration 1 twisted clockwise when torsionally buckled and twisted counter clockwise when torsionally buckled while in configuration 2. Fourth, the BiSTEMs do not behave linearly as beam theory predicts.

Chapter 5

Conclusion

Chapter 5 summarizes the work performed for this thesis and provides concluding remarks. Suggestions for future work on BiSTEM structures are also discussed based on experimental results from this thesis.

5.1 Summary of Experiments

Four experiments were conducted using the model solar array with the 1.27 cm aluminum booms. Each experiment was designed to analyze the booms and model solar array reactions to different loading conditions and displacements. The experiments conducted were: 1) axial strain as a function of vertical load, 2) bending strain distribution along the length of the boom as a function of horizontal load, 3) boom tip displacement as a function of compressive load, and 4) fundamental bending frequency as a function of load. Experiments 1 and 2 produced linear relationships between applied load and strain. Experiment 3 produced several significant results. First, near either end of the booms the values for the bending strain are at their minimums and approach zero. Second, the maximum value for the bending strain occurs near the center of the booms length. Third, with increasing compressive load imparted to the booms the overall bending strain increased. Also, illustrated by the relationship between the maximum bending strain values at 50% of the boom length for each compressive load level, the boom force approaches an asymptote near 115-

120 Newtons. Finally, with increasing load, the bending strain increases nonlinearly as the force approaches the horizontal asymptote. Experiment 4 produced two significant details. First, as the compressive load is increased, the bending vibration frequency decreases. Second, there is a distinct minimum frequency value over the test range which occurred near 115 Newtons. This last result tends to approximate classical beam theory that states, the vibration frequency approaches zero as the load approaches the critical buckling load.

There were two sets of experiments conducted using the model solar array with the BiSTEM booms. Again, each experiment was designed to analyze the booms and model solar array reaction to different loading conditions and displacements. The experiments conducted were: 1) boom tip displacement as a function of compressive load, and 2) local buckling and twist of the BiSTEMs near the critical torsional buckling load with a horizontal displacement superimposed. Experiment 1 results illustrate that the for each configuration that the boom force approaches an asymptote. Also, with increasing load the lower spreader bar twist increases nonlinearly as the force approaches the asymptote. This twisting of the lower spreader bar resulting in a twist of the model solar array was seen only with the open cross-section booms. This is specifically caused because the booms that twisted had an open cross-section as opposed to the closed cross-section of the 1.27 cm aluminum tubes. Experiment 2 illustrated that local buckling increases in magnitude and frequency with increasing compressive load and horizontal displacement. Also, a small amount of boom twist was observed at the highest compressive load in both

booms. Finally, at the highest compressive load level and largest horizontal displacement each boom was disturbed by a "flick". While there was no observable effect on boom 1, boom 2 inner and outer STEM twisted relative to each other.

5.2 Conclusions

Several significant conclusions can be made as a result of the data from this thesis and applied to the condition of the Hubble Space Telescopes solar arrays. The compressive load buckling experiment demonstrated when BiSTEMs were used as booms for the model solar array torsional buckling occurs before flexural buckling. The reverse is true if the 1.27 cm aluminum tubes are used for the booms for the model solar array. This means that the Hubble Space Telescopes solar arrays were torsionally buckled. Also, once the Hubble Space Telescopes solar arrays had torsionally buckled, thermal gradients across the BiSTEM cross sections imposed additional thermal deflections on both booms. Experiment five, loading the model solar array near its torsional critical buckling load and imposing a horizontal displacement, simulated the thermally induced tip displacements superimposed on the torsional buckling displacements. The results of this experiment suggest that the STEMs of each BiSTEM can twist in relation to each other if they are disturbed. Also, each BiSTEM can twist with the inner and outer STEM rotating together, and finally, local buckling can cause plastic deformations along the open edges of the BiSTEM.

5.3 Future Work

One area that should be explored further is cyclic heat loading and its effect on the BiSTEMs and their structure as a whole. Once the model solar array is loaded near its critical buckling load a cyclic heat loading could be imposed. This will investigate whether the booms of an orbiting satellite transitioning from daylight to night and night to day will act as a disturbance to initiate the STEMs to rotate with respect to each other. This rotation of the STEMs in relation to each other could change the manner in which the BiSTEMs react to known loading conditions. Further, cyclic heat loading of the BiSTEMs once the arrays are torsionally buckled could induce local buckling.

Appendix A: Test 1 Compressive load-angle of twist

Displacement (cm)	Load (N)
0	-34.498688
0	-34.848058
0	-34.42752
0	-34.728615
0	-34.681691
0	-34.498688
0	-34.73888
0	-34.448452
0	-34.664747
0	-34.521162
0	-34.498688
0	-34.60544
0	-34.60544
0	-34.60544
0	-34.60544
0	-34.60544
0	-34.498688
0	-34.498688
0	-34.498688
0	-34.498688
0	-34.285184
0	-34.285184
0	-34.178432
0	-34.07168
0	-33.964928
0	-34.07168
0	-33.964928
0	-33.858176
0	-33.751424
0	-33.751424
0	-33.644672
0	-33.53792
0	-33.431168
0	-33.324416
0	-33.324416
0	-33.217664
0	-33.324416
0	-33.217664
0	-33.110912
0	-33.00416
0	-33.00416

Displacement (cm)	Load (N)
0	-32.897408
0	-33.00416
0	-32.897408
0	-32.897408
0	-32.683904
0	-32.683904
0	-32.683904
0	-32.683904
0	-32.683904
0	-32.577152
0	-32.577152
0	-32.577152
0	-32.4704
0	-32.363648
0	-32.256896
0	-32.150144
0	-32.150144
0	-32.043392
0	-32.043392
0	-31.93664
0	-31.93664
0	-31.723136
0	-31.723136
0	-31.616384
0	-31.616384
0	-31.509632
0	-31.509632
0	-31.296128
0	-31.189376
0	-31.082624
0	-31.082624
0	-30.975872
0	-30.86912
0	-30.86912
0	-30.762368
0	-30.655616
0	-30.548864
0	-30.442112
0	-30.33536
0	-30.228608
0	-30.121856

Displacement (cm)	Load (N)
0	-30.121856
0	-30.015104
0	-29.908352
0	-29.8016
0	-29.694848
0	-29.588096
0	-29.481344
0	-29.374592
0	-29.26784
0	-29.161088
0	-29.054336
0	-28.947584
0	-28.840832
0	-28.627328
0	-28.520576
0	-28.413824
0	-28.307072
0	-28.307072
0	-28.093568
0	-27.986816
0	-27.880064
0	-27.773312
0	-27.773312
0	-27.559808
0	-27.559808
0	-27.453056
0	-27.453056
0	-27.453056
0	-27.346304
0	-27.239552
0	-27.239552
0	-27.1328
0	-27.1328
0	-27.026048
0	-27.026048
0	-26.919296
0	-26.812544
0	-26.812544
0	-26.705792
0	-26.705792
0	-26.59904

Displacement (cm)	Load (N)
0	-26.492288
0	-26.385536
0	-26.172032
0	-26.06528
0	-25.958528
0	-25.745024
0	-25.638272
0	-25.53152
0	-25.424768
-4E-05	-25.318016
-5.6E-05	-25.211264
-6.533E-05	-25.104512
-6.533E-05	-25.104512
-6.533E-05	-24.891008
-6.533E-05	-24.784256
-9.467E-05	-24.677504
-0.000184	-24.570752
-0.000332	-24.464
-0.000424	-24.250496
-0.000472	-24.143744
-0.0005573	-24.036992
-0.0005987	-23.93024
-0.0008467	-23.93024
-0.001144	-23.823488
-0.0015	-23.716736
-0.0021293	-23.609984
-0.0028493	-23.503232
-0.0035867	-23.39648
-0.00434	-23.182976
-0.0050986	-22.969472
-0.0057373	-22.755968
-0.0062626	-22.649216
-0.0067466	-22.542464
-0.0076519	-22.435712
-0.0088038	-22.32896
-0.0100317	-22.008704
-0.0111315	-21.901952
-0.0120141	-21.7952
-0.0130499	-21.688448
-0.0140257	-21.688448
-0.0150509	-21.368192

Displacement (cm)	Load (N)
-0.0160746	-21.26144
-0.0170304	-21.047936
-0.0178501	-20.834432
-0.0184846	-20.72768
-0.0191203	-20.514176
-0.0193776	-20.407424
-0.0195335	-20.19392
-0.0198041	-20.087168
-0.0201173	-20.087168
-0.0204412	-20.087168
-0.0209849	-19.980416
-0.0216366	-19.766912
-0.0218752	-19.66016
-0.0218645	-19.553408
-0.0217086	-19.553408
-0.0214194	-19.339904
-0.0213514	-19.1264
-0.0212715	-18.912896
-0.0214207	-18.699392
-0.0212421	-18.59264
-0.0211089	-18.59264
-0.020833	-18.379136
-0.0207224	-18.272384
-0.0207783	-18.165632
-0.0205731	-18.05888
-0.0205225	-17.952128
-0.0207357	-17.738624
-0.0207157	-17.52512
-0.0206291	-17.311616
-0.0204531	-16.99136
-0.0203452	-16.884608
-0.0203519	-16.671104
-0.0202479	-16.4576
-0.0200786	-16.350848
-0.0201439	-16.137344
-0.0201533	-16.030592
-0.0200187	-15.92384
-0.0198854	-15.817088
-0.0196068	-15.710336
-0.0196908	-15.496832
-0.0196841	-15.283328

Displacement (cm)	Load (N)
-0.0196281	-15.176576
-0.0196655	-14.963072
-0.0193962	-14.749568
-0.0194655	-14.536064
-0.0193616	-14.429312
-0.0189391	-14.32256
-0.0188244	-14.109056
-0.0186432	-14.002304
-0.0187991	-13.7888
-0.0187525	-13.575296
-0.0185539	-13.361792
-0.0183366	-13.148288
-0.0181154	-12.934784
-0.0178608	-12.72128
-0.0178128	-12.614528
-0.0178154	-12.401024
-0.0177901	-12.18752
-0.0177328	-11.974016
-0.0176248	-11.760512
-0.0175769	-11.65376
-0.0173703	-11.547008
-0.0172183	-11.333504
-0.017245	-11.226752
-0.0169544	-11.013248
-0.0168544	-10.906496
-0.0168464	-10.692992
-0.0167198	-10.58624
-0.0166158	-10.372736
-0.0164385	-10.159232
-0.0161479	-10.05248
-0.0158054	-9.945728
-0.0156267	-9.732224
-0.0155094	-9.625472
-0.0152135	-9.411968
-0.0151069	-9.305216
-0.0148509	-9.091712
-0.0147016	-8.878208
-0.0145136	-8.771456
-0.0141417	-8.557952
-0.0139871	-8.344448
-0.0140697	-8.237696

Displacement (cm)	Load (N)
-0.0138231	-8.024192
-0.0136818	-7.810688
-0.0134592	-7.597184
-0.0133965	-7.276928
-0.0132486	-7.063424
-0.0133099	-6.84992
-0.0135298	-6.743168
-0.0133392	-6.529664
-0.0133659	-6.31616
-0.0132926	-6.102656
-0.0133472	-5.889152
-0.0132059	-5.675648
-0.0131899	-5.462144
-0.0130739	-5.24864
-0.0129486	-5.035136
-0.012762	-4.821632
-0.0125273	-4.608128
-0.012578	-4.501376
-0.012374	-4.287872
-0.0123647	-3.967616
-0.0122927	-3.754112
-0.0121834	-3.64736
-0.0122101	-3.433856
-0.0121141	-3.327104
-0.0119181	-3.1136
-0.0116675	-2.900096
-0.0112049	-2.686592
-0.0107916	-2.473088
-0.0106129	-2.259584
-0.010469	-2.152832
-0.0101343	-1.939328
-0.0098997	-1.725824
-0.009877	-1.51232
-0.009661	-1.192064
-0.0097517	-0.97856
-0.0096597	-0.658304
-0.009765	-0.4448
-0.009609	-0.124544
-0.0095357	0.08896
-0.0094611	0.302464
-0.0093824	0.515968

Displacement (cm)	Load (N)
-0.0092504	0.836224
-0.0089091	1.15648
-0.0086984	1.476736
-0.0087891	1.69024
-0.0086358	2.010496
-0.0085198	2.224
-0.0085651	2.544256
-0.0084198	2.75776
-0.0084691	3.078016
-0.0085238	3.29152
-0.0085665	3.505024
-0.0083905	3.82528
-0.0082478	4.038784
-0.0079318	4.252288
-0.0077892	4.465792
-0.0075879	4.786048
-0.0074759	5.106304
-0.0072865	5.42656
-0.0068439	5.746816
-0.0066466	6.067072
-0.0065119	6.173824
-0.0065359	6.387328
-0.0063972	6.600832
-0.0062626	6.814336
-0.0059146	7.134592
-0.0056679	7.454848
-0.0055586	7.775104
-0.0053933	8.09536
-0.005244	8.415616
-0.0050386	8.842624
-0.004952	9.056128
-0.0046493	9.483136
-0.0045533	9.803392
-0.0047506	10.016896
-0.0045413	10.337152
-0.0042733	10.550656
-0.0037933	10.870912
-0.00364	11.084416
-0.0033227	11.404672
-0.0031293	11.724928
-0.0028387	12.045184

Displacement (cm)	Load (N)
-0.0023653	12.472192
-0.002168	12.792448
-0.002008	13.112704
-0.0020853	13.43296
-0.0019427	13.646464
-0.0019373	13.859968
-0.0017907	14.180224
-0.0014413	14.393728
-0.001152	14.713984
-0.0007747	15.03424
-0.000624	15.247744
-0.000404	15.568
6.5333E-05	15.995008
0.00032	16.422016
0.00041733	16.63552
0.000172	16.955776
0.00048133	17.276032
0.00063333	17.596288
0.00093067	17.916544
0.00105867	18.2368
0.00111333	18.557056
0.00126533	18.877312
0.00154533	19.197568
0.00194133	19.517824
0.00211733	19.83808
0.00247599	20.158336
0.00263466	20.478592
0.00279733	20.798848
0.00294799	21.225856
0.00307466	21.546112
0.00333465	21.97312
0.00360798	22.293376
0.00385198	22.613632
0.00411198	22.933888
0.00433331	23.360896
0.0047493	23.681152
0.00492796	24.001408
0.00504662	24.214912
0.00525728	24.64192
0.00545061	24.962176
0.00557461	25.282432

Displacement (cm)	Load (N)
0.00585993	25.70944
0.00616259	26.029696
0.00630925	26.563456
0.0066199	26.883712
0.00692122	27.31072
0.00729854	27.737728
0.00756919	28.164736
0.00790917	28.37824
0.00809582	28.698496
0.00829448	29.125504
0.00850779	29.44576
0.00882377	29.766016
0.0088891	30.193024
0.00926373	30.51328
0.0097077	30.940288
0.009993	31.367296
0.01022631	31.687552
0.01047695	32.11456
0.01085157	32.541568
0.01124353	32.968576
0.01151416	33.288832
0.01198343	33.609088
0.01226605	33.929344
0.01251935	34.2496
0.01271665	34.676608
0.01304993	34.996864
0.0133752	35.423872
0.01364449	35.957632
0.01401508	36.277888
0.01431636	36.598144
0.01458297	37.025152
0.0148669	37.345408
0.01533613	37.772416
0.01563339	38.092672
0.01574137	38.51968
0.01600263	38.946688
0.01644652	39.373696
0.01668778	39.693952
0.01695171	40.014208
0.01727428	40.441216
0.01759552	40.868224

Displacement (cm)	Load (N)
0.01757552	41.295232
0.01811269	41.615488
0.01844857	42.042496
0.01868183	42.469504
0.01886976	42.896512
0.01917232	43.216768
0.01953618	43.643776
0.0199267	44.070784
0.02033453	44.497792
0.02075968	44.9248
0.02104356	45.351808
0.0213181	45.778816
0.0216846	46.205824
0.02194847	46.632832
0.02232296	47.05984
0.02267878	47.486848
0.0230799	48.020608
0.02356097	48.447616
0.02390744	48.767872
0.0243352	49.088128
0.0248722	49.515136
0.02505875	50.048896
0.02545717	50.475904
0.02605677	50.902912
0.02659506	51.32992
0.02706139	51.756928
0.02752238	52.183936
0.02783281	52.610944
0.02811792	52.9312
0.02857355	53.358208
0.02921568	53.785216
0.02968461	54.212224
0.0301029	54.53248
0.03071301	54.852736
0.03121386	55.279744
0.03170271	55.706752
0.0322355	56.13376
0.03263508	56.454016
0.03311189	56.987776
0.03356605	57.521536
0.03402287	57.948544

Displacement (cm)	Load (N)
0.03468076	58.375552
0.03524407	58.695808
0.03553836	59.016064
0.03608833	59.549824
0.03659565	59.976832
0.03681536	60.40384
0.0373626	60.830848
0.03791116	61.257856
0.03845037	61.684864
0.03900021	62.00512
0.03976702	62.432128
0.04035807	62.859136
0.0408466	63.286144
0.04134443	63.713152
0.04196202	64.033408
0.04236131	64.460416
0.04299615	64.994176
0.04350853	65.314432
0.04425242	65.74144
0.0450974	66.061696
0.04550723	66.381952
0.04597292	66.80896
0.04660623	67.235968
0.04694149	67.556224
0.04756543	67.87648
0.04833299	68.303488
0.04896749	68.623744
0.04958998	69.050752
0.05024168	69.47776
0.05086276	69.904768
0.05122182	70.331776
0.05181491	70.652032
0.05242392	71.07904
0.05290259	71.506048
0.05348361	71.826304
0.05391171	72.253312
0.05456578	72.573568
0.05523177	73.000576
0.05568504	73.427584
0.05607847	73.854592
0.05671777	74.2816

Displacement (cm)	Load (N)
0.0575444	74.708608
0.05829521	75.135616
0.05910176	75.562624
0.05979264	75.88288
0.06073853	76.309888
0.06143725	76.630144
0.06219568	77.057152
0.0626592	77.48416
0.06303106	77.911168
0.06371497	78.338176
0.06450505	78.765184
0.06545835	79.192192
0.06610355	79.6192
0.06685488	80.046208
0.06800696	80.366464
0.06887754	80.68672
0.06959675	81.113728
0.07056398	81.540736
0.07132812	81.860992
0.07185873	82.394752
0.07264395	82.715008
0.07339327	83.035264
0.07395289	83.462272
0.07468218	83.88928
0.07506005	84.316288
0.07606894	84.743296
0.07677811	85.170304
0.0783632	85.597312
0.07926292	85.810816
0.08005123	86.237824
0.08099972	86.664832
0.08200104	87.09184
0.08349741	87.412096
0.08437388	87.732352
0.08551758	88.15936
0.08670077	88.586368
0.08840629	88.799872
0.08942222	89.22688
0.09033745	89.547136
0.09174175	89.974144
0.09285884	90.401152

Displacement (cm)	Load (N)
0.09412637	90.82816
0.0960317	91.255168
0.09728525	91.575424
0.09849888	91.89568
0.09961585	92.215936
0.10104536	92.536192
0.10125916	92.9632
0.10278186	93.283456
0.10439905	93.603712
0.10564916	94.03072
0.10689103	94.350976
0.10806799	94.884736
0.10969653	95.204992
0.11122836	95.632
0.11238972	96.059008
0.11333227	96.486016
0.11504705	96.913024
0.11709915	97.23328
0.11870068	97.553536
0.1203108	97.873792
0.12175871	98.194048
0.12299862	98.514304
0.12455454	98.83456
0.12632374	99.154816
0.12787442	99.581824
0.12975486	99.90208
0.13165667	100.22234
0.13339511	100.64934
0.13472295	101.07635
0.13641677	101.39661
0.13815166	101.71686
0.13920186	102.03712
0.14027791	102.35738
0.14156795	102.78438
0.14313835	103.10464
0.14461013	103.53165
0.14584113	103.8519
0.14718128	104.17216
0.14877389	104.49242
0.15052866	104.81267
0.15234633	105.13293

Displacement (cm)	Load (N)
0.15455483	105.55994
0.15691401	105.88019
0.1594326	106.3072
0.16181538	106.62746
0.16456484	106.94771
0.16698638	107.37472
0.16946554	107.69498
0.17235804	108.01523
0.1743671	108.33549
0.17650137	108.65574
0.17868825	108.976
0.18115465	109.40301
0.18368972	109.72326
0.18646059	110.04352
0.19000273	110.25702
0.192722	110.68403
0.19569627	111.11104
0.1986414	111.53805
0.20142434	111.96506
0.20461576	112.28531
0.20758721	112.60557
0.2106442	112.92582
0.21318779	113.35283
0.21587489	113.77984
0.21836568	114.1001
0.22170909	114.42035
0.22480168	114.74061
0.22811383	115.06086
0.23180362	115.48787
0.23558911	115.80813
0.2399855	116.23514
0.24397449	116.44864
0.24778516	116.7689
0.25149844	117.08915
0.25457412	117.40941
0.25923883	117.62291
0.2629275	117.83642
0.26705301	118.04992
0.2711321	118.47693
0.27487098	118.79718
0.27825317	119.22419

Displacement (cm)	Load (N)
0.2819573	119.54445
0.28702648	119.75795
0.29164272	120.07821
0.29615838	120.29171
0.3002553	120.61197
0.30477141	120.82547
0.30951667	121.14573
0.31404738	121.46598
0.31811497	121.78624
0.32303281	122.1065
0.3277887	122.42675
0.33258764	122.74701
0.33752267	123.17402
0.34234958	123.49427
0.34672954	123.81453
0.35215098	124.02803
0.35767374	124.34829
0.36319944	124.56179
0.36904538	124.7753
0.37480611	124.9888
0.38010171	125.2023
0.3848276	125.52256
0.3906965	125.73606
0.39655871	126.05632
0.40302202	126.37658
0.40848904	126.59008
0.41435159	126.91034
0.42041522	127.01709
0.4273642	127.12384
0.43387876	127.33734
0.44020037	127.4441
0.44707992	127.6576
0.45368819	127.76435
0.46074849	127.8711
0.47024965	128.19136
0.4770897	128.29811
0.48932805	128.51162
0.50189685	128.61837
0.5137588	128.72512
0.53070071	128.93862
0.54764283	129.04538

Displacement (cm)	Load (N)
0.56302149	129.15213
0.57692148	129.36563
0.5919696	129.47238
0.60756733	129.57914
0.62355574	129.68589
0.63838549	129.68589
0.65352489	129.89939
0.66794495	130.00614
0.68178786	130.1129
0.69586404	130.3264
0.70914168	130.43315
0.72232923	130.64666
0.73383516	130.75341
0.74395125	130.86016
0.75555081	131.07366
0.76314527	131.18042
0.77045661	131.39392
0.77801552	131.60742
0.78231469	131.71418
0.7865209	131.82093
0.79115279	131.92768
0.7964189	132.03443
0.80077995	132.14118
0.80414313	132.24794
0.80744348	132.35469
0.81075539	132.56819
0.81376839	132.88845
0.81670919	132.88845
0.81970123	132.88845
0.82250081	133.10195
0.82519892	132.88845
0.82764947	132.9952
0.83077442	132.9952
0.83294808	132.88845
0.83487114	133.2087
0.83632905	133.02329
0.83769738	133.17312
0.83901733	133.08939
0.75948165	132.9952
0.80890921	124.98324
0.84236132	133.07145

Displacement (cm)	Load (N)
0.80355074	122.92903
0.84394207	133.17312
0.84489969	133.04372
0.84547498	133.52896

Appendix B: Test 2 Compressive load-angle of twist

Displacement (cm)	Load (N)
0	-37.914752
0	-38.34176
0	-37.98592
0	-38.34176
0	-38.036754
0	-38.34176
0	-38.07488
0	-38.216169
0	-38.104533
0	-38.117019
0	-38.128256
0	-37.914752
0	-37.808
0	-37.701248
0	-37.808
0	-37.701248
0	-38.021504
0	-37.701248
0	-38.128256
0	-37.808
0	-38.235008
0	-37.808
0	-38.128256
0	-37.808
0	-38.128256
0	-37.808
0	-37.914752
0	-37.808
0	-37.808
0	-37.914752
0	-37.701248
0	-37.914752
0	-37.701248
0	-38.021504
0	-37.701248
0	-38.128256
0	-37.701248
0	-38.128256
0	-37.701248
0	-38.021504
0	-37.701248

Displacement (cm)	Load (N)
0	-37.914752
0	-37.808
0	-37.808
0	-37.808
0	-37.808
0	-38.021504
0	-37.808
0	-38.021504
0	-37.594496
0	-38.021504
0	-37.701248
0	-38.021504
0	-37.594496
0	-37.914752
0	-37.594496
0	-37.808
0	-37.594496
0	-37.701248
0	-37.594496
0	-37.594496
0	-37.701248
0	-37.487744
0	-37.701248
0	-37.380992
0	-37.701248
0	-37.27424
0	-37.594496
0	-37.380992
0	-37.808
0	-37.487744
0	-37.701248
0	-37.594496
0	-37.701248
0	-37.594496
0	-37.594496
0	-37.594496
0	-37.380992
0	-37.701248
0	-37.380992
0	-37.701248
0	-37.27424

Displacement (cm)	Load (N)
0	-37.594496
0	-37.27424
0	-37.594496
0	-37.167488
0	-37.487744
0	-37.27424
0	-37.27424
0	-37.167488
0	-37.167488
0	-37.167488
0	-36.953984
0	-37.167488
0	-36.847232
0	-37.060736
0	-36.74048
0	-37.060736
0	-36.633728
0	-36.953984
0	-36.526976
0	-36.847232
0	-36.526976
0	-36.633728
0	-36.420224
0	-36.526976
0	-36.526976
0	-36.420224
0	-36.526976
0	-36.313472
0	-36.526976
0	-36.20672
0	-36.633728
0	-36.099968
0	-36.526976
0	-36.20672
0	-36.526976
0	-36.20672
0	-36.313472
0	-36.099968
0	-36.099968
0	-35.993216
0	-35.993216

Displacement (cm)	Load (N)
0	-36.099968
0	-35.886464
0	-36.099968
0	-35.67296
0	-35.993216
0	-35.67296
0	-35.993216
0	-35.566208
0	-35.886464
0	-35.459456
0	-35.779712
0	-35.459456
0	-35.459456
0	-35.245952
0	-35.1392
0	-35.1392
0	-34.925696
0	-35.032448
0	-34.712192
0	-34.925696
0	-34.498688
0	-34.818944
0	-34.391936
0	-34.712192
0	-34.285184
0	-34.498688
0	-33.964928
0	-33.964928
0	-33.751424
0	-33.644672
0	-33.53792
0	-33.324416
0	-33.324416
0	-33.00416
0	-33.217664
0	-32.790656
0	-33.110912
0	-32.790656
0	-33.110912
0	-32.683904
0	-32.897408

Displacement (cm)	Load (N)
0	-32.4704
0	-32.4704
0	-32.256896
0	-32.150144
0	-31.93664
0	-31.829888
0	-31.93664
0	-31.616384
0	-31.723136
0	-31.296128
0	-31.509632
0	-31.082624
0	-31.40288
0	-30.975872
0	-31.189376
0	-30.762368
0	-30.762368
0	-30.33536
0	-30.228608
0	-30.015104
0	-29.8016
0	-29.8016
0	-29.481344
0	-29.588096
0	-29.161088
0	-29.481344
0	-28.947584
0	-29.161088
0	-28.627328
0	-28.840832
0	-28.413824
0	-28.627328
0	-28.307072
0	-28.307072
0	-28.093568
0	-27.986816
0	-27.880064
0	-27.66656
0	-27.773312
0	-27.453056
0	-27.773312

Displacement (cm)	Load (N)
0	-27.1328
0	-27.346304
0	-26.705792
0	-26.919296
0	-26.278784
0	-26.385536
0	-25.958528
0	-26.06528
0	-25.851776
0	-25.745024
0	-25.53152
0	-25.211264
0	-25.104512
0	-24.677504
0	-24.677504
0	-24.143744
0	-24.357248
0	-23.716736
0	-23.823488
0	-23.182976
0	-23.503232
0	-23.076224
0	-23.182976
0	-22.86272
0	-22.755968
0	-22.542464
0	-22.32896
0	-22.115456
0	-21.581696
0	-21.581696
0	-21.047936
0	-21.154688
0	-20.620928
0	-20.834432
0	-20.300672
0	-20.514176
0	-19.980416
0	-20.087168
0	-19.66016
0	-19.66016
0	-19.339904

Displacement (cm)	Load (N)
0	-19.019648
0	-18.912896
0	-18.59264
0	-18.59264
0	-18.165632
0	-18.165632
0	-17.631872
0	-17.952128
0	-17.418368
0	-17.631872
0	-17.098112
0	-17.204864
-1.867E-05	-16.671104
-2.4E-05	-16.671104
-9.733E-05	-16.350848
-0.000104	-16.137344
-0.000132	-15.92384
-0.000132	-15.603584
-0.000156	-15.496832
-0.000516	-14.963072
-0.0010973	-15.069824
-0.0015253	-14.429312
-0.001764	-14.429312
-0.002024	-13.7888
-0.002712	-13.895552
-0.004084	-13.361792
-0.0055066	-13.575296
-0.0070585	-12.934784
-0.0083918	-12.828032
-0.009673	-12.401024
-0.0114328	-12.18752
-0.0132419	-11.867264
-0.0152681	-11.547008
-0.0175542	-11.440256
-0.0195362	-11.013248
-0.0215713	-10.906496
-0.0236423	-10.479488
-0.0255598	-10.479488
-0.0274185	-9.838976
-0.0290638	-9.945728
-0.0305638	-9.198464

Displacement (cm)	Load (N)
-0.0320131	-9.411968
-0.0339456	-8.878208
-0.0356183	-8.98496
-0.0368007	-8.4512
-0.037545	-8.237696
-0.0381322	-7.810688
-0.0383532	-7.597184
-0.0389976	-7.38368
-0.0395367	-6.84992
-0.03959	-6.743168
-0.0397204	-6.209408
-0.0394582	-6.209408
-0.0390681	-5.462144
-0.0388285	-5.462144
-0.0385462	-4.928384
-0.0383306	-4.821632
-0.0384104	-4.18112
-0.0384291	-4.18112
-0.0383053	-3.64736
-0.0382919	-3.540608
-0.0382959	-3.006848
-0.037802	-2.686592
-0.0379511	-2.259584
-0.0381881	-1.832576
-0.0379937	-1.725824
-0.0377993	-1.192064
-0.0379844	-1.085312
-0.0378113	-0.4448
-0.0379857	-0.4448
-0.038031	0.195712
-0.0380297	0.195712
-0.0383505	0.836224
-0.038256	0.836224
-0.0383306	1.476736
-0.03824	1.69024
-0.0382294	2.330752
-0.0381708	2.651008
-0.0379831	3.184768
-0.0379285	3.611776
-0.0377381	3.82528
-0.0375716	4.465792

Displacement (cm)	Load (N)
-0.0375983	4.572544
-0.0373746	5.213056
-0.0370271	5.319808
-0.0368114	6.280576
-0.0368793	6.280576
-0.0366383	7.134592
-0.0366356	7.241344
-0.0363973	7.988608
-0.0363373	8.202112
-0.0362494	8.842624
-0.0359778	9.16288
-0.0358699	9.69664
-0.0356289	10.2304
-0.0357967	10.657408
-0.0356649	11.191168
-0.0353719	11.404672
-0.0354878	12.045184
-0.0351202	12.258688
-0.0347234	13.112704
-0.0347101	13.112704
-0.0345729	14.073472
-0.0342866	14.180224
-0.0341933	14.927488
-0.0340935	15.03424
-0.0337805	15.888256
-0.0337898	16.10176
-0.0335634	16.742272
-0.0334049	17.16928
-0.0332704	17.70304
-0.0330213	18.450304
-0.0327256	18.77056
-0.032743	19.624576
-0.0326377	19.83808
-0.0325405	20.692096
-0.0325338	20.798848
-0.032422	21.652864
-0.0322435	21.866368
-0.0324939	22.720384
-0.0324939	22.933888
-0.0325085	23.894656
-0.032366	24.214912

Displacement (cm)	Load (N)
-0.0321796	24.962176
-0.0321423	25.495936
-0.0320117	26.029696
-0.0318213	26.670208
-0.0317227	27.203968
-0.031359	27.951232
-0.0311299	28.37824
-0.0308782	29.232256
-0.0305252	29.339008
-0.0305212	30.406528
-0.0302921	30.620032
-0.030027	31.5808
-0.0296886	31.794304
-0.0294382	32.755072
-0.0290585	33.18208
-0.0286828	34.142848
-0.028415	34.78336
-0.0282565	35.530624
-0.0277609	36.171136
-0.0278008	36.704896
-0.0277569	37.558912
-0.0272066	37.98592
-0.0271253	38.946688
-0.0269668	39.266944
-0.0266031	40.334464
-0.0266643	40.65472
-0.0266137	41.615488
-0.0263899	41.935744
-0.0265644	43.110016
-0.026138	43.537024
-0.0259435	44.39104
-0.0259582	44.9248
-0.0257636	45.885568
-0.0255624	46.632832
-0.0257117	47.273344
-0.0256157	47.913856
-0.0252386	48.340864
-0.0251773	49.301632
-0.025208	49.72864
-0.0250108	50.79616
-0.0248362	51.116416

Displacement (cm)	Load (N)
-0.0251041	52.290688
-0.0249801	52.610944
-0.0248642	53.785216
-0.0247829	54.212224
-0.0246017	55.279744
-0.0243845	55.813504
-0.0240607	56.774272
-0.0237209	57.414784
-0.0235397	58.162048
-0.0231905	59.122816
-0.0229626	59.763328
-0.0226321	60.724096
-0.022207	61.151104
-0.0219098	62.325376
-0.0215753	62.859136
-0.0212701	64.033408
-0.0210862	64.460416
-0.0209596	65.634688
-0.0204931	66.061696
-0.0202919	67.235968
-0.0197348	67.769728
-0.0192576	68.837248
-0.019059	69.47776
-0.0184792	70.331776
-0.0181114	71.185792
-0.0177955	71.933056
-0.0174995	72.893824
-0.0170917	73.427584
-0.0171716	74.495104
-0.017069	74.922112
-0.0171157	76.096384
-0.0170623	76.523392
-0.0166118	77.804416
-0.0163252	78.231424
-0.0166265	79.405696
-0.0163612	79.939456
-0.015944	81.006976
-0.0158653	81.647488
-0.0155481	82.608256
-0.0153015	83.462272
-0.0148536	84.209536

Displacement (cm)	Load (N)
-0.014539	85.277056
-0.0142817	85.917568
-0.0140018	86.985088
-0.0138151	87.518848
-0.0134232	88.799872
-0.0138898	89.333632
-0.0138951	90.614656
-0.0137165	91.148416
-0.0137858	92.322688
-0.0136658	92.9632
-0.0135418	94.03072
-0.014407	94.671232
-0.0150495	95.738752
-0.0150055	96.592768
-0.0167651	97.553536
-0.0170637	98.621056
-0.0170543	99.36832
-0.0192443	100.542592
-0.019924	101.183104
-0.0213554	102.464128
-0.0225748	102.891136
-0.0229706	104.278912
-0.0243179	104.919424
-0.0244551	106.3072
-0.0258116	106.84096
-0.025685	108.015232
-0.026735	108.762496
-0.0283391	109.936768
-0.0296913	110.790784
-0.0320703	111.6448
-0.0336699	112.71232
-0.0359126	113.566336
-0.0375344	114.740608
-0.0392106	115.487872
-0.03826	116.768896
-0.0401611	117.302656
-0.0418396	118.58368
-0.041998	119.11744
-0.0422295	120.398464
-0.0436602	120.932224
-0.0446676	122.32

Displacement (cm)	Load (N)
-0.0470998	122.960512
-0.0531765	124.134784
-0.0565902	124.882048
-0.0585145	125.949568
-0.0616644	126.910336
-0.0643125	127.764352
-0.0650733	128.938624
-0.0672292	129.79264
-0.0713188	131.180416
-0.0731811	131.820928
-0.0771214	133.208704
-0.0790973	133.742464
-0.0835583	135.023488
-0.0872486	135.557248
-0.0944634	136.838272
-0.1009873	137.585536
-0.1098349	138.86656
-0.1211242	139.720576
-0.1354836	140.894848
-0.1442667	141.748864
-0.1637356	142.816384
-0.1778424	143.777152
-0.1959439	144.524416
-0.21094	145.698688
-0.2274508	146.3392
-0.241482	147.620224
-0.2596685	148.047232
-0.275339	149.328256
-0.2881299	149.862016
-0.3024815	151.14304
-0.3142247	151.6768
-0.3271217	152.851072
-0.339077	153.491584
-0.3526396	154.559104
-0.3622228	155.306368
-0.3730799	156.053632
-0.3827285	156.694144
-0.3931802	157.0144
-0.4012222	157.654912
-0.4169807	157.868416
-0.4241571	158.508928

Displacement (cm)	Load (N)
-0.4334088	158.508928
-0.4419198	159.14944
-0.4534113	159.042688
-0.4618732	159.789952
-0.4720123	159.6832
-0.4786709	160.21696
-0.4875428	159.896704
-0.497279	160.003456
-0.5104335	159.896704
-0.5246984	159.789952
-0.5407175	159.6832
-0.5550978	159.469696
-0.5683023	159.362944
-0.5803308	158.935936
-0.5913082	159.042688
-0.6021298	158.61568
-0.6119348	158.829184
-0.6220066	158.402176
-0.6307917	158.61568
-0.6390086	158.08192
-0.6455162	158.402176
-0.6515864	157.975168
-0.6568881	158.08192
-0.6635246	157.441408
-0.6709932	157.121152
-0.6800975	156.587392
-0.6886518	156.373888
-0.6959701	156.053632
-0.7006678	155.519872
-0.7031402	155.199616
-0.7045304	154.772608
-0.706676	154.452352
-0.710353	153.918592
-0.7149725	153.705088
-0.7184591	153.249987
-0.7215688	153.218773
-0.7243386	152.807115
-0.7256235	152.74432
-0.7260571	152.246144
-0.7258036	152.134309
-0.7264448	151.512566

Displacement (cm)	Load (N)
-0.7279765	151.32096
-0.7306922	150.706327
-0.7331892	150.60928

Displacement (cm) Load (N)

References

1. Chaisson, Eric J., *The Hubble Wars*, New York: Harper Collins Publishers, 1994

2. Pellegrino, S., "Large Retractable Appendages in Spacecraft," Journal of Spacecraft and Rockets, Vol. 32, No. 6, November-December 1995, pp. 1006-1014.

3. Foster, C. L., Tinker, M. L., Nurre, G.S., and Till, W. A., "Solar-Array-Induced Disturbance of the Hubble Space Telescope Pointing System," *Journal of Spacecraft and Rockets*, Vol. 32, No. 4, July-August 1995, pp. 634-644.

4. Deloo, P., Klein, M., and Reynolds, J., "Solar Array Deployed Finite Element Model: Volume 2," European Space Research and Technology Center, ESA Document TN-SA-0011, Vol. 2, Noordwijk, Netherlands, March 1989.

5. Thornton, Earl A. and Kim, Yool A., "Thermally Induced Bending Vibrations of a Flexible Rolled-Up Solar Array," *Journal of Spacecraft and Rockets*, Vol. 30, No. 4, July/August 1993, pp. 438-448.

6. Foster, C. L., Tinker, M. L., Nurre, G.S., and Till, W. A., "The Solar Array-Induced Disturbance of the Hubble Space Telescope Pointing System," Proceedings of the 61st Shock and Vibration Symposium, Vol. 4, October 1990, pp. 19-37.

7. Chung, Peter W. and Thornton, Earl A. "Torsional Buckling and Vibrations of a Flexible Rolled-Up Solar Array," AIAA Paper pp. 95-1355 April 1995.

8. Rauschenbach, H.S., *Solar Cell Array Design Handbook*, Litton Educational Publishing, Inc., 1980.

9. Anonymous, STEM Design Characteristics and Parameters, AAC-B-006, Astro Aerospace Corp., 1985.

10. Anonymous, System 4000 Equipment Reference Manual, Measurements Group, Inc., 1990.

11. Beer, Ferdinand P. and Johnston Jr., E. Russell, Mechanics of Materials, McGraw-Hill Book Company, 1981.

DISTRIBUTION LIST

1 - 3 National Aeronautics and Space Administration
Goddard Space Flight Center
Greenbelt, MD 20771
301-286-6279

Attention: Mr. John Decker, Code 722.1
Mechanical Systems Division

4 Gloria R. Blanchard, Code 286.1
National Aeronautics and Space Administration
Goddard Space Flight Center
Greenbelt, MD 20771
301-286-8511

5 NASA Scientific and Technical Information Facility
P. O. Box 8757
Baltimore/Washington International Airport
Baltimore, MD 21240

6 - 7 E. A. Thornton

8 R. D. Flack, Jr.

* SEAS Postaward Research Administration

9 - 10 M. Rodeffer, Engineering Library

11 SEAS Preaward Research Administration

*Cover Letter

JO#7205:ph